The Dissertation Committee for Jamie Michael Kropka Certifies that this is the approved version of the following dissertation:

Polymer Behavior under the Influence of Interfacial Interactions

Committee:

_____
Venkat Ganesan, Supervisor

_____
Peter F. Green, Co-Supervisor

_____
Roger T. Bonnecaze

_____
Donald R. Paul

_____
Arumugam Manthiram

Polymer Behavior under the Influence of Interfacial Interactions

by

Jamie Michael Kropka, B.S.

Dissertation

Presented to the Faculty of the Graduate School of

The University of Texas at Austin

in Partial Fulfillment

of the Requirements

for the Degree of

Doctor of Philosophy

The University of Texas at Austin

May 2008

Dedication

To my wife Kim and daughter Jordan

Acknowledgements

There are a number of people that have contributed to making my experiences in graduate school rewarding, and I would like to use this opportunity to express my gratitude to some of them. First I would like to thank my dissertation advisor, Dr. Peter Green, for his support. In particular, he allowed me the freedom to direct my own path towards this degree, which has been a very challenging but rewarding journey. Dr. Venkat Ganesan also played a large role in my development as a scientist, as he has challenged the thoroughness of my understanding of a number of topics. I would also like to thank professors Roger Bonnecaze, Donald Paul and Arumugam Manthiram for graciously serving as members on my dissertation committee.

I am also very grateful to have had the opportunity to conduct neutron scattering experiments at the National Institute of Standards and Technology (NIST). The staff at the NIST Center for Neutron Research were always very inviting, which made the opportunity to use a world class facility all that more enjoyable. I am particularly indebted to Dr. Victoria Garcia Sakai, who was instrumental in helping run the experiments and teaching me to use the data analysis software developed by NIST. I also appreciate the kind and encouraging comments from Dr. Dan Neumann during my visits; he seemed to always find time in his schedule to ask how things were coming along. Both Peter and now Dr. Brian Besancon played a significant role in getting me involved

with this work and I will be forever grateful for that. A number of people from the polymers division at NIST were also very helpful, particularly Dr. Christopher Soles and Dr. Jack Douglas, who opened the door to use their laboratory facilities and were willing to talk about the science going on within the division and elsewhere.

I would also like to acknowledge the many colleagues and friends who helped me to make the most of my time in graduate school. I would especially like to thank Brian, who not only helped me get involved with the work at NIST, but was also my travel partner to many conferences and a great resource for discussing research problems. Karl Putz and Joseph Pham were very helpful and supportive in getting me acquainted with the ways of the Green group in my early days. I am also indebted to Abraham Arceo and Luciana Meli, both for their technical help in the early days and, especially, for standing up to take the lead of the group when it was split between two universities. My thanks goes to Yuan Li as well, both for her help with instrumentation issues and for keeping me company in the office during the days when she and I were the only Texas group members. I am also thankful for help from a number of people outside the Green group. Michael Dickey and Frank Palmieri were gracious enough to allow me access to facilities in the Willson group. Landry Khounlavong was immensely helpful in making the transition from experimental to computational work as smooth as possible. I also am grateful for the bright spots in the day that came along with the office transition to CPE. Mark Pond's good mood and genuine interest in your daily activities was always uplifting. The coffee scavengers, Bill Krekelberg, Gaurav Gupta, Gaurav Goel, and Manas Shaw, brought a welcomed break to the rigors of research as well.

My family deserves the most thanks of all. My mother encouraged me to pursue my own interests during childhood, and that laid the foundation for what I have been able to do since then. Finally and most importantly, my thanks go to my wife Kim. Without

her support, the pursuit of my dream would not have been possible. She has always been there to encourage me and to make sure that my sights remained broader than the details of any single problem that I was trying to solve on a given day. I do not think that there is anything that the two of us could not handle together, and I look forward to the rest of my life with her.

Polymer Behavior under the Influence of Interfacial Interactions

Publication No._____

Jamie Michael Kropka, Ph.D.

The University of Texas at Austin, 2008

Supervisors: Peter F. Green and Venkat Ganesan

The properties of polymers, thin films or bulk, are profoundly influenced by interactions at interfaces with dissimilar materials. Thin, supported, polymer films are subject to interfacial instabilities, due largely to competing intermolecular forces, that cause them to rupture and dewet the substrate. The addition of nanoparticles (such as clay sheets, metallic or semiconductor nanocrystals, carbon nanotubes, etc.) to polymers can substantially affect bulk properties, such as the glass transition and viscosity, and influence the processability of the material. In this dissertation, we contribute to a fundamental understanding of the role of interfacial interactions on both the instabilities exhibited by polymer thin films and the properties displayed by polymer-nanoparticle mixtures.

While conditions under which the destabilization of compositionally homogeneous thin films occurs are relatively well understood, the mechanisms of film stabilization in many two-component thin film systems are still unresolved.   We demonstrate that the addition of a miscible component to an unstable film can provide an effective means of stabilization.   The details of the stabilization mechanism are

understood in terms of the compositional dependence of both the macroscopic wetting parameters and the effective interface potential for the system. We find that the suppression of dewetting in the system is not an equilibrium stabilization process and propose a mechanism by which the increased resistance to dewetting may occur.

There is also significant interest in understanding the extraordinary property enhancement of polymers that are enabled by the addition of only small concentrations of nanoparticles. If these effects could be distilled down to a few simple rules, they could be exploited in the design of materials for specific applications. In this work, the influence of C_{60} nanoparticles on the bulk dynamical properties of three polymers is examined. Based on the findings from a range of measurement techniques, including differential scanning calorimetry, dynamic mechanical analysis, dynamic rheology and neutron scattering, we propose that the changes in the glass transition temperature for the polymer-C_{60} mixtures can be understood in terms of a percolation interpretation of the glass transition. The proposed mechanism is also characterized computationally.

Table of Contents

xi

List of Tables

List of Figures

xvi

Chapter 1: Introduction

The research detailed in this dissertation focuses on the behaviors of polymers under the influence of interfacial interactions, both in thin film geometries and in polymer-nanoparticle mixtures. The objective of the research is to further the development of a predictive understanding of the factors that control both (1) interfacial instabilities associated with dewetting in thin polymer films and (2) the dynamical properties exhibited by polymer-based nanocomposites (PNCs). In the following sections, we describe the motivation for this work and provide a brief overview of the current understanding of the topics to be addressed.

1.1   MOTIVATION AND OVERVIEW

Advances in polymers have come a long way since their initial commercialization. Thirty years ago, the applications of polymers were limited, and plastics were often viewed as "cheap" alternatives that did not exhibit the same strength or durability as more traditional materials, such as metals. Today, synthetic polymers are ubiquitous, with commercial applications that range from textiles and automobile parts to sensors and organic electronics; in some instances, such as when mechanical flexibility is required, polymer-based materials present the only option to meet all the demands that an application requires.

New uses for these versatile organic materials continue to emerge. Polymer thin films are used for lithographic patterning,[1, 2] as organic light emitting diodes and transistors,[3, 4] and as gas separation membranes.[5, 6] The incorporation of nanoparticles, such as C_{60} fullerenes, carbon nanotubes and layered silicates, into polymer hosts to create PNCs has also recently been shown to significantly enhance the

mechanical,[7, 8] electrical, and barrier[5, 6] properties of the polymer at very small concentrations of the additive. This provides hope for overcoming the limitations of property optimization of conventional composites, in which compromises generally must be made between properties such as stiffness, toughness and optical clarity.

A common element between the polymer thin films and PNCs used in many emerging applications is the fact that a large fraction of the polymer chains are subject to interfacial interactions. In the films, the interactions are with the external interfaces that confine the film, while in the PNCs, the interactions are with the surfaces of the particles within the bulk of the material. The interfacial interactions in these systems are known to play a significant role in the properties they exhibit; polymer thin films can exhibit both a thickness dependence of their physical properties[9-12] and structural instabilities[13-15] as film thickness decrease below ~ 100 nm, while the addition of nanoparticles induces changes in the bulk properties exhibited by PNCs.[16-19] These effects bring both new challenges and opportunities for devices constructed from these materials, as device fabrication and performance rely on both the initial properties and the long-term stability of the materials of construction. Examples of challenges that can be encountered when dealing with these materials include the following: (1) a change in the glass transition temperature (T_g) of an amorphous polymeric material upon the addition of nanoparticles could significantly alter the necessary processing conditions to mold a structural component within dimensional specifications; (2) if a thin, chemically amplified photoresist film possessed enhanced mobility relative to its bulk counterpart, excessive photoacid diffusion through the resist film could lead to blurring of the latent lithographic image;[1] (3) in a gas separation membrane, changes in polymer packing densities at interfaces could change the permeation properties of gases through the film[6] as well as the rate at which the permeability changes over the lifetime of the membrane;[20] (4) the

2

operation of organic electronic devices depends on the ability to transport charge carriers from the point of excitation to the electrode on the outer surface of the device, and disruption of the charge transport path, such as by a breakup of the thin film charge transporting layer, would significantly compromise the function of the device. Clearly, understanding how interfacial interactions affect the properties of materials in these devices is key to preventing catastrophic device failures and wielding the property changes exhibited by the materials in favor of device fabrication and performance.

Unfortunately, global rules to describe the behaviors of polymers under the influence of interfacial interactions have not yet been established. A desire to mature understanding of the topic has motivated studies in a number of areas, which include the following: the thickness dependence of the T_g,[10, 11, 21-25] viscosity,[26-29] and diffusion coefficient[12, 30-35] of polymer thin films; interfacial instabilities that occur in thin polymer films;[13-15, 36-40] and viscoelastic and thermal behaviors of PNCs.[16, 17, 19, 41-46] In this work, we address two classes of phenomena induced by the role of interfacial interactions: structural instabilities of thin polymer films and the ability of nanoparticles to alter the bulk properties of PNCs. The following subsections will provide a brief background to serve as the context in which to interpret the remainder of the dissertation. Specifically, the structural stability of supported thin polymer films is discussed, followed by an introduction to the influence of nanoparticles on the properties exhibited by polymers.

1.1.1 Structural Stability of Supported Polymer Films

Rupture and dewetting of a polymer film from the underlying substrate can occur during processing or device aging. For example, smooth polymer films can be achieved on a substrate by spin casting, even if this is not the energetically favorable state. When

3

conditions exist such that the film acquires sufficient mobility, destabilization will occur through the formation of topographical patterns at the free interface that grow over time. Eventually the morphological structure evolves to form droplets on the substrate (dewetting). The conditions under which destabilization occurs are relatively well understood and are briefly summarized here.

The wetting of a macroscopic liquid film on a solid substrate is determined entirely by the energies (or surface tensions) of the involved interfaces. Whether a liquid spreads or beads up to form droplets on a surface is determined by the spreading coefficient, S,

$$S = \gamma_{sv} - \left(\gamma_{lv} + \gamma_{ls}\right) \tag{1.1}$$

where γ_{sv} is the substrate-vapor interfacial energy, γ_{lv} is the liquid-vapor interfacial energy, and γ_{ls} is the liquid-substrate interfacial energy. When $S > 0$, the liquid will wet (spread) the surface. Otherwise, the liquid will dewet and form droplets.

When film thickness is reduced to the nanoscale, $< \sim 100$ nanometers, long-range intermolecular interactions can induce instabilities in an otherwise stable film.[47-49] The stability of the system and the mechanism of film breakup can be understood in terms of an effective interface potential, or equivalently, the excess free energy (per unit area) of the film due to the presence of the two interfaces. The effective interface potential, Φ, can be characterized by the following expression,[50, 51]

$$\Phi(h) = S^p \exp\left[\frac{d_o - h}{l}\right] - S^{LW}\left(\frac{d_o^2}{h^2}\right) \tag{1.2}$$

where S^p and S^{LW} are the polar and apolar dispersion contributions, respectively, to the spreading coefficient, h is the film thickness, l is the decay length of the polar interactions, and $h = d_o$ is the contact distance. For $h < d_o$, the interface potential will increase sharply to infinity due to Born repulsion. The distinction between stable,

4

metastable, and unstable films can be made in terms of Φ using Figure 1-1. Curve 1 in Figure 1-1a describes the stable case; $\Phi(h) > 0$ for all h, with a global minimum at infinite thickness. Curve 2 displays a global minimum, Φ_{min}, at $h = h^*$. The minimum in the potential indicates the system can minimize energy by changing its film thickness to h^*. If the initial film thickness is greater than h^*, the film will autophobically dewet, forming droplets on top of a uniform layer of thickness h^* as shown schematically in Figure 1-1b. Two mechanisms about which the droplets can be formed include (i) the nucleation and growth of holes and (ii) spinodal dewetting, or the spontaneous amplification of surface capillary waves. Spinodal dewetting is only possible in an unstable system, when $\Phi''(h) < 0$. This condition holds to large film thicknesses for curve 2 in Figure 1-1a. Curve 3 in Figure 1-1a exhibits both a global minimum and a local maximum, $\Phi_{max,}$. The minimum has the same implications as for curve 2, while the presence of the local maximum displays a change in curvature ($\Phi''(h)$ becomes positive) for larger film thicknesses. When $\Phi''(h) > 0$, the system is termed metastable and the film can only rupture by the nucleation and growth of holes

Polystyrene (PS) thin films supported by oxidized silicon substrates provide a model system for experimental investigations of interfacial instabilities. Oxidized silicon substrates provide a readily attainable smooth surface upon which a uniform polymer films can be spin cast. The PS film destabilizes upon heating above T_g, yet is non-volatile and thus the mass of the film is conserved. The dynamics of the film break up can also be tuned, by varying anneal temperature and polymer molecular weight, to resolve the mechanism of destabilization. Early studies of the destabilization of PS thin films, on oxidized silicon substrates in the presence of air or vacuum, used optical methods to evaluate the mechanism and dynamics of film destabilization.[14, 15] These studies were sensitive to the formation and growth of holes in the liquid film that

(a)

Φ

Φ_{max}

1

3

$\Phi'' > 0$

0

Φ_{min}

2

$\Phi'' < 0$

Φ_{min}

h^* h^* h_{max} **film thickness, h**

(b)

h^*
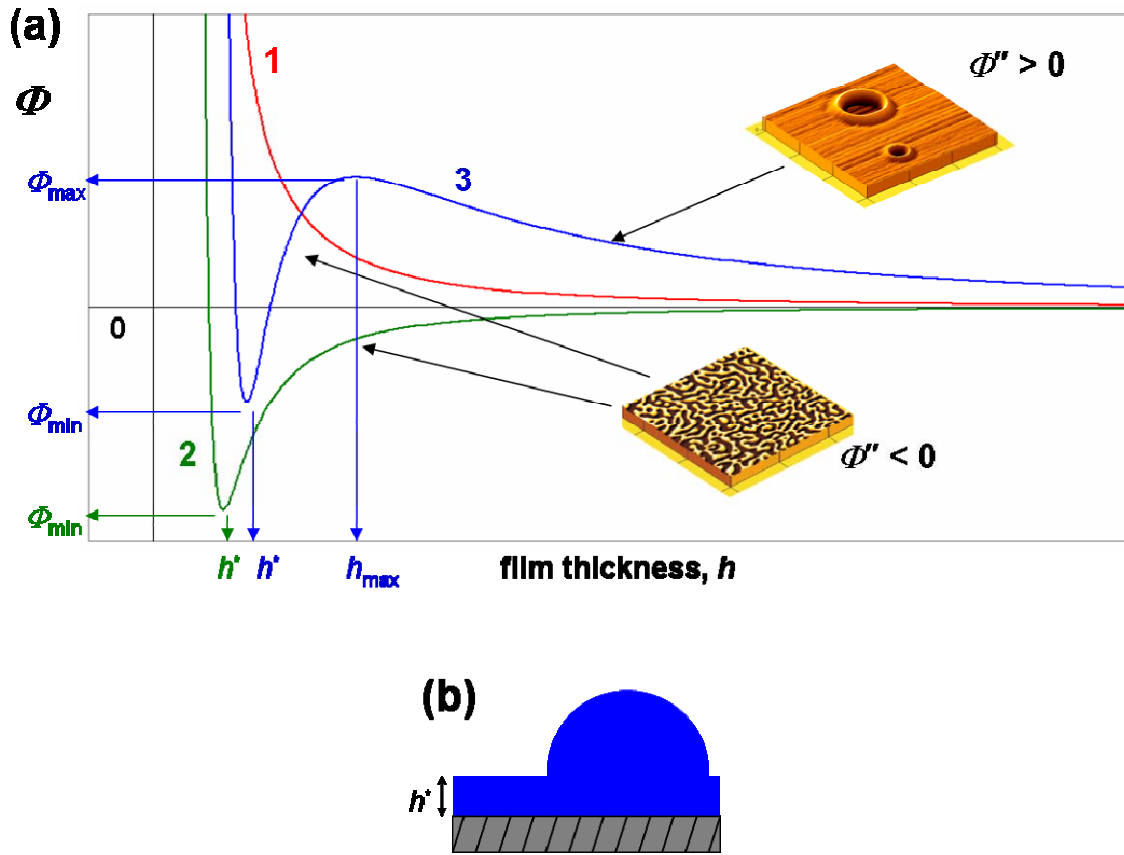
Figure 1-1: (a) Schematic of the effective interface potential as a function of film thickness for (1) stable, (2) unstable, and (3) metastable films. The inset atomic force microscopy micrographs illustrate film breakup through the nucleation and growth of holes ($\Phi'' > 0$) and through a spinodal process ($\Phi'' < 0$). (b) Schematic of a macroscopic droplet over a nanoscopic wetting layer of thickness h^*.

eventually led to the formation of droplets residing on the substrate surface. However, it was not until the use of higher resolution techniques, such as scanning probe microscopy (SPM), that a quantitative reconstruction of the interface potential for the system was possible.[38] The SPM studies found that this system exhibited an effective interface potential of type 2 or 3 from Figure 1-1a, depending on the thickness of the underlying silicon oxide layer. A nanoscopic wetting layer underlying the microscopic dewet droplets, as depicted in Figure 1-1b, was also confirmed by reflectivity measurements performed with the polymer in the liquid state.[38, 39] Ex-situ SPM measurements of dewet samples after cooling to room temperature discern that the nanoscopic wetting layer breaks up to form nanoscopic droplets.[36] The nanodroplets were reasoned to result from the rupture of the thin wetting layer of thickness h^* upon cooling the film below T_g. Self-consistent field calculations have suggested that the rupture of the wetting layer is due to a local minimum in $\Phi(h)$ at $h \approx 0$ becoming stable relative to the minimum at h^* at low temperatures.[39]

Since the performance of most thin film devices relies on uniform films, a number of strategies have been utilized in attempts to stabilize polymer films against breakup. Polymer brush layers, to enable the film to interact with like molecules and reduce unfavorable substrate-film interactions, have been fabricated through the introduction of end-functionalized polymers that can adsorb to the substrate[52-57] or block copolymers with an adsorbing anchor.[58-60] Other strategies include sulfonation and metal complexation of polymer films,[61] surface roughening,[62] and the addition of nanoparticles.[29, 63-65] The retardation of dewetting in these systems is attributed to phenomena that include an increase in film viscosity and/or changes in polymer-substrate interactions. Many of these mechanisms are kinetic in nature, though often the films are stabilized over long time scales that are indicative of an equilibrium phenomenon. We

note, however, that none of the above mentioned studies evaluated the effective interface potential of the system to determine the nature of stabilization. In our studies, we will utilize the detailed understanding of PS thin film stability on oxidized silicon substrates to try to understand the nature of film stabilization by the addition of a miscible polymer component, tetramethyl bisphenol-A polycarbonate (TMPC).

1.1.2 Influence of Nanoparticles on the Properties of Polymers

In addition to exhibiting property enhancements at much smaller particle concentrations than their conventional composite counterparts, PNCs also exhibit some unique, and even unexpected, behaviors. For example, Mackay et al.[18, 66] have observed a decrease in viscosity upon the addition of PS nanoparticles to a PS host. This finding contrasts with the century old Einstein equation for a suspension of hard spheres, where the viscosity is predicted to increase in proportion to the volume fraction of the particles in the system. Other experiments on the rheology of PNCs have reported dramatic enhancements in the low frequency elasticity (storage modulus) at very low particle loadings.[17, 41, 67] This effect manifests at particle concentrations well below the percolation threshold of the particles and cannot be attributed solely to jamming of the hard particles in the mixture. A final example is a change in the bulk T_g upon the addition of nanoparticles to a polymer host. This effect has been seen in a number of different systems, manifesting both increases[19, 44-46] and decreases[42-44] in T_g with nanoparticle concentration. Particle-induced regions of altered polymer mobility are generally proposed to underlie the T_g changes in these materials, but whether the mobility changes are restricted to a region close to the vicinity of the particle or extend tens to hundreds of nanometers from the surface of the particle is still widely debated. And very little is known about how the regions of altered polymer mobility interact to induce the

8

bulk T_g changes in the system. Clearly, nanoparticles in these materials are affecting the properties of the polymer host, but much is left to be understood about the origin of these effects.

The unique behaviors PNCs exhibit are often attributed to the effects illustrated schematically in Figure 1-2: large particle-polymer interfacial areas of contact within the material; polymer chain confinement between particles, where interparticle distances in the system become smaller than the unperturbed size of the polymer molecule; and/or polymer bridging of particles, where a single polymer chain can link multiple particles into a "polymer mediated particle aggregate". Molecular dynamics[68-72] simulations reveal that interfacial interactions alone can induce changes in monomer packing that lead to the formation of "shells" of perturbed polymer density around a nanoparticle. These "shells" exhibit dynamics that differ from the neat polymer, and the simulations suggest that such dynamical heterogeneities can provide a rationale for the observed changes in the bulk T_g and viscosity of the PNCs.[68-70, 73] One would expect the effects to be even more extreme when interparticle distances become smaller than the unperturbed polymer chain size and confinement and bridging become active. The precise manner in which these features interplay and impact material properties, however, remains to be clarified for many applications. And it is such an understanding that is paramount to being able to harness the full potential of PNCs. Our efforts in this area will be directed towards examining how nanoparticles influence the thermal and viscoelastic properties of model PNCs, narrow molecular weight distribution amorphous polymers into which C_{60} fullerene particles are incorporated, and describing the relation of these property changes to the changes in microscopic structure and dynamics of the polymer molecules induced by the presence of the C_{60} particles.

Interfacial Interactions
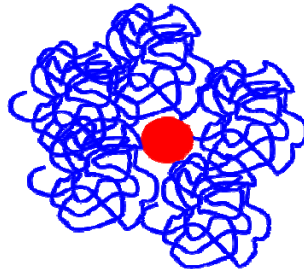
Interparticle Distance < Polymer Chain Size

Polymer Chain Confinement

Polymer Bridging of Particles
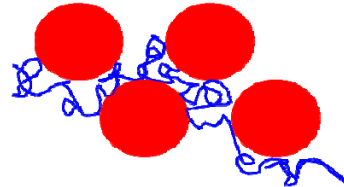
Figure 1-2:   Schematic of particle-polymer interfacial interactions, polymer chain
confinement between particles, and polymer bridging of particles.

1.2 OUTLINE OF DISSERTATION

Now that a context for the dissertation work has been provided, we close this chapter with a brief outline of the chapters to follow, in which the details of the work are described.

1.2.1 Controlling Interfacial Instabilities in Thin Polymer Films with the Addition of a Miscible Component (Chapter 2)

In this chapter, the factors that control the morphological structure of thin film, compatible, mixtures of polystyrene (PS) and tetramethyl bisphenol-A polycarbonate (TMPC) are examined. We look not only at the conditions under which film stabilization occurs, but also characterize the morphological features of the equilibrium structures developed leading up to the stabilization. This information is used to evaluate the topographical stability of the films in terms of the compositional dependence of both the macroscopic wetting parameters and the effective interface potential.

1.2.2 New Observations of Nanodroplet Structure in Polymer-Polymer Thin Film Mixtures (Chapter 3)

Here, we show that while the morphology of secondary nanoscopic dewetting structures remains constant for PS homopolymer films, the nanodroplet structure changes with both composition and initial film thickness when the film consists of a mixture of compatible polymer components. We consider the ability to account for the morphological changes of the nanostructures in terms of the following factors: overlying microscopic droplet structure, system thermodynamic parameters (the film surface tension, Hamaker constant, and wetting layer thickness), and/or increased surface segregation of one component from throughout the thickness of the film.

1.2.3 Origin of Dynamical Properties in PMMA-C_{60} Nanocomposites (Chapter 4)

In this chapter, we examine how nanoparticles influence the bulk properties of PNCs. To this end, the thermal and viscoelastic properties of a model PNC, narrow molecular weight distribution poly(methyl methacrylate) into which C_{60} fullerene particles are incorporated, are evaluated. The results are assessed in the context of the dispersion of the C_{60} within the polymer host, and a mechanism is proposed by which the changes in the dynamics of the system can be explained.

1.2.4 Local Polymer Dynamics in Polymer-C_{60} Mixtures (Chapter 5)

The effects of C_{60} on the thermal and viscoelastic properties of two other polymer hosts, PS and TMPC, are investigated, and the influences of the nanoparticles on local polymer motions are probed using neutron scattering measurements. The findings from these measurements are interpreted in light of the results from Chapter 4, which leads to the proposal of a percolation description of the glass transition in order to describe the changes in T_g observed in the PNCs.

1.2.5 Percolation Model to Describe the Glass Transition Temperature in Polymer Nanocomposites (Chapter 6)

Finally, a computational model is developed to characterize the changes in T_g exhibited by PNCs within a percolation description of the glass transition. Within the model, the glass transition is associated with the percolation, or spanning to all outer interfaces of the system, of slow domains. The manner in which the addition of nanoparticles affects the percolation of slow domains in the system is evaluated and related to a change in the system T_g. The ability of the model to account for experimental

observations of T_g changes in PNCs is assessed. The model is also used to examine the correspondence of T_g behaviors between PNCs and polymer thin films.

1.3   REFERENCES

[1]   E. K. Lin *et al.*, Science **297**, 372 (2002).

[2]   C. W. Frank *et al.*, Science **273**, 912 (1996).

[3]   K. Ziemelis, Nature **393**, 619 (1998).

[4]   C. D. Dimitrakopoulos, and D. J. Mascaro, IBM J. Res. Dev. **45**, 11 (2001).

[5]   H. Q. Lin *et al.*, Science **311**, 639 (2006).

[6]   T. C. Merkel *et al.*, Science **296**, 519 (2002).

[7]   L. J. Bonderer, A. R. Studart, and L. J. Gauckler, Science **319**, 1069 (2008).

[8]   P. Podsiadlo *et al.*, Science **318**, 80 (2007).

[9]   G. Reiter, Europhysics Letters **23**, 579 (1993).

[10]   J. L. Keddie, R. A. L. Jones, and R. A. Cory, Europhysics Letters **27**, 59 (1994).

[11]   J. H. van Zanten, W. E. Wallace, and W.-l. Wu, Physical Review E: Statistical Physics, Plasmas, Fluids, and Related Interdisciplinary Topics **53**, R2053 (1996).

[12]   B. Frank *et al.*, Macromolecules **29**, 6531 (1996).

[13]   B. M. Besancon, and P. F. Green, Physical Review E: Statistical, Nonlinear, and Soft Matter Physics **70**, 051808/1 (2004).

[14]   G. Reiter, Physical Review Letters **68**, 75 (1992).

[15]   G. Reiter, Langmuir **9**, 1344 (1993).

[16]   R. Krishnamoorti, R. A. Vaia, and E. P. Giannelis, Chemistry of Materials **8**, 1728 (1996).

[17]   Q. Zhang, and L. A. Archer, Langmuir **18**, 10435 (2002).

[18]   M. E. Mackay *et al.*, Nat. Mater. **2**, 762 (2003).

[19]   J. M. Kropka *et al.*, Macromolecules (Washington, DC, United States) **40**, 5424 (2007).

[20]   Y. Huang, and D. R. Paul, Polymer **45**, 8377 (2004).

[21]   J. L. Keddie, R. A. L. Jones, and R. A. Cory, Faraday Discussions, 219 (1994).

[22]   J. A. Forrest *et al.*, Physical Review Letters **77**, 2002 (1996).

[23]   C. J. Ellison, and J. M. Torkelson, Nat. Mater. **2**, 695 (2003).

[24]   J. Q. Pham, and P. F. Green, Journal of Chemical Physics **116**, 5801 (2002).

[25]   B. M. Besancon, C. L. Soles, and P. F. Green, Physical Review Letters **97** (2006).

[26]   A. N. Semenov, Physical Review Letters **80**, 1908 (1998).

[27]   K. Dalnoki-Veress *et al.*, Physical Review E: Statistical Physics, Plasmas, Fluids, and Related Interdisciplinary Topics **59**, 2153 (1999).

[28]   J.-L. Masson, and P. F. Green, Physical Review E: Statistical, Nonlinear, and Soft Matter Physics **65**, 031806/1 (2002).

[29]   B. M. Besancon, and P. F. Green, Macromolecules **38**, 110 (2005).

[30]   E. K. Lin *et al.*, Macromolecules **32**, 3753 (1999).

[31]   P. Doruker, and W. L. Mattice, Macromolecules **32**, 194 (1999).

[32]   E. K. Lin, W.-l. Wu, and S. K. Satija, Macromolecules **30**, 7224 (1997).

[33]   X. Zheng *et al.*, Physical Review Letters **74**, 407 (1995).

[34]   X. Zheng *et al.*, Physical Review Letters **79**, 241 (1997).

[35]   Y. Pu *et al.*, Physical Review Letters **87**, 206101/1 (2001).

[36]   P. Muller-Buschbaum *et al.*, Europhysics Letters **40**, 655 (1997).

[37]   G. Reiter *et al.*, Langmuir **15**, 2551 (1999).

[38]   R. Seemann, S. Herminghaus, and K. Jacobs, Physical Review Letters **86**, 5534 (2001).

[39]   M. Muller *et al.*, Journal of Chemical Physics **115**, 9960 (2001).

[40]   J. M. Kropka, and P. F. Green, Macromolecules **39**, 8758 (2006).

[41] F. Du *et al.*, Macromolecules **37**, 9048 (2004).

[42] B. J. Ash, R. W. Siegel, and L. S. Schadler, Journal of Polymer Science, Part B: Polymer Physics **42**, 4371 (2004).

[43] A. Bansal *et al.*, Nat. Mater. **4**, 693 (2005).

[44] A. Bansal *et al.*, Journal of Polymer Science Part B-Polymer Physics **44**, 2944 (2006).

[45] P. Rittigstein, and J. M. Torkelson, Journal of Polymer Science, Part B: Polymer Physics **44**, 2935 (2006).

[46] P. Rittigstein *et al.*, Nat. Mater. **6**, 278 (2007).

[47] A. Vrij, Discussions of the Faraday Society **No. 42**, 23 (1966).

[48] P. G. De Gennes, Reviews of Modern Physics **57**, 827 (1985).

[49] J. N. Israelachvili, *Intermolecular and Surface Forces* (Academic Press, London, 1991), p. 291 pp.

[50] A. Sharma, Langmuir **9**, 861 (1993).

[51] A. Sharma, and A. T. Jameel, Journal of Colloid and Interface Science **161**, 190 (1993).

[52] R. Yerushalmi-Rozen, J. Klein, and L. J. Fetters, Science (Washington, DC, United States) **263**, 793 (1994).

[53] R. Yerushalmi-Rozen, and J. Klein, Journal of Physics: Condensed Matter **9**, 7753 (1997).

[54] G. Reiter, P. Auroy, and L. Auvray, Macromolecules **29**, 2150 (1996).

[55] G. Reiter *et al.*, Europhysics Letters **33**, 29 (1996).

[56] G. Henn *et al.*, Macromolecules **29**, 4305 (1996).

[57] A. Voronov, and O. Shafranska, Langmuir **18**, 4471 (2002).

[58] Y. Liu *et al.*, Physical Review Letters **73**, 440 (1994).

[59] R. Oslanec *et al.*, Macromolecules **33**, 5505 (2000).

[60] A. C. Costa, R. J. Composto, and P. Vlcek, Macromolecules **36**, 3254 (2003).

[61] Y. Feng *et al.*, Macromolecules **31**, 484 (1998).

[62] T. Kerle, R. Yerushalmi-Rozen, and J. Klein, Europhysics Letters **38**, 207 (1997).

[63] D. H. Cole *et al.*, Macromolecules **32**, 771 (1999).

[64] K. A. Barnes *et al.*, Macromolecules **33**, 4177 (2000).

[65] R. S. Krishnan *et al.*, Langmuir **21**, 5770 (2005).

[66] A. Tuteja *et al.*, Macromolecules **38**, 8000 (2005).

[67] P. Potschke, T. D. Fornes, and D. R. Paul, Polymer **43**, 3247 (2002).

[68] F. W. Starr, T. B. Schroder, and S. C. Glotzer, Physical Review E **64**, 021802 (2001).

[69] F. W. Starr, T. B. Schroder, and S. C. Glotzer, Macromolecules **35**, 4481 (2002).

[70] G. D. Smith *et al.*, Journal of Chemical Physics **117**, 9478 (2002).

[71] D. Brown *et al.*, Macromolecules **36**, 1395 (2003).

[72] T. Desai, P. Keblinski, and S. K. Kumar, Journal of Chemical Physics **122**, 134910/1 (2005).

[73] V. Pryamitsyn, and V. Ganesan, Macromolecules **39**, 844 (2006).

Chapter 2: Control of Interfacial Instabilities in Thin Polymer Films with the Addition of a Miscible Component[*]

In this chapter, we show that while polystyrene (PS) thin films are structurally unstable on oxidized silicon wafers, the addition of as little as a few weight percent tetramethyl bisphenol-A polycarbonate (TMPC) has a stabilizing effect on the topographical structure of the films. The stabilization is evident from the existence of a threshold TMPC concentration, ϕ_t, and a threshold thickness, h_t, beyond which films do not dewet. The concentration threshold occurs for $\phi_{TMPC} \leq 0.10$. An examination of the effective interface potential, which accounts for short and long-range intermolecular interactions, indicates that this dewetting inhibition is metastable.

2.1 INTRODUCTION

A diverse range of applications, from coatings and adhesives to active components in organic electronic devices, rely on the properties and performance of polymer thin films. Both confinement and interactions between the polymer segments and the external interfaces can have a profound influence on the properties exhibited by thin polymer films. Film thickness dependencies of glass transition temperatures (T_g),[1-9] viscosities,[10, 11] and phase transitions exhibited by polymer-polymer mixtures and block copolymers[12-15] are all consequences of confinement and interfacial interactions.

In addition to the finite size dependence of physical properties, morphological instabilities also arise in thin polymer films.[16-19] For thin, supported, apolar

homopolymer films of thicknesses larger than a few nanometers, morphological destabilization is due to long-range van der Waals forces (though defects and impurities can also be problematic[20, 21]).[22-26]   The destabilization process begins with the formation of topographical patterns (e.g. spinodal patterns or holes) at the free interface that grow over time. Eventually the morphological structure evolves to form droplets on the substrate (dewetting). The stability of the system and the mechanism of film break-up can be understood in terms of an effective interface potential, or equivalently, the excess free energy (per unit area) of the film due to the presence of the two interfaces.

Since the performance of most applications relies on uniform films, a number of strategies have been utilized in attempts to stabilize polymer films against break-up. Polymer brush layers, to enable the film to interact with like molecules and reduce unfavorable substrate-film interactions, have been fabricated through the introduction of end-functionalized polymers that can adsorb to the substrate[27-32] or block copolymers with an adsorbing anchor.[33-35]   Other strategies include sulfonation and metal complexation of polymer films,[36] surface roughening,[37] and the addition of nanoparticles.[38-41]   The retardation of dewetting in these systems is attributed to phenomena that include an increase in film viscosity and/or changes in polymer-substrate interactions. Many of these mechanisms are kinetic in nature, though often the films are stabilized over long time scales that are indicative of an equilibrium phenomenon.   We note, however, that none of the above-mentioned studies evaluated the effective interface potential of the system to determine the nature of stabilization.

In the remaining sections of this chapter, we examine the factors that control the morphological structure of thin film, compatible, mixtures of polystyrene (PS) and tetramethyl bisphenol-A polycarbonate (TMPC). The majority of studies on polymer-polymer blend thin films have focused on mixtures in the two-phase regime and

characterized the interplay between phase separation and dewetting.[42-48] The topographical patterns that develop during both processes are similar and a careful analysis is necessary to understand their origin. No effects of phase separation are present in our miscible system. Therefore, the topological instabilities that develop are due to long-range van der Waals interactions. We show that while PS thin films are readily destabilized on oxidized silicon wafers, the addition of as little as a few wt % TMPC has a stabilizing effect on the topographical structure of the film. The nature of the stabilization is evaluated in terms of the compositional dependence of both the macroscopic wetting parameters and the effective interface potential, which includes an assessment of both short and long-range intermolecular interactions.

2.2   EXPERIMENTAL DESCRIPTION

Thin films of PS - (Pressure Chemical; M_w = 4 kg/mol, M_w/M_n < 1.06) TMPC (Bayer; M_w = 37.9 kg/mol, M_w/M_n = 2.75) mixtures were spin cast from toluene solution onto clean oxidized silicon wafers. The initial thickness of the polymer film was controlled between 5-100 nm by varying solution concentration and spin speed. Silicon (100) wafers (Wafer World, Inc.) with a 2200 nm thermally grown oxide layer were used as substrates. Prior to coating, the wafers were cleaned in an acid solution to remove residual organic contaminants. The acid cleaning consisted of two steps: (1) a 30 minute soak in an equal weight mixture of methanol and hydrochloric acid, and (2) a 30 minute soak in concentrated sulfuric acid. Both acid soaks were followed by rinsing in deionized water and drying by spinning. Immediately before coating, the substrates were rinsed with fresh toluene.

The thickness of the substrate oxide layer and cast films was measured by spectroscopic ellipsometry at room temperature. Films were annealed in a vacuum

furnace at $T = 180^{\circ}$C, which is sufficiently above the glass transition temperature[7] but below the lower critical temperature for mixture phase separation.[49] The samples were annealed until the film broke up to form droplets (if indeed droplets were formed), ≤ 10 minutes, and then further annealed and examined until no further structure changes occurred (annealing was continued for up to 2 hours for films that dewet and longer than 16 hours for films that did not dewet). After annealing, the samples were quenched to room temperature. Surface structure of the substrates, films and droplets was characterized by optical microscopy and atomic force microscopy (AFM). Optical micrographs were recorded using an Axioskop 2 MAT (Zeiss) with an attached Axiocam MRc5 CCD (Zeiss). All AFM images presented in the results were collected with an Autoprobe CP (Park Scientific) in contact mode with a gold coated sharpened microlever. The microlevers had a nominal tip radius of 30 nm and a spring constant of 0.05 N/m. Aware of the possibility that contact mode AFM may damage soft polymer structures, we also analyzed selected samples with a Dimension 3100 (Veeco) in intermittent contact. The cantilevers for the Dimension 3100 had a tip radius < 10 nm, a nominal spring constant of 42 N/m, and a nominal resonance frequency of 330 kHz. Both AFMs measured equivalent structures over all regions of the substrates and no regions of damage were noted when reinvestigating samples using intermittent contact. Hence, we only present the originally measured contact mode micrographs. All samples were imaged at room temperature. Images were captured over several locations across the sample to evaluate uniformity across the entire substrate, and scan size was controlled to focus on the pertinent morphological structures.

2.3   RESULTS AND DISCUSSION

Optical micrographs of PS-TMPC thin film mixtures, after annealing, are shown in Figure 2-1 and exhibit topographies which range from droplets (due to dewet films) to smooth films, depending on the composition, ϕ_{TMPC}, and initial film thickness, h_o. Stabilization of the films with the addition of TMPC is evident from the following observations. As the TMPC fraction in the film is increased, a composition is reached at which a threshold thickness, h_t, is observed. Beyond h_t, films remain smooth despite annealing at elevated temperatures for longer than 16 hours. The threshold film thickness decreases with increasing TMPC concentration until a threshold composition, ϕ_t, is reached, beyond which films do not dewet regardless of thickness. Beyond the thresholds, film uniformity is observed over spatial scales probed by both optical and atomic force microscopy and over time scales 2 orders of magnitude longer than the time it takes for the unstable films to dewet. Determining the underlying factors controlling the observed inhibition of dewetting and whether the stabilization is a kinetic or equilibrium effect will be the focus of the following discussion.

2.3.1   Macroscopic Wetting Parameters

When the spreading coefficient for the film is negative, an independent measure of wettability can be obtained from the contact angle, θ_e, that the polymer droplets make with the substrate.[50] The data in Figure 2-2a, obtained from AFM line profiles of the droplets after the samples had been quenched to room temperature, indicate that the average contact angle decreases with increasing TMPC concentration. To analyze whether the reported contact angles were of equilibrium structures, we compared measurements at the contact line to calculations based on a spherical cap structure and
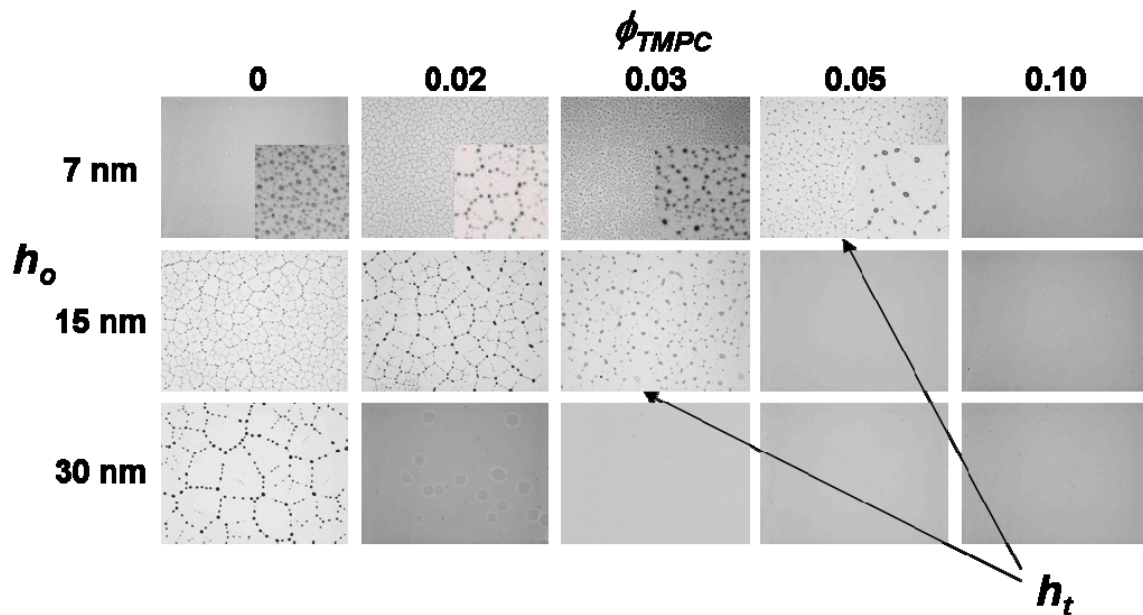
Figure 2-1: Optical micrographs of PS-TMPC thin film mixtures after annealing.
Magnification of all samples is equivalent and shows ~ 1 mm in the lateral
direction. The 7 nm dewet samples include insets that provide a higher
magnification to detail droplet structure. The closely spaced droplets of the
7 nm PS film are the result of spinodal dewetting, whereas the polygonal
patterned droplets are the result of hole nucleation and growth. As TMPC
concentration increases, droplet shape and patterns become more irregular.
In some cases, hole growth was arrested, as in the 30 nm $\phi_{TMPC} = 0.02$
sample. Anneal time varied among individual samples. Films dewet in ≤ 10
minutes and were further annealed for up to 2 hours to verify no further
structure changes. Uniform films were further annealed for ≥ 16 hours with
no changes in topography.
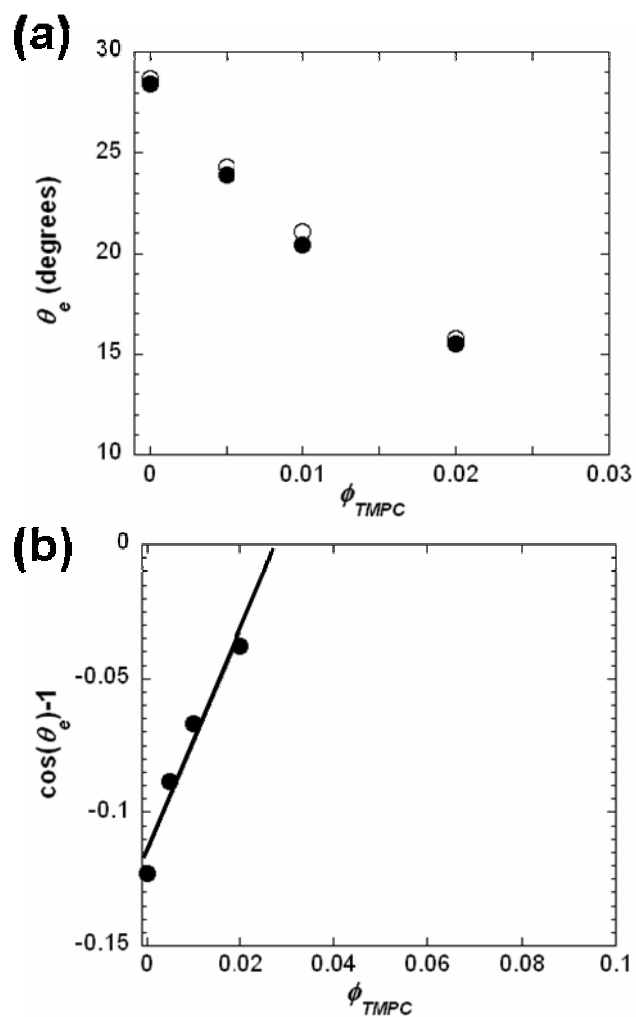
Figure 2-2: (a) The average contact angle polymer droplets make with the substrate as a function of film composition. Filled points refer to contact line measurements and open points to the spherical cap calculations from droplet diameter and height. The size of the points bound the maximum and minimum contact angle measurements. (b) Linear fit of $(\cos\theta_e-1)$ versus concentration data and extrapolation to $(\cos\theta_e-1) = 0$.

found good agreement, as depicted in Figure 2-2a. We also found no changes in droplet structure upon further annealing. Further, linear fits of $\cos\theta_e$ versus contact line curvature (not shown) yielded estimates of the line tension on the order of 10^{-10} J/m, which results in contact angle changes of less than one degree with droplet size over the measured range of droplet radii, ~ 1.5-3 µm, to produce the data in Figure 2-2. The decrease in contact angle with increasing TMPC concentration signifies a decrease in the driving force for dewetting, which is not sufficiently strong to break up films at concentrations of $\phi_{TMPC} \geq 0.10$. In fact, if the concentration dependence of $(\cos\theta_e\text{-}1)$ is linearly extrapolated to higher concentrations (see Figure 2-2b), it would reach zero at $\phi_{TMPC} < 0.10$. This suggests an equilibrium nature of the observed dewetting inhibition at $\phi_{TMPC} \geq 0.10$.

The contact angle data enable calculation of the spreading coefficient, S,

$$S = \gamma_f \left(\cos\theta_e - 1 \right) \qquad\qquad (2.1)$$

where γ_f is the surface free energy of the film. S is plotted as a function of film composition in Figure 2-3a. In all calculations of S, the bulk PS surface energy (29.2 mJ/m^2) is used for γ_f.[51] This approximation is substantiated by the fact that mixture compositions are of $\phi_{TMPC} \leq 0.10$, and PS enriches the free interface of the system.[52]. We note that the surface tension of PS has been measured to change when film thickness is decreased below 100 nm,[53] but such changes are sufficiently small as to not alter the conclusions of the following analysis.

To evaluate the origin of TMPC's stabilizing effect, it is instructive to consider both the apolar, dispersion contribution, S^{LW}, and the polar contribution, S^p, of the spreading coefficient,

$$S = S^{LW} + S^p \qquad\qquad (2.2)$$

derived from the apolar and polar components of the interfacial tensions, respectively.
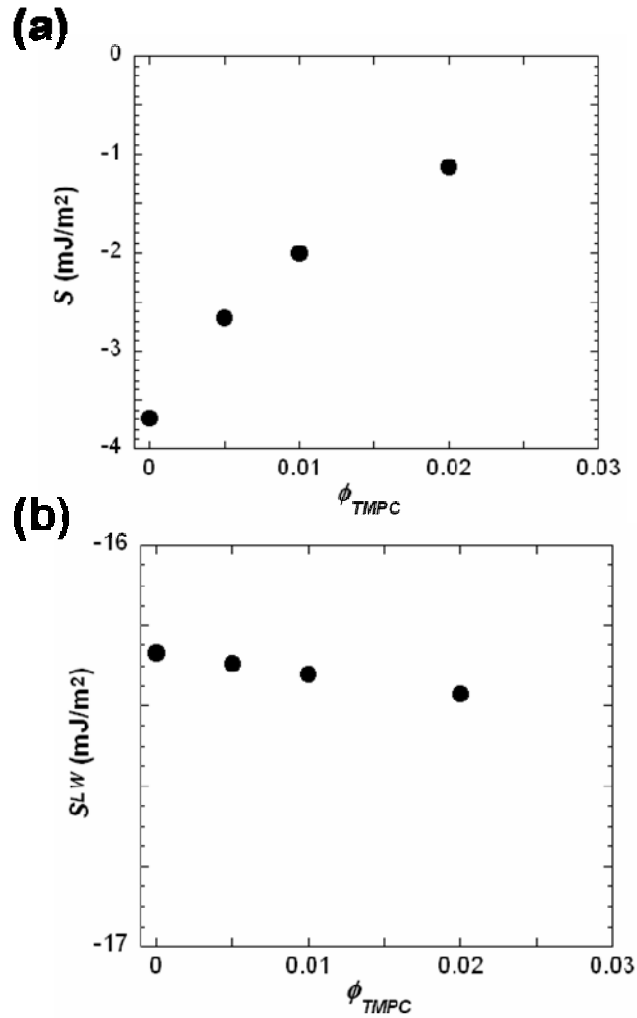
Figure 2-3: (a) The total spreading coefficient, *S*, and (b) the dispersion component of spreading coefficient, S^{LW}, plotted as a function of film composition. S^{LW} was calculated using the indices of refraction and dielectric constants of materials; $n_{PS}=1.557$, $n_{TMPC}=1.586$, $n_{SiOx}=1.448$, $\varepsilon_{PS}=2.55$, $\varepsilon_{TMPC}=3.17$, $\varepsilon_{SiOx}=3.8$.

S^{LW} and the effective Hamaker constant, A, of the thin film system are related such that,[54]

$$S^{LW} = \frac{-A}{12\pi d_o^2}$$ (2.3)

where d_o is the separation distance between materials in van der Waals contact, ~ 0.15 nm.[55] Equation 2-3 indicates that knowledge of the Hamaker constant, which can be calculated from refractive indices and dielectric constants of the materials in the layered system,[22] enables the determination of the dispersion component of the spreading coefficient. Using equation 2-3 and assuming additivity of the refractive indices of the film constituents,[56] S^{LW} is evaluated as a function of film composition as shown if Figure 2-3b. The polar component of the spreading coefficient may subsequently be deduced as the difference between the total spreading coefficient and the dispersion component via equation 2-2.

From the data in Figure 2-3, it is evident that the decrease in contact angle with increasing TMPC content in the film yields an increase in the total spreading coefficient, as $(\cos\theta_e - 1)$ approaches zero. On the other hand, the dispersion component of the spreading coefficient decreases with increasing TMPC concentration. Clearly, changes in the dispersion interactions act to destabilize the film as TMPC content is increased and cannot explain the stabilization observed. Therefore, the polar contribution is responsible for the stabilizing effect of TMPC.

We can resolve the increase in S^p by evaluating its contributing components,

$$S^p = \gamma_s^p - \gamma_{sf}^p - \gamma_f^p$$ (2.4)

where γ_s^p and γ_f^p are the polar components of the surface free energies of the substrate and film, respectively, and γ_{sf}^p is the polar component of the substrate-film interfacial energy. TMPC enriches the substrate (oxide layer) interface in this system,[52] reflecting favorable TMPC-substrate interactions relative to PS-substrate interactions. Hence, an

increase in TMPC coverage of the substrate results in a decrease in $\gamma_{sf}{}^p$. There is no change in $\gamma_s{}^p$ with changes in film composition, and negligible change is expected in $\gamma_f{}^p$ since we investigated only low TMPC film fractions and PS enriches the free surface of the film.[52] Therefore, it is reasonable to conclude that changes in $\gamma_{sf}{}^p$ determine changes in S^p, and the decrease in $\gamma_{sf}{}^p$ with increasing TMPC concentration results in the increase in S^p.

2.3.2   Effective Interface Potential

We have shown that a decrease in $\gamma_{sf}{}^p$ with increasing TMPC concentration leads to a decrease in the driving force for topographical destabilization of PS-TMPC thin film mixtures and that extrapolation of contact angle measurements suggests an equilibrium nature of the dewetting inhibition at $\phi_{TMPC} \geq 0.10$. However, the onset of the threshold thickness, h_t, beyond which films do not dewet is yet to be explained. To evaluate the stability of the films as a function of film thickness, h, it is convenient to calculate the excess free energy (per unit area) of the film due to the presence of the two interfaces. The excess free energy is the sum of the apolar and polar energies of interaction[22, 54, 55, 57-60] and is often referred to as the effective interface potential of the film, $\Phi(h)$,

$$\Phi(h) = \Phi_o^p \exp[\frac{d_o - h}{l}] - \frac{A}{12\pi h^2} \qquad (2.5)$$

Here, $\Phi_o{}^p$ is the polar component of the energy of adhesion for interactions at contact ($h = d_o$), l is the decay length of the polar interactions, and A is the effective Hamaker constant. Equation 2-5 is valid for $h \geq d_o$. For $h < d_o$, the interface potential will increase sharply to infinity due to Born repulsion. Equation 2-5 may also be written in terms of the macroscopic wetting parameters,[54, 61]

$$\Phi(h) = S^p \exp[\frac{d_o - h}{l}] + S^{LW}(\frac{d_o^2}{h^2}) \qquad (2.6)$$

Therefore, determination of S^p and S^{LW} enables the depiction of the short-range interactions, which decay exponentially with film thickness, and long-range van der Waals interactions, respectively. We use the values of the spreading coefficients as calculated above, and take $l = 0.2$ nm, to plot the effective interface potential for three film compositions in Figure 2-4.

We first note that our PS potentials are in agreement with those obtained by Seemann et al.[25] for film thicknesses $h > \sim 1$ nm. This is to be expected, as the contribution of the dispersion interactions in both analyses is equivalent. However, Seemann[25] calculated the short-range contributions to the potential by fitting the position of a global minimum to $h \sim 1$ nm, $\Phi_{min} \sim -0.25$ mJ/m^2 (defined by a measured thin wetting layer thickness and spreading coefficient, respectively). As mentioned by Muller et al.,[24] such an analysis fails to capture the existence of an additional minimum at short distances that they find through self-consistent field calculations. Our analysis shows that plots of equation 2-6 exhibit both minima, which are separated by a barrier in the potential, as in the calculations by Muller.[24] So our analysis provides a method to experimentally describe the contributions of the short-range interactions to the interface potential. Further, the addition of TMPC acts to increase the barrier height and change the contact angle of the macroscopic droplets, but has only minor effects on the position of the potential minimum at $h \sim 1$ nm. These effects are similar to those observed by Muller[24] for changes in the contact potential in their calculations. We conclude that TMPC primarily affects the short-range interactions in our system.

The effective interface potential is now examined in light of the nature of the observed dewetting inhibition. We have established that the addition of TMPC primarily affects short-range interactions in the system. This results in the global minimum of the potential residing at a finite thickness even when the value of the potential at contact, $h =$
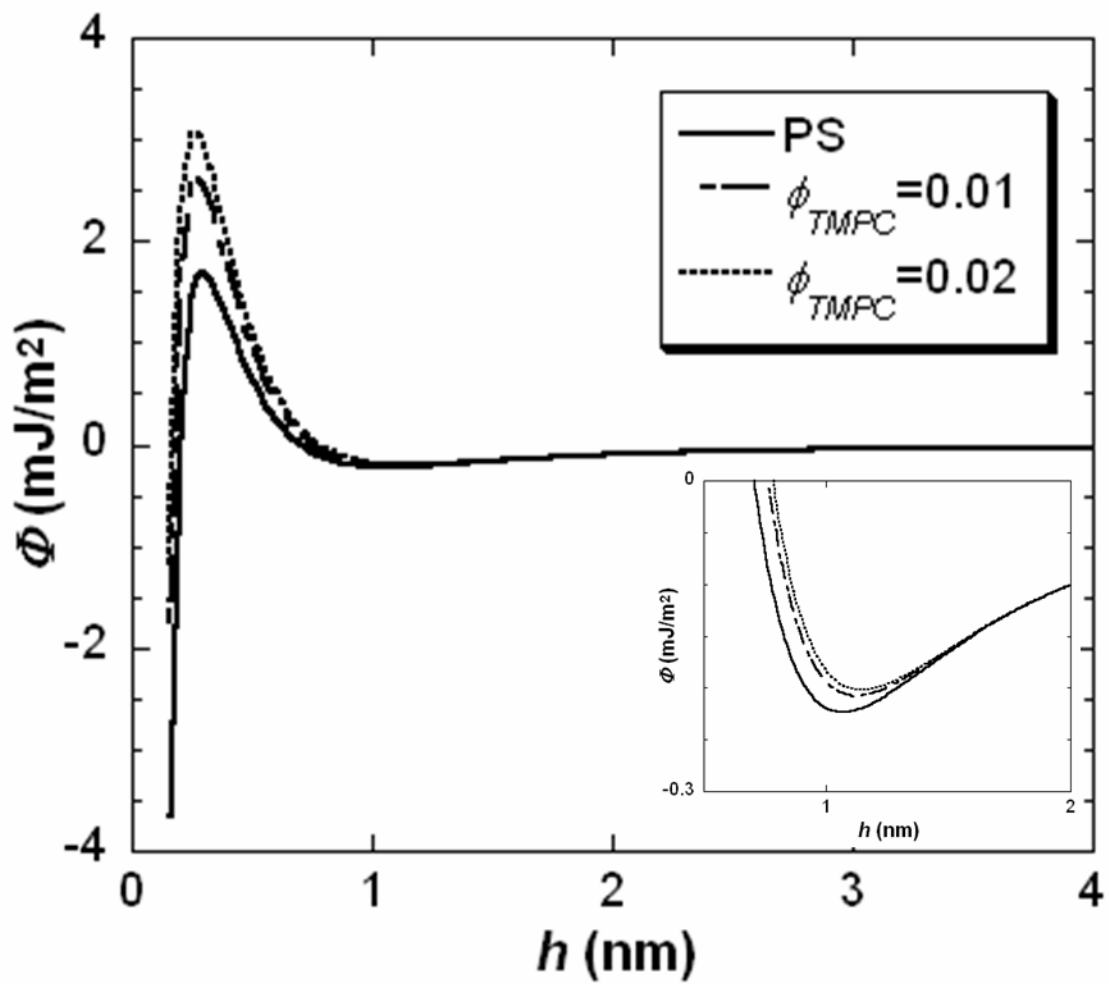
Figure 2-4:   Effective interface potentials for selected film compositions. The plot is of equation 2-6 and is therefore valid only for $h \geq d_o$. For $h < d_o$, the interface potential will increase sharply to infinity due to Born repulsion. All plotted potentials have a global minimum at d_o, shown as the point at minimum h in the figure. The inset displays the local minima at $h \sim 1$ nm.

d_o, exceeds the value at $h = \infty$ (i.e. $S > 0$), due to the negative contribution of the long-range van der Waals interactions. This means an autophobic dewetting process, resulting in polymer droplets on a smooth polymer film of thickness h_{min}, corresponding to the location of the minimum in the potential, is thermodynamically predicted when h_{min} is less than the initial film thickness. For our system, h_{min} ($\sim$ 1 nm) is less than the thinnest films tested ($\sim$ 7 nm), and therefore autophobic dewetting is anticipated, thermodynamically, for our samples. This signifies that the dewetting inhibition observed with the addition of TMPC is metastable, a conclusion that could not be drawn from analysis of the macroscopic wetting parameters alone.

The existence of h_t and/or ϕ_t could result from the development of an energy barrier to reach the minimum in the effective interface potential or a change in the curvature of the potential with the addition of TMPC, kinetically trapping the film in the uniform state. However, as displayed in Figure 2-4, changes in the interface potential with TMPC addition are essentially limited to $h <\sim$ 1 nm and fail to provide insight into the stabilization of thicker films. We therefore question whether the existence of the observed thresholds can be rationalized through analyses of the effective interface potential alone or whether there are additional long-range interactions that are not accounted for in eq 2-6. Hence, we discuss the possibility of additional stabilization mechanisms below.

2.3.3 Additional Film Stabilization Mechanisms

The addition of TMPC to the film decreases the dynamics of the system; both the average molecular weight and T_g of the film increase. Changes in dynamics due to an enhancement of film viscosity,[62] however, are less than a factor of two and cannot predict an increase in hole nucleation time of two orders of magnitude that would be

required to explain our stabilization observations. In other analyses of dewetting retardation, the development of surface heterogeneities has been suggested to play a role in stabilization.[34, 37, 39, 41]

In our system, nanodroplets[24, 63] are detected by AFM measurements in regions of the substrate between the macroscopic droplets, as shown in Figure 2-5. From the micrographs in Figure 2-5, it is clear that the nanodroplets vary in size and spatial distribution with film composition and effectively roughen the substrate surface. As TMPC fraction in the film increases, the nanoscale morphology (nanodroplets) more densely covers the substrate. If the more dense coverage is due to "sticking" of the TMPC chain segments to the substrate and the TMPC chains remain "entangled" with PS neighbors, an increased resistance to dewetting would ensue. Such an effect may, along with the decreasing spreading coefficient, lead to the overall stabilization of the film. Further, with increased initial film thickness, there is more TMPC in the film available to enrich the substrate interface, and the resistance force may increase relative to thinner films. Such a height dependence of the resistance force may play a role in the onset of h_t.

The change in nanodroplet coverage of the substrate is analogous to a change in grafting density of polymer brush layers[32] or nanoparticle substrate coverage with increasing particle concentrations.[39, 41] All of these strategies can result in inhibition of dewetting over long time scales that are indicative of a thermodynamic stabilization. However, the exact force that resists the destabilizing van der Waals interactions in these systems remains elusive.

2.4 CONCLUSIONS

We have demonstrated how morphological analyses of thin film mixtures can be used to deduce changes in the stability of the system with changes in film composition
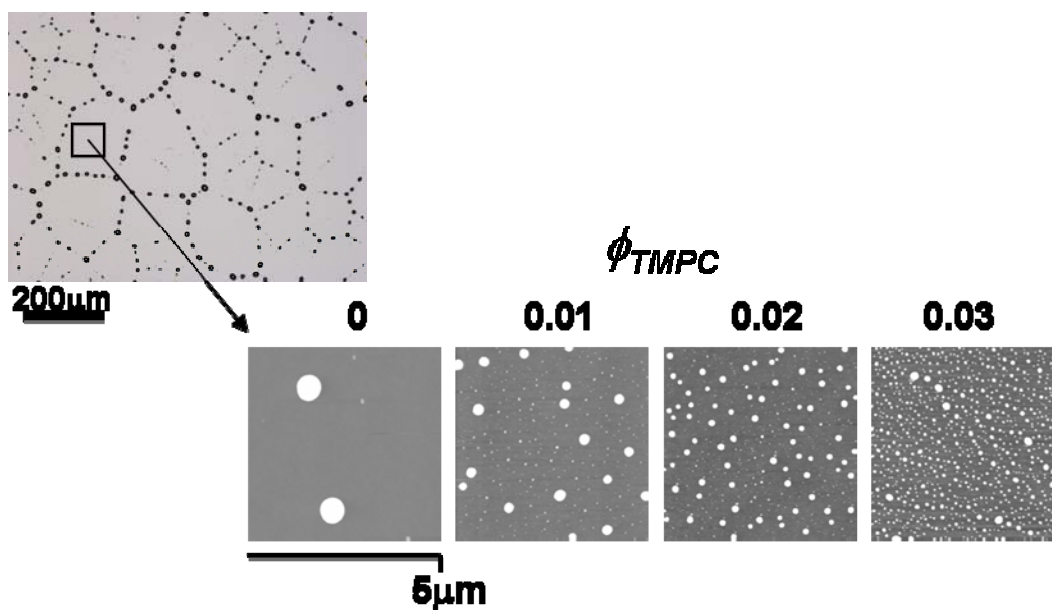
Figure 2-5: AFM micrographs of PS-TMPC thin film nanostructure after annealing. The optical micrograph in the upper left denotes the region of the samples the AFM micrographs are recorded from. Brighter regions in the AFM micrographs represent larger heights above the substrate. The height range (nm) depicted in the micrographs was set to focus on the pertinent morphological structures and is, from L-R: 40, 25, 15, and 15.

and initial film thickness. The addition of TMPC has a stabilizing effect on the topographical structure of PS films on oxidized silicon substrates, even at concentrations as low as a few wt %. An analysis of the macroscopic wetting parameters alone suggests a thermodynamic nature of the dewetting inhibition observed in the optical micrographs of Figure 2-1. However, the change in these parameters is due to changes in the short-range polar interactions between the substrate and polymer film. Although the change in short-range polar interactions dominate changes in energy at contact, $h = d_o$, these interactions become insignificant at distances $h > \sim 1$ nm from the substrate-film interface and long-range van der Waals interactions determine the film behavior. In our system, changes in these long-range interactions with TMPC addition act to destabilize the film. Therefore, even when interactions at contact are favorable (i.e. $S > 0$), there still exists a minimum in the effective interface potential at $h \sim 1$ nm that defines the thermodynamically stable state of the system: dewet droplets on a thin polymer wetting layer. Additional mechanisms that may stabilize the film against the van der Waals interactions are proposed, but the exact underlying forces remain elusive.

2.5   REFERENCES

[1]   J. L. Keddie, R. A. L. Jones, and R. A. Cory, *Europhysics Letters* **27**, 59 (1994).

[2]   J. A. Torres, P. F. Nealey, and J. J. de Pablo, *Physical Review Letters* **85**, 3221 (2000).

[3]   J. A. Forrest, and K. Dalnoki-Veress, *Advances in Colloid and Interface Science* **94**, 167 (2001).

[4]   D. Long, and F. Lequeux, *European Physical Journal E: Soft Matter* **4**, 371 (2001).

[5]   J. D. McCoy, and J. G. Curro, *Journal of Chemical Physics* **116**, 9154 (2002).

[6]   J. Q. Pham, and P. F. Green, *Macromolecules* **36**, 1665 (2003).

[7]   J. Q. Pham, and P. F. Green, *Journal of Chemical Physics* **116**, 5801 (2002).

[8]   J. Q. Pham *et al.*, *Journal of Polymer Science, Part B: Polymer Physics* **41**, 3339 (2003).

[9]   B. M. Besancon, C. L. Soles, and P. F. Green, *Physical Review Letters* **97**, 057801 (2006).

[10]   J.-L. Masson, and P. F. Green, *Physical Review E: Statistical, Nonlinear, and Soft Matter Physics* **65**, 031806/1 (2002).

[11]   G. Reiter, *Macromolecules* **27**, 3046 (1994).

[12]   R. Limary, P. F. Green, and K. R. Shull, *European Physical Journal E: Soft Matter* **8**, 103 (2002).

[13]   K. Binder, *Advances in Polymer Science* **138**, 1 (1999).

[14]   A. Arceo, and P. F. Green, *Journal of Physical Chemistry B* **109**, 6958 (2005).

[15]   T. P. Russell, *Current Opinion in Colloid & Interface Science* **1**, 107 (1996).

[16]   G. Reiter, *Physical Review Letters* **68**, 75 (1992).

[17]   G. Reiter, *Langmuir* **9**, 1344 (1993).

[18]   J.-L. Masson, and P. F. Green, *Physical Review Letters* **88**, 205504/1 (2002).

[19]   B. M. Besancon, and P. F. Green, *Physical Review E: Statistical, Nonlinear, and Soft Matter Physics* **70**, 051808/1 (2004).

[20]   T. G. Stange, D. F. Evans, and W. A. Hendrickson, *Langmuir* **13**, 4459 (1997).

[21]   K. Jacobs, S. Herminghaus, and K. R. Mecke, *Langmuir* **14**, 965 (1998).

[22]   J. N. Israelachvili, *Intermolecular and Surface Forces* (Academic Press, London, 1991).

[23]   G. Reiter *et al.*, *Langmuir* **15**, 2551 (1999).

[24]   M. Muller *et al.*, *Journal of Chemical Physics* **115**, 9960 (2001).

[25]   R. Seemann, S. Herminghaus, and K. Jacobs, *Physical Review Letters* **86**, 5534 (2001).

[26]   A. Sharma, and R. Khanna, *Physical Review Letters* **81**, 3463 (1998).

[27]   R. Yerushalmi-Rozen, J. Klein, and L. J. Fetters, *Science* **263**, 793 (1994).

[28]   R. Yerushalmi-Rozen, and J. Klein, *Journal of Physics: Condensed Matter* **9**, 7753 (1997).

[29]   G. Reiter, P. Auroy, and L. Auvray, *Macromolecules* **29**, 2150 (1996).

[30]   G. Reiter *et al.*, *Europhysics Letters* **33**, 29 (1996).

[31]   G. Henn *et al.*, *Macromolecules* **29**, 4305 (1996).

[32]   A. Voronov, and O. Shafranska, *Langmuir* **18**, 4471 (2002).

[33]   Y. Liu *et al.*, *Physical Review Letters* **73**, 440 (1994).

[34]   R. Oslanec *et al.*, *Macromolecules* **33**, 5505 (2000).

[35]   A. C. Costa, R. J. Composto, and P. Vlcek, *Macromolecules* **36**, 3254 (2003).

[36]   Y. Feng *et al.*, *Macromolecules* **31**, 484 (1998).

[37]   T. Kerle, R. Yerushalmi-Rozen, and J. Klein, *Europhysics Letters* **38**, 207 (1997).

[38]   D. H. Cole *et al.*, *Macromolecules* **32**, 771 (1999).

[39]   K. A. Barnes *et al.*, *Macromolecules* **33**, 4177 (2000).

[40]   B. M. Besancon, and P. F. Green, *Macromolecules* **38**, 110 (2005).

[41]   R. S. Krishnan *et al.*, *Langmuir* **21**, 5770 (2005).

[42]   A. Karim *et al.*, *Macromolecules* **31**, 857 (1998).

[43]   P. Mueller-Buschbaum *et al.*, *Macromolecules* **31**, 5003 (1998).

[44]   P. Muller-Buschbaum, J. S. Gutmann, and M. Stamm, *Journal of Macromolecular Science, Physics* **B38**, 577 (1999).

[45]   P. Mueller-Buschbaum, J. S. Gutmann, and M. Stamm, *Macromolecules* **33**, 4886 (2000).

[46]   H. Wang, and R. J. Composto, *Journal of Chemical Physics* **113**, 10386 (2000).

[47]   H. Wang, and R. J. Composto, *Europhysics Letters* **50**, 622 (2000).

[48]   P. Mueller-Buschbaum *et al.*, *Journal of Physics: Condensed Matter* **17**, S363 (2005).

[49] E. Kim *et al.*, *Journal of Polymer Science, Part B: Polymer Physics* **33**, 467 (1995).

[50] E. Vitt, and K. R. Shull, *Macromolecules* **28**, 6349 (1995).

[51] S. Wu, *Polymer interface and adhesion* (M. Dekker, New York, 1982).

[52] E. Kim *et al.*, *Macromolecules* **27**, 5927 (1994).

[53] K. M. Ashley *et al.*, *Langmuir* **21**, 9518 (2005).

[54] A. Sharma, *Langmuir* **9**, 861 (1993).

[55] C. J. Van Oss, M. K. Chaudhury, and R. J. Good, *Chemical Reviews (Washington, DC, United States)* **88**, 927 (1988).

[56] J. C. Seferis, and R. J. Samuels, *Polymer Engineering and Science* **19**, 975 (1979).

[57] R. M. Pashley, *Journal of Colloid and Interface Science* **83**, 531 (1981).

[58] C. J. Van Oss, *Journal of Dispersion Science and Technology* **12**, 201 (1991).

[59] C. J. Van Oss, M. K. Chaudhury, and R. J. Good, *Advances in Colloid and Interface Science* **28**, 35 (1987).

[60] W. A. Ducker, T. J. Senden, and R. M. Pashley, *Nature (London, United Kingdom)* **353**, 239 (1991).

[61] A. Sharma, and A. T. Jameel, *Journal of Colloid and Interface Science* **161**, 190 (1993).

[62] C. Wisniewsky, G. Marin, and P. Monge, *European Polymer Journal* **20**, 691 (1984).

[63] P. Muller-Buschbaum *et al.*, *Europhysics Letters* **40**, 655 (1997).

Chapter 3: New Observations of Nanodroplet Structure in Polymer-Polymer Thin Film Mixtures

The development of secondary nanoscopic dewetting structures, in addition to the larger microscopic dewetting features commonly observed by optical microscopy, in polystyrene (PS) thin films on oxidized silicon substrates has been reported to be due to the rupture of a nanoscopic wetting layer that resides beneath the microscopic pattern of the overlying dewet film. In this chapter, we show that while the structure of these nanodroplets is constant for PS homopolymer films, when the film consists of a mixture of compatible polymer components, PS and tetramethyl bisphenol-A polycarbonate (TMPC), the nanodroplet structure changes with both composition and initial film thickness. We propose that the origin of nanodroplet structure changes is a change in polymer dynamics at the substrate interface that is associated with an enrichment of the TMPC component at the interface.

3.1   INTRODUCTION

Wetting phenomena are present in everyday observances, e.g., writing onto paper with ink or water droplet bead-up on a car, yet a complete understanding of such behaviors requires knowledge spanning fields such as physical chemistry, statistical physics, and fluid dynamics. The complexity of wetting phenomena proves to make a general analysis on the subject quite challenging.[1] Still, the wetting behavior of thin polymeric films on solid substrates has attracted remarkable attention.[2-10] This is likely due to the wealth of applications, e.g., coatings, adhesives, photolithography, organic electronic devices, that rely on the stability of such films and require an understanding of wetting behavior to design reliable devices.

37

Insight into the wetting behavior of thin liquid films can be obtained from the effective interface potential, $\Phi(h)$. The effective interface potential is the excess free energy of the film, of thickness h, due to the presence of the two bounding interfaces and contains information about the static and dynamic wetting properties. Intermolecular interactions in the system give rise to both a short- and long-range contribution to $\Phi(h)$. Short-range contributions to the effective interface potential decay exponentially with film thickness and stem from sources including polar interactions, liquid density distortions in the vicinity of the substrate, and entropy loss due to film confinement.[4, 5, 11, 12] For non-polar systems, van der Waals interactions account for the long-range contribution to the effective interface potential: $\Phi_{vdW} = -A/12\pi h^2$.[13] The Hamaker constant, A, characterizes the strength of these interactions, which can be attractive (destabilizing) or repulsive (stabilizing). The superposition of these contributing interactions determines the shape of the effective interface potential and the wetting behavior of the film.

The interface potential of interest here is depicted in Figure 3-1. The global minimum of the potential lies at finite thickness, $h = h^*$. This system can minimize energy by changing its film thickness to h^*, and films of initial thickness, h_o, greater than h^* dewet to form droplets on top of a wetting layer of thickness h^* (see schematic in Figure 3-1). This is the type of behavior that is exhibited by polystyrene (PS) films on oxidized silicon substrates in the presence of air or vacuum,[7, 12] which is a model system for experimental investigations for a number of reasons: (1) the oxidized silicon substrates provide a readily attainable smooth and uniform surface, (2) uniform polymer films can be easily spin cast onto the substrates, (3) PS films destabilize upon heating above the glass transition temperature (T_g) yet are non-volatile and thus the mass of the film is conserved, and (4) the dynamics of the film break up can be tuned to resolve the
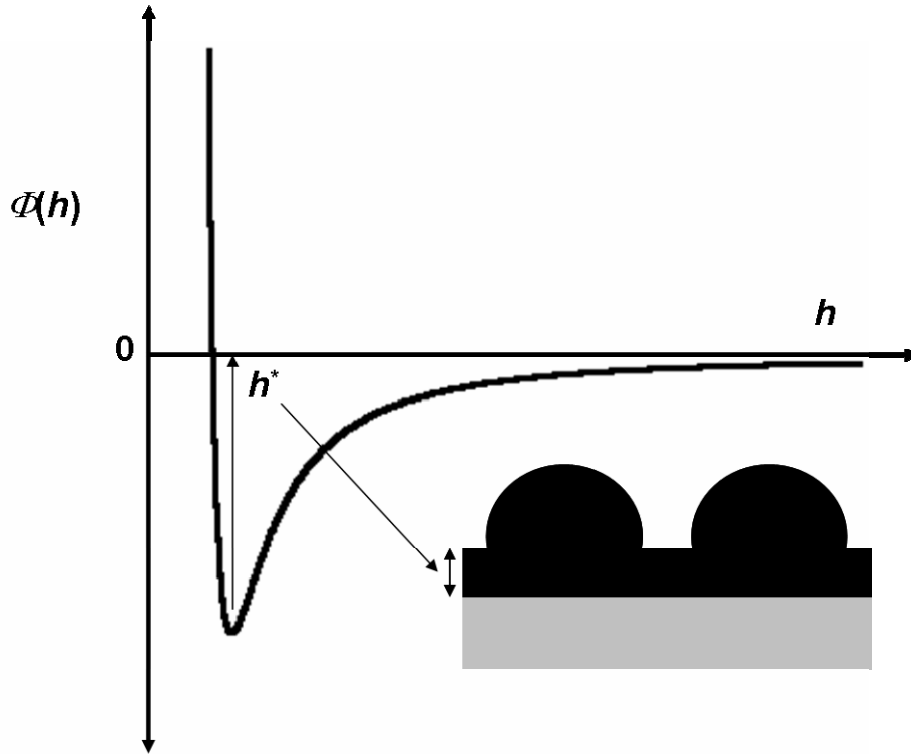
Figure 3-1: Interface potential schematic along with a schematic of the resulting equilibrium morphology of an initially homogeneous thin film. In the morphology schematic, the gray area refers to the substrate and the overlying black region to the liquid. The film thickness corresponding to the global minimum in the potential, h^*, also corresponds to the thickness of the wetting layer beneath the dewet macroscopic droplets in the morphology schematic.

mechanism of destabilization.

Early studies of polymer thin film dewetting used optical methods to evaluate the mechanism and dynamics of film destabilization.[2, 3] The use of higher resolution techniques, such as scanning probe microscopy, enabled the quantitative reconstruction of the effective interface potential[7] and uncovered the presence of much smaller structures than could be observed optically, nanodroplets.[12, 14] The nanodroplets were reasoned to result from the rupture of the thin wetting layer of thickness h^* upon cooling the film below T_g. Self-consistent field calculations[12] have suggested that the rupture of the wetting layer is due to a local minimum in $\Phi(h)$ at $h \approx 0$ becoming stable relative to the minimum at h^* at low temperatures. The resulting nanodroplets have been suggested to play a role in the development of densely branched dewetting morphologies[9] and the stabilization of polymer-polymer mixture thin films.[10]

If nanodroplets are the result of the h^* wetting layer rupture, then their morphology should be independent of initial film thickness unless the overlying macroscopic droplets influence the wetting layer destabilization. In this manuscript, we show that this constraint holds for the PS homopolymer films, confirming the lack of influence of overlying droplets on the break up of the thin wetting layer. However, when the film consists of a mixture of PS and a compatible polymer component, tetramethyl bisphenol-A polycarbonate (TMPC), the behavior is changed. Nanodroplet morphology for the mixtures is a function of both film composition and initial film thickness. We characterize the differences in observed morphology, and a mechanism that could explain the changes in structure is proposed.

3.2   EXPERIMENTAL DESCRIPTION

Thin films of PS- (Pressure Chemical; M_w = 4 kg/mol, M_w/M_n < 1.06) TMPC (Bayer; M_w = 37.9 kg/mol, M_w/M_n = 2.75) mixtures were spin-cast from toluene solution onto clean oxidized silicon wafers.   The initial thickness of the polymer film was controlled between 5 and 100 nm by varying solution concentration and spin speed. Silicon (100) wafers (Wafer World, Inc.) with a 2200 nm thermally grown oxide layer were used as substrates. Prior to coating, the wafers were cleaned in an acid solution to remove any residual organic contaminants. The acid cleaning consisted of two steps: (1) a 30 minute soak in an equal weight mixture of methanol and hydrochloric acid, and (2) a 30 minute soak in concentrated sulfuric acid. Both acid soaks were followed by rinsing in deionized water and drying by spinning. Immediately before coating, the substrates were rinsed with fresh toluene.

The thickness of the substrate oxide layer and cast films was measured by spectroscopic ellipsometry at room temperature.   Films were annealed in a vacuum furnace at T = 180°C, which is sufficiently above the glass transition temperature (T_g)[15] but below the lower critical temperature for mixture phase separation.[16] The samples were annealed for 3 hours and then were quenched to room temperature. Surface structure of the substrates, films and droplets was characterized by atomic force microscopy (AFM). AFM micrographs were obtained with a Dimension 3100 (Veeco) in intermittent contact. The cantilevers for the Dimension 3100 had a tip radius < 10 nm, a nominal spring constant of 42 N/m, and a nominal resonance frequency of 330 kHz. All samples were imaged at room temperature. Images were captured over several locations across the sample to evaluate uniformity across the entire substrate, and scan size was controlled to focus on the pertinent morphological structures.

3.3   RESULTS AND DISCUSSION

Figure 3-2 depicts nanodroplet structure over a range of compositions, ϕ_{TMPC}, and initial films thicknesses, h_o, for the PS-TMPC thin film mixtures. Nanodroplet structure is found to be independent of h_o for the pure PS films. This is not surprising, as h^* is independent of h_o and there is no reason to suspect that the rupture mechanism of the thin wetting layer would vary with h_o, i.e., with the size of the overlying droplets. Even if the overlying droplets did influence the rupture mechanism of the wetting layer, this influence would likely remain in the local vicinity of the droplet. Therefore, since the diameter of the polygons formed by the overlying droplets ($\sim h^2$ with $h \geq 6$ nm)[2] is much larger than the dominant wavelength of the h^* layer instability predicted by spinodal theory ($\sim h^2$ with $h \approx 1$ nm), any influence of the overlying droplets would be transparent to large regions of the h^* layer.

In the mixtures, Figure 3-2 depicts a clear change in nanodroplet structure with both ϕ_{TMPC} and h_o. Changes in nanodroplet structure with ϕ_{TMPC} in the mixtures is also not too surprising, as changes in both nanodroplet surface density, $<\rho>$, and height, $<h>$, have been noted with changes in only the molecular weight of PS films.[9, 12] TMPC addition not only changes the average molecular weight of the film, but also influences local film-substrate and polymer-polymer interactions and shifts the location of the global minimum in $\Phi(h)$.[10] What is surprising is the dependence of nanodroplet structure on h_o in the mixtures. Just as in the case of the pure PS films, h^* is independent of h_o in a given mixture and there is no reason to suspect that the rupture mechanism of the thin wetting layer would vary with the size of the overlying droplets. So what is the origin of the changes in nanodroplet morphology with h_o? Since film rupture times, based on spinodal theory, scale as h^5, the rupture dynamics of the wetting layers of thickness h^* (h^* ~ 1-2 nm for the systems studied here) are orders of magnitude faster than for films ≥ 10
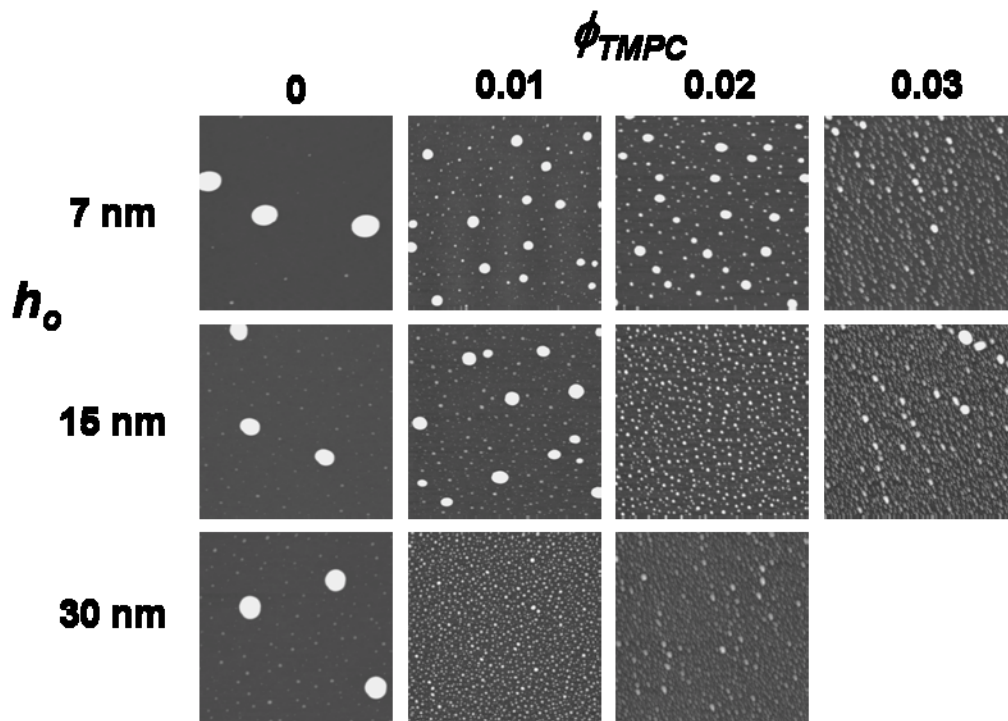
Figure 3-2: AFM micrographs of the PS-TMPC thin film mixture nanodroplet structure. Lateral scan range of all samples is equivalent and shows 5 x 5 μm. Brighter regions in the AFM micrographs represent larger heights above the substrate. The height range (nm) depicted in the micrographs was set to focus on the pertinent morphological structures and is listed, from left to right, in the following: 7 nm: 40, 20, 20, 15; 15 nm: 40, 20, 15, 15; 30 nm: 40, 15, 15.

nm thick, and experimental observation of the rapid break up of these ultrathin films is not practical. We can, however, characterize the structure of the resulting droplets as a function of ϕ_{TMPC} and h_o and use this information to reason through the origins of the structure changes.

In Figure 3-2, it is clear that nanodroplets exist on two scales; the two scales will heretofore be referred to as large and small nanodroplets. The large nanodroplets decrease in size and increase in number density with increases in ϕ_{TMPC} and/or h_o (for $\phi_{TMPC} > 0$). On the other hand, the size of the small nanodroplets remains relatively constant with changes in ϕ_{TMPC} and/or h_o while their number density increases. At some point ($\phi_{TMPC} = 0.01$ and $h_o = 30$ nm, $\phi_{TMPC} = 0.02$ and $h_o = 15$ nm, and $\phi_{TMPC} = 0.03$ and $h_o = 7$ nm) the structure of the large and small nanodroplets merge to create a uniform height distribution of droplets. When ϕ_{TMPC} or h_o is increased beyond the merger position, the nanodroplets further increase in number density and a fraction of the droplets begin to increase in size. Figure 3-3 plots the average droplet height and number density of both the small and large nanodroplets as a function of ϕ_{TMPC} and h_o to depict these changes.

We first note the deviation of the nanodroplet sizes of Figure 3-2 to those reported previously for PS films, which were only on the order of 3-10 nm in height.[9, 12, 14] At low ϕ_{TMPC} and h_o, the height of the large nanodroplets in Figure 3-2 is an order of magnitude larger than these previous observations. We can only guess that the earlier works focused on what we are referring to as the small nanodroplets, as the sizes of the small nanodroplets match well with the previous observations. But our measurements clearly show the existence of both sizes of nanodroplets inside the macroscopic droplet patterns, and a calculation of the average polymer height above the substrate in these regions, h_{avg}, for the PS case (including the large nanodroplets) yields $h_{avg} \approx 1$ nm, in

44
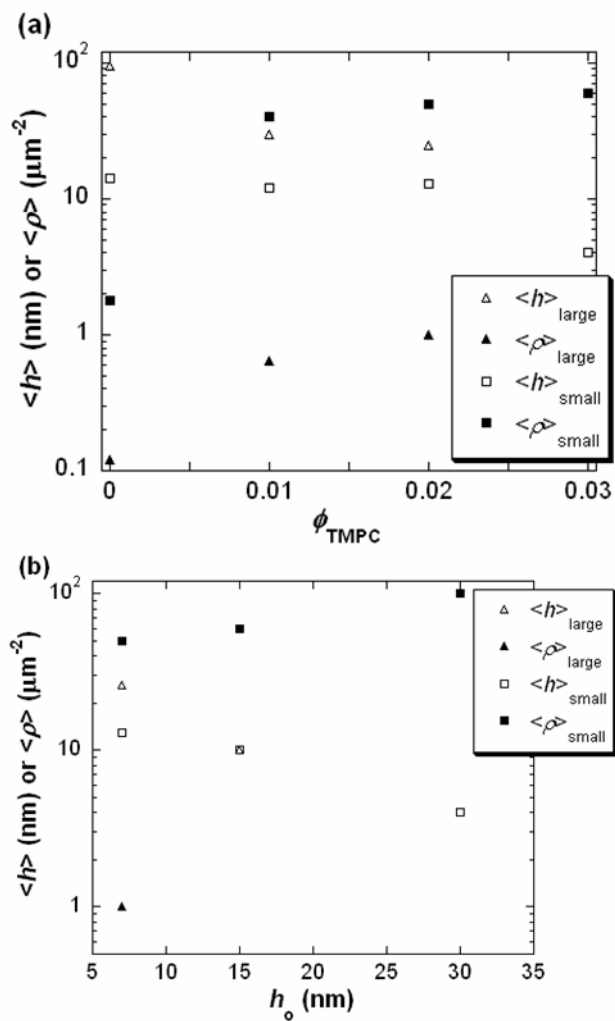
Figure 3-3: Average height $\langle h \rangle$ and number density $\langle \rho \rangle$ of PS-TMPC nanodroplets as a function of (a) composition at $h_o = 7$ nm and (b) initial film thickness at $\phi_{TMPC} = 0.02$. Quantities are plotted for both the large and small nanodroplets, as referred to in the text.

good agreement with in-situ reflectivity measurements of the thickness of the wetting layer beneath the macroscopic droplets.[7, 12, 14] If the large nanodroplets are not taken into account, volume conservation between the original thin wetting film and nanodroplets would not hold. These observations clearly depict the need to include the large nanodroplets in our discussion.

As already described, the rupture dynamics of the wetting layer of thickness h^* are so rapid that experimental investigations into the process are impractical. That denies us the ability to directly observe the dewetting process that leads to the formation of the nanodroplets. We can, however, reason through mechanisms by which the changes in structure may occur. We start by asking what may be theoretically expected for changes in the nano-dewetting structures. Spinodal theory predicts a dominant wavelength of the instability, $\lambda = 2\pi(h^*)^2(4\pi\gamma/A)^{1/2}$, where γ is the film surface tension, that corresponds to the fastest growing mode. This suggests that changes in the wetting layer thickness, the film surface tension, and/or the Hamaker constant may play a role in shaping the dewetting morphology of the thin wetting layer. These parameter do not vary with h_o, but do have a ϕ_{TMPC} dependence.[10] Here, the dominant factor is expected to be h^*, as increases in h^* with ϕ_{TMPC} are predicted to be as much as 8 % over the relevant compositions, while A changes less than 1 % and γ changes are also expected to be insignificant.[10] The increase in h^* with ϕ_{TMPC} tends to increase λ and therefore increase the size and separation distance between the resulting droplets. This is the opposite effect of that observed in Figure 3-2 with increasing ϕ_{TMPC} and implies that changes in h^* are not likely the origin of the changes in the nanodroplet structure with ϕ_{TMPC}.

The denser packing of smaller droplets noted with an increase in ϕ_{TMPC} could be explained by a limitation of coarsening in the system. This would require that the initial

46

break up of the h^* wetting layer results in small, closely packed droplets that later coarsen. Such a mechanism would be consistent with the bimodal distribution of droplet sizes observed. Coarsening limitation may be anticipated with the decrease in dynamics, due to the increase in average molecular weight and T_g, associated with TMPC addition to PS and the limited amount of time, the interval between cooling below the instability temperature of the thin wetting layer and freezing motions in the glassy state, to coarsen. A coarsening limitation with increasing h_o is more difficult to reason, unless a higher fraction of TMPC enriches the substrate interface with increasing initial film thickness. However, the inability to affect nanodroplet morphology by changing the cooling rate of the sample suggests against a coarsening explanation.

The following description may be the most plausible explanation for the changes in nanodroplet structure. TMPC is known to interact strongly with oxidized silicon substrates.[15] The strong interactions could lead to an essential "immobilization" of TMPC segments on the substrate. Such an effect could result in more tightly packed nanostructures, as the frozen segments (and segments associated with the same molecule and any other entrapped molecules) are left on the substrate while the molecules without such constraints withdraw due to the film instability. In this case, a very local effect on polymer dynamics is active and may be able to explain the changes in nanodroplet structure with both ϕ_{TMPC} and h_o if a higher fraction of TMPC enriches the substrate interface with increasing initial film thickness. This type of mechanism may also be able to account for a bimodal distribution of droplet sizes. The small nanodroplets may be the result of the immobilized TMPC segments along with any neighboring chains they may trap, whereas the larger drops are the result of the dewetting chains without such constraints. As the local concentration of the TMPC at the substrate increases, the number of constrained chains increases, creating a barrier to the formation of the large

47

nanodroplets and hence reducing their size and trapping them in more localized vicinities. Eventually, there are enough constrained sights to prevent a dewetting flow of the h^* layer over large areas and a high density of the constrained chains remain on the substrate as small nanodroplets. With further increases in local TMPC concentration the constrained regions may grow in size, resulting in the morphologies observed beyond the merger of the large and small nanodroplets in Figure 3-2.

3.4   CONCLUSIONS

The variation in the height and number density of nanodroplets formed from PS-TMPC thin film mixtures was evaluated as a function of ϕ_{TMPC} and h_o. Changes in the system thermodynamic parameters, the film surface tension, Hamaker constant, and wetting layer thickness, were shown unlikely to be the origin of changes in nanodroplet structure, and mechanisms for changes in polymer dynamics at the substrate interface were proposed that could explain the changes in nanodroplet structure observed. The proposed mechanism is primarily based upon an increase in TMPC enrichment at the substrate, and hence the changes in nanodroplet structure might be interpreted as an indirect observation of increased segregation of the TMPC component to the substrate interface. The rapid dynamics of nanodroplet formation, however, prevented a direct observation of the dewetting process that leads to the formation of the nanodroplets, and a confirmation of the proposed mechanism may have to await simulation evaluations of the system.

3.5   REFERENCES

[1]   P. G. De Gennes, *Reviews of Modern Physics* **57**, 827 (1985).

[2]   G. Reiter, *Physical Review Letters* **68**, 75 (1992).

[3]   G. Reiter, *Langmuir* **9**, 1344 (1993).

[4]   A. Sharma, *Langmuir* **9**, 861 (1993).

[5]   A. Sharma, and A. T. Jameel, *Journal of Colloid and Interface Science* **161**, 190 (1993).

[6]   A. Sharma, and R. Khanna, *Physical Review Letters* **81**, 3463 (1998).

[7]   R. Seemann, S. Herminghaus, and K. Jacobs, *Physical Review Letters* **86**, 5534 (2001).

[8]   J.-L. Masson, and P. F. Green, *Physical Review Letters* **88**, 205504/1 (2002).

[9]   B. M. Besancon, and P. F. Green, *Physical Review E: Statistical, Nonlinear, and Soft Matter Physics* **70**, 051808/1 (2004).

[10]   J. M. Kropka, and P. F. Green, *Macromolecules* **39**, 8758 (2006).

[11]   C. J. Van Oss, M. K. Chaudhury, and R. J. Good, *Chemical Reviews (Washington, DC, United States)* **88**, 927 (1988).

[12]   M. Muller *et al.*, *Journal of Chemical Physics* **115**, 9960 (2001).

[13]   J. N. Israelachvili, *Intermolecular and Surface Forces* (Academic Press, London, 1991).

[14]   P. Muller-Buschbaum *et al.*, *Europhysics Letters* **40**, 655 (1997).

[15]   J. Q. Pham, and P. F. Green, *Journal of Chemical Physics* **116**, 5801 (2002).

[16]   E. Kim *et al.*, *Journal of Polymer Science, Part B: Polymer Physics* **33**, 467 (1995).

Chapter 4: Origin of Dynamical Properties in PMMA-C$_{60}$ Nanocomposites[*]

In this chapter, poly(methyl methacrylate) (PMMA)-C$_{60}$ nanocomposites, with compositions in the range $0 \leq \phi_{C60}{}^{wt} \leq 0.05$, are shown to exhibit systematic increases in dynamic shear moduli, in glass transition temperature (T_g), and in the longest relaxation time of the polymer (τ_R) with increasing fullerene concentration. We show that while the $\phi_{C60}{}^{wt}$ dependence of the plateau modulus can be reconciled with a conventional "filler" effect, the systematic increases in T_g and in τ_R are associated with specific interactions between the C$_{60}$ and the polymer segments. In the melt, these segment-C$_{60}$ interactions are proposed to reduce polymer segmental mobility in the vicinity of the particle surface and ultimately suppress polymer dynamics, as measured mechanically, in a manner consistent with an increase in the polymer segmental friction coefficient.

4.1 INTRODUCTION

The influence of particles on the viscoelastic properties of conventional polymer-based composites, i.e., polymers filled with particles that have dimensions on the order of microns or larger, can often be described solely in terms of the volume fraction of particles.[1] The success of such a "filler" effect model relies on the influence of specific interactions between polymer segments and particles being negligible. However, when particles possess dimensions on the order of nanometers, even small particle concentrations can lead to a breakdown of this "continuum-solvent" wisdom. These polymer nanocomposite (PNC) materials exhibit changes in glass transition temperatures

(T_gs)[2-7] and enhancements in viscoelastic properties[8-15] unprecedented in conventional composites.

The unique properties of PNCs are attributed to the high filler surface area-to-volume ratios, which result in significant interfacial areas of contact between the polymer and the particles. The large interfacial areas of contact enable a substantial fraction of polymer segments to interact directly with filler particles, even at low particle concentrations. In addition, interparticle distances can become comparable to the size of the polymer chains at low particle volume fractions in PNCs. Consequently, both chain confinement and polymer bridging between particles can occur and may also influence the properties of the PNC. For many applications, however, the precise manner in which the preceding features interplay and impact material properties remains to be clarified.

The rheological behavior of PNCs has attracted significant interest in recent years,[8-12, 14-20] both for scientific and technological reasons. Apart from providing an assessment of processability, rheological measurements give insight into the connection between the molecular structure and dynamics of polymers. Experimentally, PNCs typically exhibit solid-like viscoelastic behavior at particle volume fractions much smaller than predicted for conventional composites.[8, 11, 14] Explanations for this phenomenon range from jamming of a highly anisotropic particulate phase[9, 16, 21] to the creation of a polymer mediated particle network.[11, 14] Simulations suggest that changes in monomer packing near the polymer-particle interface[19, 22-27] lead to local segmental dynamics that differ from that of the homopolymer. In the case of attractive polymer-particle interactions, the dynamics and can be highly heterogeneous,[19] particularly at high loading fractions.[20] These dynamic heterogeneities, which arise due to the presence of nanofillers, have been suggested to underlie changes in the T_g and the viscosity observed in PNCs.[19, 20, 25, 26] Additional experimental studies aimed at

51

discerning the nature of the material heterogeneities would be useful to gain further insight into these observations.

In this chapter we examine how nanoparticles influence the viscoelastic behavior of PMMA based PNCs and probe the underlying mechanism(s) of the effect. To this end, the thermal and viscoelastic properties of a model PNC, narrow molecular weight distribution PMMA into which C_{60} fullerene particles are incorporated, are evaluated. The diameter of a C_{60} particle is approximately 1 nm; so individually dispersed particles within the polymer matrix would therefore result in average interparticle distances comparable to the size of the polymer radius of gyration, $R_g \sim 14$ nm, at volume fractions as low as $3x10^{-5}$. Considering the similarities noted between PNCs and polymer thin films,[6, 25] and noting that polymer thin film physical properties exhibit changes at film thicknesses greater than the polymer R_g,[28-33] the properties of PMMA should be expected to exhibit changes even at such low C_{60} fractions. Our investigations confirm that the addition of C_{60} to PMMA has ramifications beyond that of a conventional "filler" effect. Dynamic mechanical analysis (DMA) and differential scanning calorimetric (DSC) measurements both reveal a systematic increase in the T_g of the PNCs, and melt rheological measurements show that an increase in the polymer chain relaxation time accompanies the change in T_g. An assessment of the C_{60} dispersion within the polymer, considered together with recent computer simulation findings and incoherent neutron scattering experiments, suggests that transient interactions between the polymer chain segments and C_{60} aggregates are responsible for the reduction in dynamics.

4.2   EXPERIMENTAL DESCRIPTION

4.2.1   Materials

The PNCs were made via a solution dissolution-solvent evaporation method. The C_{60} (Alpha Aesar, 99+%) was added to toluene up to a concentration of 0.15 weight percent and sonicated (Sonicor, SC-40) for 15 minutes to disperse the fullerenes into solution.   PMMA (Pressure Chemical; M_w = 254.7 kg/mol, M_w/M_n = 1.15) was also dissolved in toluene, and the two solutions were mixed in proportion to create the appropriate nanocomposite concentration.   The toluene was subsequently evaporated from the mixture at 348 K. Residual solvent was removed by drying the samples under high vacuum at 453 K for 15 hours. The pure polymer and PNCs were compression molded at 453 K into cylindrical and rectangular geometries for rheological and dynamic mechanical (DMA) testing, respectively.

4.2.2   Thermal Characterization

Differential scanning calorimetry measurements of the samples were taken on a DSC 7 (Perkin-Elmer) after residual solvent removal. Approximately ten milligrams of material was heated from 298 to 473 K at a rate of 10 K per minute in three cycles. Between each heat ramp, the material was annealed at 473 K for five minutes to erase previous thermal history and then cooled back to 298 K. The samples were then held at 298 K for five minutes to ensure temperature equilibration before beginning the next heat ramp.   All measurements reported are of the second heating cycle, which was indistinguishable from the third heating cycle.

The dynamic mechanical behavior of the PNCs was examined using a Mark V DMTA (Rheometrics Scientific) in the single cantilever bending geometry.   The

experimental specimens were 30 mm long, 10 mm wide and 1.1 mm thick. The samples were cooled to 123 K and held there for 10 minutes. Then the storage modulus (E'), loss modulus (E'') and loss tangent (tanδ) were analyzed at discrete frequencies of 0.1, 1, 10 and 50 Hz under a strain of 0.1 % while the sample was heated from 123 to 483 K at a rate of 1 K/min. Strain sweeps verified that the reported measurements were within the linear viscoelastic regime. All samples were relaxed above their glass transition temperature just before testing.

4.2.3 Rheology

The melt viscoelastic properties of the PNCs were characterized using an advanced rheometric expansion system (ARES) rheometer (Rheometrics Scientific) equipped with 25 mm parallel plates under small amplitude oscillatory shear strain. The average gap between the plates was 1 mm and applied strains ranged from 5 to 10 %. The frequency dependent elastic ($G'(\omega)$) and loss ($G''(\omega)$) shear moduli were measured over a temperature range of 433 to 513 K by performing frequency, ω, sweeps from 0.1 to 100 rad/s. Strain sweeps verified that all reported measurements were within the linear viscoelastic regime. Master curves at 443 K were generated using Orchestrator (TA Instruments) software, which determined the horizontal shift factors (a_T) necessary to match the loss tangent (tanδ). Subsequent vertical shift factors (b_T) were required to superpose moduli due to changes in material density and variations in the separation gap with temperature.

4.2.4 Incoherent Neutron Scattering

Aluminum boats containing the polymer samples were placed in an annular, thin-walled aluminum cell that was mounted on the high flux backscattering spectrometer (HFBS)[34] on the NG2 beam line at the NIST Center for Neutron Research and cooled to 50 K under vacuum. The spectrometer operated in fixed window mode (stationary Doppler drive) with the elastic intensity recorded over a Q range of 0.25 to 1.75 Å^{-1}. The sample temperature was increased at a rate of 1 K/min to 525 K, and the elastic intensity was summed over intervals of 1 K. The HFBS energy resolution of ~ 0.8 μeV (FWHM) implies that dynamics on a time scale of 200 MHz (approximately a nanosecond) or slower contribute to elastic scattering, whereas faster processes contribute to inelastic scattering and a subsequent reduction in the elastic intensity.

The incoherent scattering cross section of hydrogen is approximately 20 times greater than the total scattering cross section of C or O and ~ 40 times larger than its own coherent scattering cross section. Hence, in the C_{60}-PMMA PNCs tested, the scattering is dominated by the incoherent scattering of the hydrogen atoms of the PMMA and only the polymer dynamics is probed. The thickness of the sample films was ~ 0.05 mm, to achieve > 90% transmission and minimize multiple scattering. Raw data were normalized to monitor and to the intensity at the lowest measured temperature.

4.2.5 Dispersion

C_{60} dispersion within the PMMA matrix was characterized by transmission optical microscopy and transmission electron microscopy (TEM). Transmission optical micrographs of the cast films were recorded using an Axioskop 2 MAT (Zeiss) equipped with an Axiocam MRc5 CCD (Zeiss). For TEM analysis, portions of the dried films were cut into sections, approximately 50 nm in thickness, with a diamond knife using an

Ultracut UCT ultramicrotome (Leica). Sections were placed on a 400 mesh copper grid and subsequently examined at an accelerating voltage of 80 kV using an EM 208 (Philips).

4.3   RESULTS

4.3.1   Thermal Characterization

The dynamic mechanical moduli show no significant changes upon C_{60} addition for materials in the glassy or rubbery state (data not shown due to the absence of changes). This observation holds at all tested frequencies (0.1, 1, 10, and 50 Hz). All changes in the moduli are limited to the α-transition region and are due to changes in the onset of the transition. At the α-transition, a substantial drop in E' occurs while E'' exhibits a peak, which is indicative of viscous damping. When C_{60} is added to PMMA, the position of the peak exhibited by $\tan\delta$ (E''/E') shifts to higher temperatures; the peak height and peak width, however, remain unchanged (Figure 4-1(a)). Similarly, the change in heat capacity of the materials associated with the glass transition (Figure 4-1(b)) shifts to higher temperatures upon particle addition, but the magnitude and breadth of the change remain unaltered. The frequency dependence of the α-transition is also unaffected by particle addition (Figure 4-1(c)).

The change in T_g from that of pure PMMA for the PMMA-C_{60} PNCs, as measured by both DSC and DMA, is shown in Figure 4-2. The DSC T_g was determined in the following manner: 1) straight lines were fit to the heat flow versus temperature curves before, during, and after the glass transition, 2) the points of intersection were taken as the onset and endpoint of the transition, and 3) the T_g was taken as one half the change in heat capacity between the onset and endpoint of the transition. The DMA T_g

56
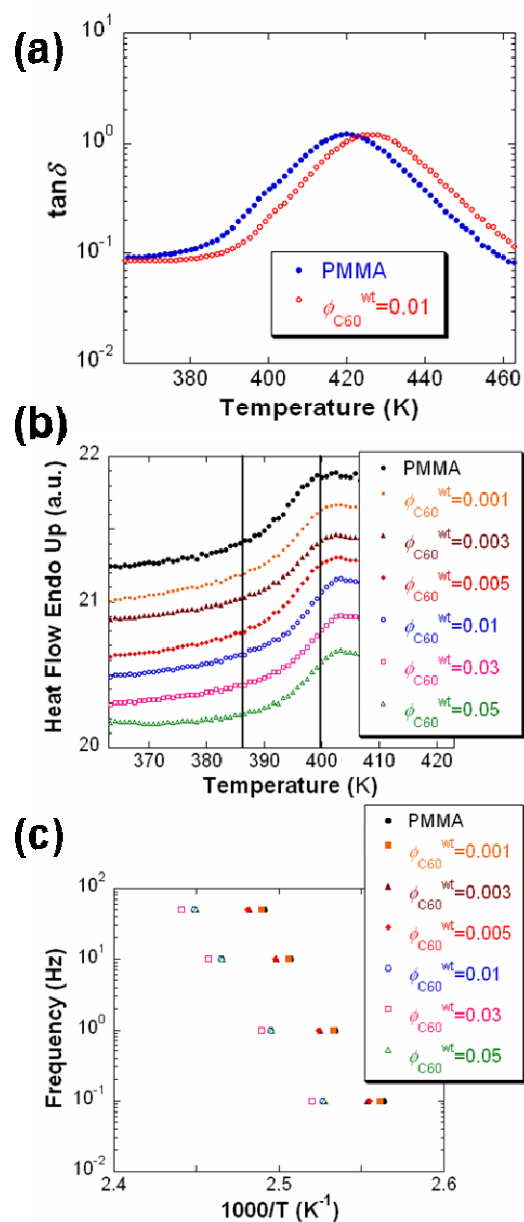
Figure 4-1: (a) Dynamic mechanical loss tangent, $\tan\delta$, as a function of temperature in the α-transition region for the pure polymer and PNC at a frequency of 10 Hz. For clarity, only the data for PMMA and the $\phi_{C60}{}^{wt} = 0.01$ PNC are shown. All other PNCs show similar behavior. (b) Differential scanning calorimetry thermograms for the pure polymer and PNCs. For clarity, the data has been shifted along the heat flow axis and only every fifth data point is shown. The vertical lines are drawn to aid in discerning the temperature shift of the transition. (c) Frequency dependence of the mechanical loss maximum associated with the α-transition for the pure polymer and PNCs.

57
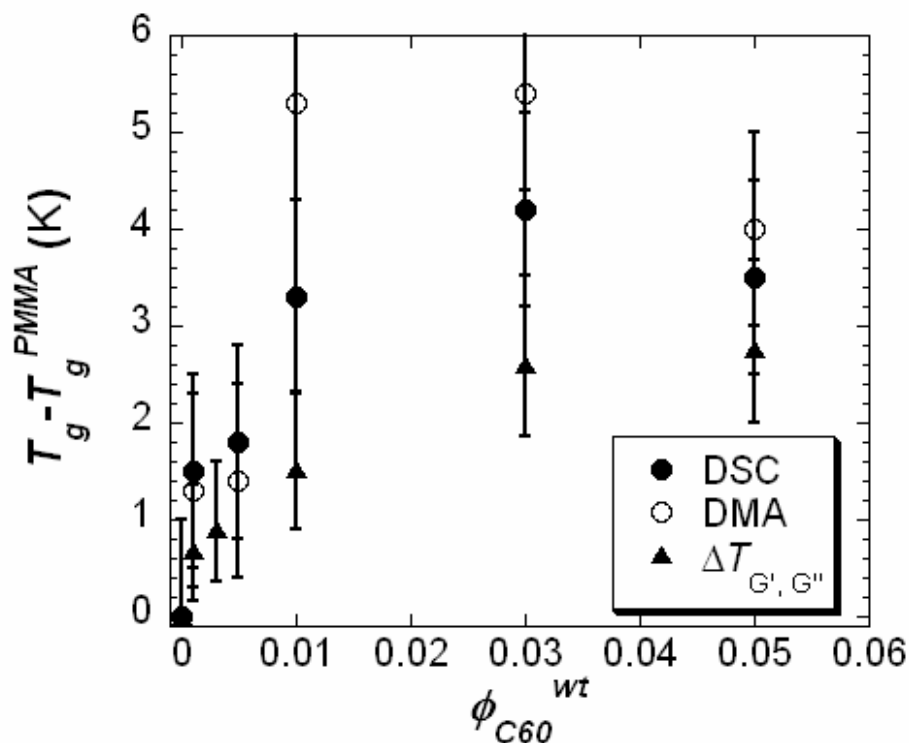
Figure 4-2: The change in the glass transition temperature from that of pure PMMA for the PMMA-C_{60} PNCs, T_g-T_g^{PMMA}, as measured by both DSC and DMA. The temperature shift necessary to superpose rheological moduli, $\Delta T_{G',G''}$, is also plotted for comparison. The error bars for the DSC measurements are associated with the range of values that can be obtained for reasonable choices of curve fits (as described in the text). For the DMA measurements, error bars are associated with the temperature difference between data points (i.e., the uncertainty with which the peak position is identified). The error bars for $\Delta T_{G',G''}$ are associated with both the measurement uncertainty of the crossover point of the storage and loss moduli (as described therein) and the range of WLF constants that gave a reasonable fit to the shift factor temperature dependence (C_1^o = 9.1-9.9, C_2^o = 140-160).

was identified as the high temperature peak position of $\tan\delta$ plotted as a function of temperature. It is clear from Figure 4-2 that the T_g of the material increases with the addition of C_{60}.

4.3.2 Rheology

Dynamic rheological measurements were conducted to determine the effect of C_{60} on the dynamics and topology of the polymer melt. Master curves of the shear storage modulus and of the shear loss modulus at a reference temperature, $T_\text{o} = 443$ K, are shown in Figure 4-3. It is evident from these data that the effect of C_{60} is to shift the storage and loss moduli to higher magnitudes and lower frequencies. The change in the magnitude of the storage modulus with $\phi_{C60}{}^\text{wt}$ is evaluated in terms of the plateau modulus, $G_\text{N}{}^\text{o}$, and the frequency shift in the moduli is evaluated in terms of the longest relaxation time of the polymer, τ_R, which is the Reptation time for the highly entangled PMMA in our studies. An estimate of $G_\text{N}{}^\text{o}$ for the materials is obtained from the value of the elastic shear modulus at the point of maximum elasticity,[35-37]

$$G_N^o = \left[G'(\omega)\right]_{\min(\tan\delta)} \tag{4-1}$$

and is depicted as a function of $\phi_{C60}{}^\text{wt}$ in Figure 4-4. The longest relaxation time of the polymer is estimated as the crossover point of the storage and loss moduli at low frequency,[38]

$$\tau_R = \left(\frac{2\pi}{a_T\omega}\right)_{G'=G''_{low\omega}} \tag{4-2}$$

and is plotted against $\phi_{C60}{}^\text{wt}$ in Figure 4-5. The two parameters, $G_\text{N}{}^\text{o}$ and τ_R, can be used to rescale the modulus and frequency axes, respectively, of the data in Figure 4-3 to account for strictly vertical and horizontal shifts in the moduli. The rescaling results in the superposition of all data over the entire frequency range, as depicted in Figure 4-6.

59
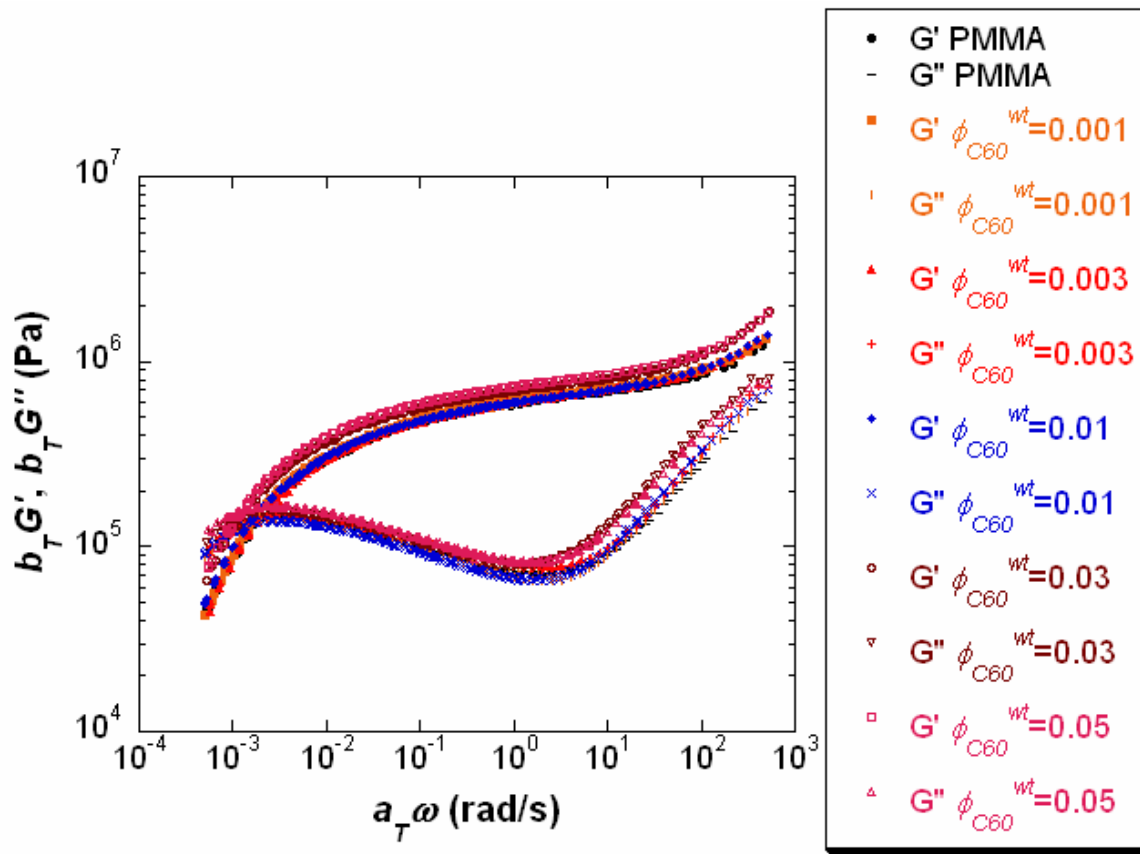
Figure 4-3: The frequency dependence of the dynamic shear moduli of the polymer and PNCs. Master-curves were obtained by application of time-temperature superposition and were shifted to a reference temperature of 443 K.
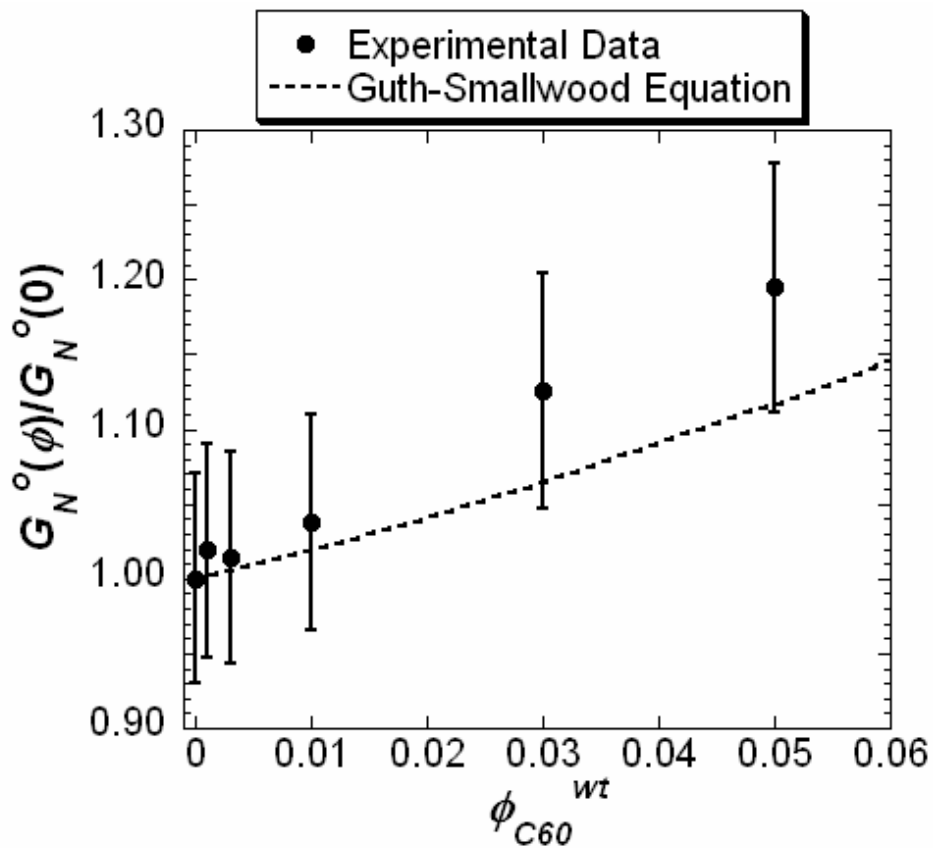
Figure 4-4: The ratio of the plateau moduli of the PNCs to that of pure PMMA as a function of C_{60} loading. The relation in equation 4-5 is plotted along with the data for comparison. The error bars for the plateau moduli are associated with the variability (~ 5 %) of equivalent measurements on material standards and all replicate PNC measurements fell within this range.
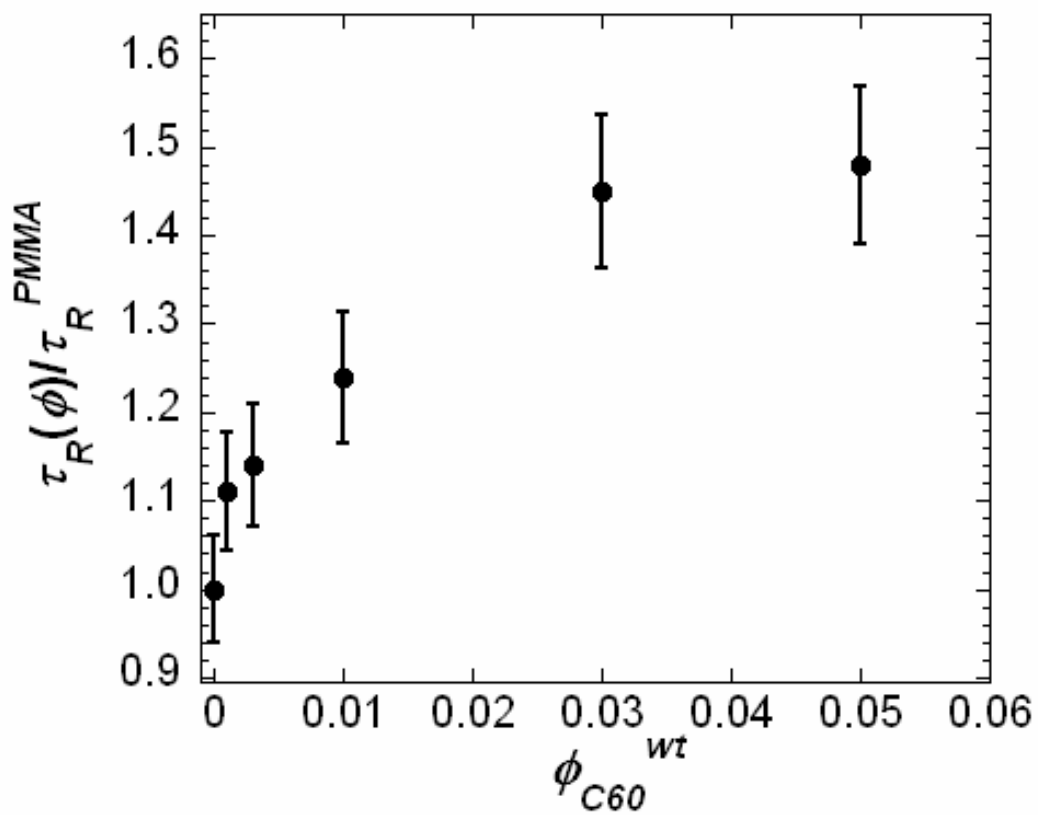
Figure 4-5: The ratio of the longest relaxation time for the PNCs to that of pure PMMA as a function of C_{60} loading. The error bars for the relaxation times are associated with the variability ($\sim$ 3 %) of equivalent measurements on material standards and all replicate PNC measurements fell within this range.
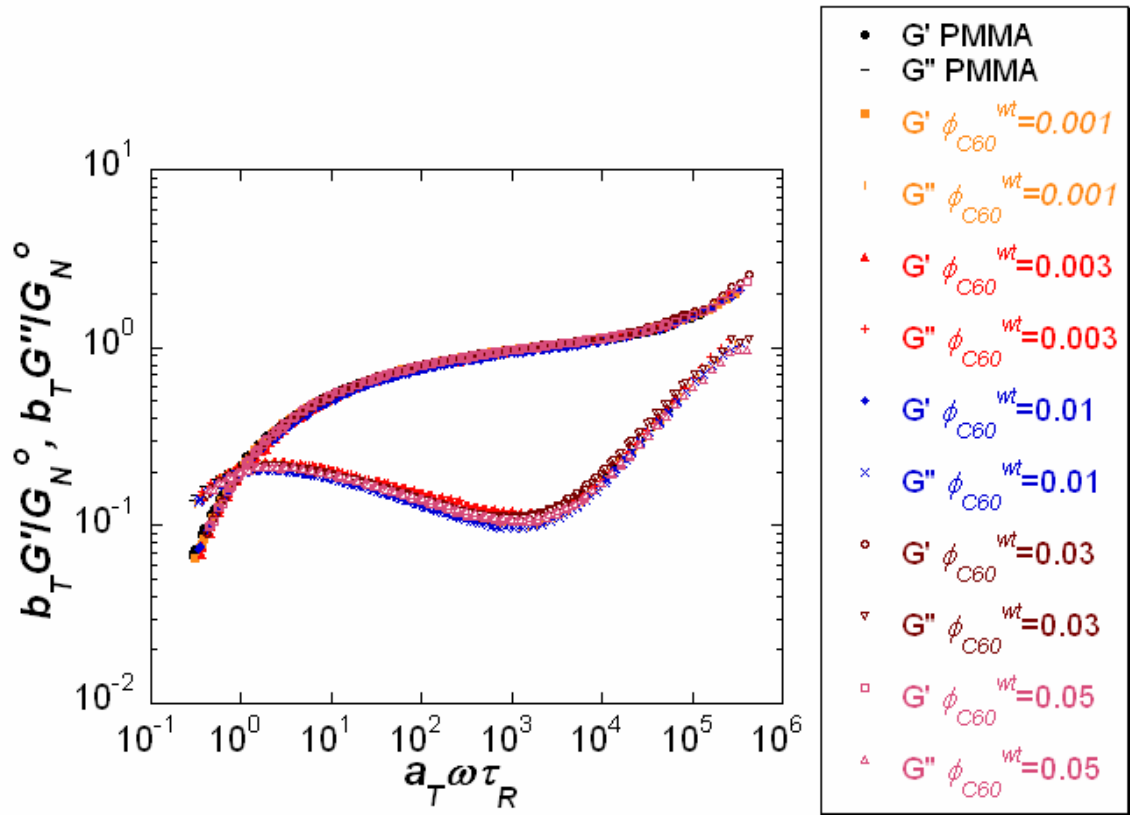
Figure 4-6:   Superposition of the dynamic shear moduli by a rescaling of the axes as described in the text.

The shift factors, a_T, necessary to construct the master curves of the viscoelastic data for each PNC are plotted as a function of temperature in Figure 4-7. The data from all samples superimpose onto a single curve that can be described by the Williams-Landel-Ferry (WLF) equation,[39]

$$\log a_T = \frac{-C_1^o (T - T_o)}{C_2^o + T - T_o}$$

(4-3)

with constants $C_1^o = 9.5$ and $C_2^o = 150$ at a reference temperature $T_o = 443$ K. The ability to describe all data in Figure 4-7 by a single fit of equation 4-3 demonstrates the independence of both C_1^o and C_2^o on C_{60} concentration for the PNCs.

We conclude the rheological results and relate them to the thermal results by revealing the increase in τ_R with ϕ_{C60}^{wt}, shown in Figure 4-5, can be reconciled solely with the change in T_g of Figure 4-2. This relation is demonstrated by using equation 4-3 to calculate a temperature shift, $\Delta T_{G',G''}$, that is equivalent to the frequency shift, α, necessary to equate the longest relaxation times.

$$\alpha = \frac{\tau_R(\phi)}{\tau_R^{PMMA}}$$

(4-4)

$\Delta T_{G',G''}$ is plotted along with the experimentally determined T_g shift in Figure 4-2. The data show good agreement, supporting the notion that the changes in chain dynamics are determined by changes in the polymer matrix properties due to the influence of C_{60}.

4.3.3 Dispersion

Since nanoparticles are known to aggregate into clusters when dried from solution,[40] it is important to monitor particle dispersion in solution-fabricated materials. A visual observation of the polymer films that remained after solvent evaporation provided an initial assessment of C_{60} dispersion within the PMMA matrix. Prior to annealing, all films were translucent, with a purple hue. However, after
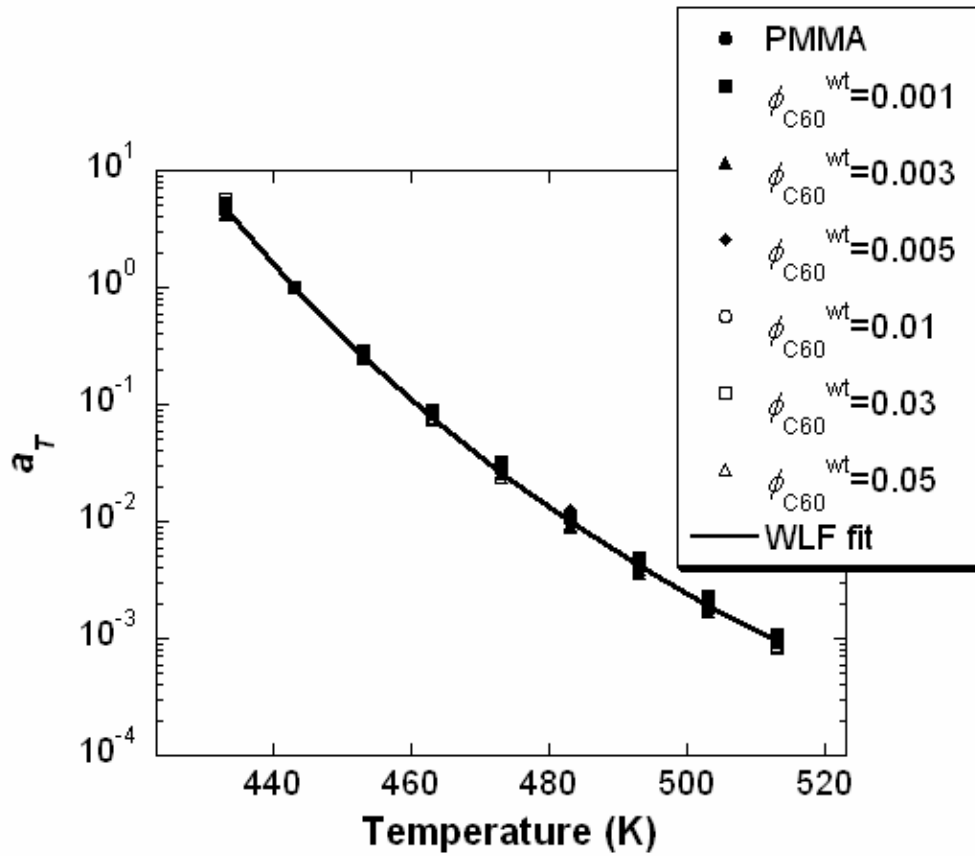
Figure 4-7: Frequency shift factors, a_T, used for the development of the master-curves in Figure 4-3 as a function of temperature.

annealing above T_g, samples of $\phi_{C60}^{wt} \geq 0.03$ became opaque. The opacity of the $\phi_{C60}^{wt} = 0.03$ and 0.05 samples is an indication of large particle agglomerates in the material, as nanoscopic fillers do not scatter light significantly.

Cross sectional transmission electron microscopy (TEM) images of the PNCs, Figure 4-8, reveal that the C_{60} exists as nanoscopic agglomerates with diameters on the order of 20 nm for $\phi_{C60}^{wt} < 0.01$. Also evident from Figure 4-8, is the invariance of agglomerate size and increase in the number density of agglomerates with increasing ϕ_{C60}^{wt} for $\phi_{C60}^{wt} < 0.01$. These observations suggest that although the fullerenes have not been individually dispersed, aggregates at these low concentrations can still be described as nanoparticles and have dimensions on the order of the polymer chain size, $\sim$ 10-20 nm.

At higher concentrations, $\phi_{C60}^{wt} \geq 0.01$, C_{60} agglomerates were detectable by both transmission optical microscopy and TEM. Figure 4-8 illustrates the coexistence of both nanoscopic and micron sized agglomerates at $\phi_{C60}^{wt} = 0.01$. From the TEM micrographs of the agglomerate structure at $\phi_{C60}^{wt} = 0.05$, it is evident that the morphology of the micron sized agglomerates is characterized by features on two additional length scales: (1) the large agglomerates consist of "bundles" of the nanoscopic aggregates that exist in the mixtures at low concentrations, and (2) crystal planes are evident within the nanoscopic aggregates. In fact, the relative abundance of the ordered nanometer agglomerates at high concentrations is likely the source of x-ray diffraction peaks observable by us (not shown) and by others[41] in these materials.
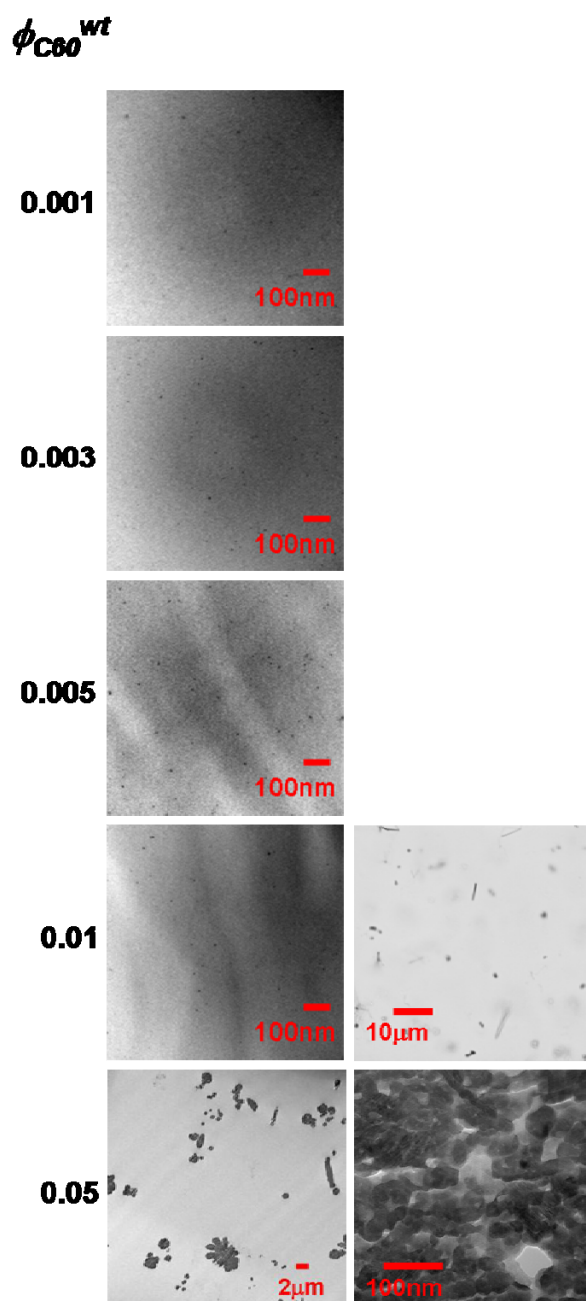
Figure 4-8: TEM and optical micrographs of the PMMA-C_{60} PNCs. The dark features are C_{60} agglomerates. At $\phi_{C60}^{wt} < 0.01$, C_{60} agglomerates are ~ 20 nm in diameter. At $\phi_{C60}^{wt} = 0.01$ nanoscale agglomerates coexist with micron sized agglomerates. The micron sized agglomerates at $\phi_{C60}^{wt} = 0.05$ consists of "bundles" of the nanoscale agglomerates that exist at low C_{60} concentrations and these nanoscale agglomerates exhibit ordered packing of C_{60} particles.

4.4   DISCUSSION

As described in the Introduction, property enhancements exhibited by PNCs can result from two effects: (1) a "filler" effect that can be completely described by the volume fraction of particles and has been well characterized through studies of conventional composites and/or (2) changes in the polymer matrix properties due to specific interactions between the polymer chain segments and the nanoparticles. While the latter is relevant in many systems,[2-6, 11, 12, 14, 15] the specific mechanisms behind the influences are often not fully understood. Simulations[19, 22-27] suggest the presence of nanoparticles change local monomer packing and that such changes in structure can contribute to property enhancements. For instance, a decrease in fractional free volume associated with increased monomer packing density, due to the influence of nanoparticles, could account for the increase in T_g exhibited by the PMMA-C_{60} PNCs, assuming the glass transition is an iso-free volume process. The increase in T_g could, in turn, account for the slow down in melt dynamics. Another scenario might be that an increase in polymer entanglement density arises from increased monomer packing density, or direct polymer-particle contacts. The resulting decrease in the number of monomers between entanglements, N_e, from such an effect could account for increases in the plateau modulus, $G_N^o \sim N_e^{-1}$, and chain relaxation time, $\tau_R \sim N_e^{-1}$, exhibited by the PMMA-C_{60} PNCs. However, in what follows we will show that our experimental observations are not consistent with the foregoing interpretations. It will be shown that the increase in G_N^o with C_{60} concentration is associated with the "filler" effect. In addition, we illustrate that the perturbing influence of the nanoparticles on the polymer matrix does not derive from polymer chain confinement or polymer bridging between particles. Instead, we argue that the increases in τ_R and T_g reflect the subtle influence of transient interactions between the fullerene surfaces and the PMMA chain segments.

68

4.4.1 Free Volume and Polymer Entanglement Density

As just described, changes in system free volume and/or polymer entanglement density, due to an influence of nanoparticles on polymer packing, could be responsible for changes in T_g, τ_R and G_N^o in PNCs. For instance, in PMMA-POSS PNCs, a WLF analysis enables a rationalization of the changes in system T_g in terms of changes in free volume with POSS concentration.[42] The rheological measurements of the PMMA-C_{60} PNCs, however, fail to resolve any such changes in structure. The WLF constants are independent of C_{60} concentration in these materials, which suggests that free volume changes cannot explain the trends exhibited in T_g.

An analysis of the breadth of the plateau region of the rheological data reveals that the PMMA entanglement density is independent of C_{60} concentration. The breadth of the plateau region is defined by the difference between τ_R and τ_e; the latter denoting the Rouse time of an entanglement strand. Since $\tau_R \sim N_e^{-1}$ and $\tau_e \sim N_e^2$, a change in N_e would result in a change in the breadth of the plateau region. However, Figure 4-6 illustrates the invariance of the breadth of the plateau region with C_{60} concentration; the data for the homopolymer and all PNCs superpose over the entire frequency range, which extends beyond the plateau region at both high and low frequencies, after rescaling to account for strictly horizontal and vertical shifts in the moduli. Since no change in the breadth of the plateau region occurs upon C_{60} addition, changes in the entanglement density cannot account for the observed changes in plateau modulus or polymer melt dynamics. These findings suggest the need for alternative explanations for the behavior of the PMMA-C_{60} PNCs, and the goal of the following discussion will be to identify the mechanisms behind the C_{60} influence on the properties of the PNCs.

4.4.2 The "Filler" Effect

We now examine the increase in melt plateau modulus with C_{60} concentration using a continuum theory which describes the effect of hard, non-interacting, spherical fillers on the moduli of polymers. The theory relates the modulus of the composite, $G_N^o(\phi^{vol})$, to that of the polymer, $G_N^o(0)$, by a filler volume fraction, ϕ^{vol}, dependent term.[43, 44]

$$G_N^o(\phi^{vol}) = G_N^o(0)\left(1 + 2.5\phi^{vol} + 14.1\left(\phi^{vol}\right)^2\right) \qquad (4\text{-}5)$$

While equation 4-5, often referred to as the Guth-Smallwood equation, under predicts the compositional dependence of the modulus depicted in Figure 4-4, the small discrepancy can be accounted for by a number of factors. The TEM images in Figure 4-8 show that the micron sized agglomerates which exist for $\phi_{C60}^{wt} > 0.01$ are anisotropic and contain voids (the light areas within the C_{60} agglomerates). The anisotropy of the particles alone contribute to deviations from equation 4-5,[43] and the voids within the agglomerate structure lead to larger effective volume fractions of the filler. Both effects tend to increase the magnitude of G_N^o beyond the theoretical predictions. Although it would be difficult to quantify the deviations from equation 4-5 due to these effects, we argue that they account for the discrepancies in Figure 4-4 and attribute the origin of the increase of G_N^o with C_{60} concentration to the "filler" effect.

4.4.3 Factors of Influence on PMMA Matrix Properties

Our results show that C_{60} perturbs the polymer matrix in such a manner as to increase the T_g and polymer chain relaxation time. The confinement of chains between filler particles, polymer bridging between particles, and polymer-particle interfacial interactions may all contribute towards the influence that nanoparticles have on the

properties of polymers. We now examine the relative role these factors play in shaping the properties exhibited by the PMMA-C$_{60}$ PNCs.

Chain confinement effects are expected be significant when interparticle distances become smaller than the size of the polymer, $\sim 2R_g$. An estimate of the C$_{60}$ interparticle distance, h, using the relation,

$$\frac{h}{D} = \left(\frac{\phi_m^{vol}}{\phi^{vol}}\right)^{\frac{1}{3}} - 1, \phi_m^{vol} = 0.638 \tag{4-6}$$

where D is the particle diameter and ϕ_m^{vol} is the maximum random packing volume fraction, predicts that $h \sim 2R_g$ for $\phi_{C60}^{vol} \sim 2.6\text{x}10^{-5}$ ($\phi_{C60}^{wt} \sim 4.5\text{x}10^{-5}$). This calculation is based on the assumption that the C$_{60}$ particles are individually dispersed and suggests that the polymer molecules in the PMMA-C$_{60}$ PNCs evaluated, $\phi_{C60}^{wt} \geq 0.001$, are highly confined between particles. However, the TEM images in Figure 4-8 reveal that much of the C$_{60}$ exists as aggregates. For $\phi_{C60}^{wt} < 0.01$, the average size of the aggregates is on order of 20 nm in diameter; for higher C$_{60}$ concentrations the dimensions of the aggregates reach the order of microns. Based on equation 4-6, the distance between these aggregates is greater than the size of the polymer, $h > 2R_g$, at all C$_{60}$ concentrations. This conclusion is consistent with the observation of interparticle distances in the micrographs of Figure 4-8. Therefore, confinement of the polymer chains between particles does not contribute to the observed changes in T_g and chain dynamics for the PMMA-C$_{60}$ PNCs.

Polymer chain bridging between particles also requires that the size of the polymer chain exceed the interparticle distances. However, we have already established that $h > 2R_g$ in the PMMA-C$_{60}$ mixtures, so any mechanism based solely on particle bridging would not be significant. Moreover, the lack of formation of a percolated filler network mediated by polymer chains, associated with polymer bridging between particles, is also evident from the melt dynamic shear moduli in Figure 4-3. Such a

network restrains long-range motions of polymer chains; the liquid-like terminal behavior associated with homopolymers at long time scales transitions to solid-like behavior.[9, 11, 14, 20] An example of this phenomenon was observed by Du et al.[14] in PMMA-single-walled carbon nanotube (SWNT) PNCs. The dynamic viscoelastic moduli of the PMMA-SWNT PNCs exhibit a weak low frequency dependence for SWNT loadings higher than 0.2 wt %, thereby revealing the restraint of the long-range polymer chain motions at these SWNT concentrations. However, the PMMA-C_{60} materials exhibit homopolymer-like terminal flow behavior, $G' \sim \omega^2$ and $G'' \sim \omega$, at all C_{60} loadings; only a shift in the onset of terminal flow to lower frequencies (Figure 4-3) occurs. This frequency shift in the rheological behavior with C_{60} addition is present throughout the entire frequency range, suggesting that polymer chain dynamics are affected equally on all length scales. This behavior is in contrast to that of a percolated network, where influence would primarily be in the terminal flow regime. Hence, both interparticle distances that exceed polymer chain size and the terminal flow behavior of the materials indicate that polymer bridging between particles is not the contributing influence to the changes in T_g and chain dynamics observed for the PMMA-C_{60} PNCs.

The absence of polymer chain confinement and polymer bridging between particles in the PMMA-C_{60} PNCs leaves interfacial interactions to account for the observed changes in PMMA matrix properties. This finding, in conjunction with the observations of C_{60} agglomerate size as a function of ϕ_{C60}^{wt} (Figure 4-8), makes the origin of the plateau of T_g and of τ_R at $\phi_{C60}^{wt} > 0.01$ (observed in Figures 4-2 and 4-5 respectively) apparent. The formation of large particle agglomerates at the higher concentrations prevents the growth of polymer-particle interfacial area of contact and hence inhibits the influence of the particles on the polymer dynamics from growing with

further increases in C_{60} concentration. We now turn our attention to the manner by which interfacial interactions exert influence on the bulk behavior of the PMMA-C_{60} PNCs.

4.4.4 Role of Transient Interactions at Interfacial Contact

There is reasonable insight into ways that interfacial interactions influence the properties of polymers, particularly from measurements of the glass transition temperature of thin polymer films[28-33, 45-48] and of PNCs.[2-7] In PNCs, particles are generally described to influence the glass transition of the material in one of two manners. The first is a relatively long-ranged gradient in T_g, extending tens of nanometers from the interface, that influences the average T_g of the material.[6] The second is a more localized effect denoted by marked changes in polymer dynamics at direct interfacial contact with the particles while, at the same time, homopolymer-like dynamics are exhibited away from the particle surface.[2, 3, 49] For the PMMA-C_{60} system, the invariance of the tanδ α-relaxation peak height and peak width with filler concentration (Figure 4-1a) is not consistent with either of the foregoing descriptions. A long-ranged gradient in the polymer T_g within the interfacial region would be anticipated to produce a broader distribution of polymer relaxation times compared to the homopolymer and hence broaden the width of the α-transition peak for the PNCs relative to the homopolymer. A marked change in dynamics at interfacial contact would be anticipated to shift the relaxation of a fraction of polymer segments outside the spectrum of the homopolymer α-transition peak and hence reduce the height of the α-transition peak for the PNCs relative to the homopolymer. The absence of either effect suggests that the C_{60} particles slow the α-relaxation dynamics uniformly throughout the bulk of the PNC.

Simulations[19, 20, 25, 26] indicate that local dynamic heterogeneities in PNC melts, associated with polymer-particle interfacial interactions, can lead to a change in the macroscopic properties of the polymer. These simulations suggest that weakly attractive polymer-particle interactions lead to transient immobilization of polymer segments at the surfaces of particles; the duration of the immobilization persists on time scales, τ_{ps}, that are much shorter than the longest relaxation time, τ_R, of a polymer chain, $\tau_{ps} \ll \tau_R$. Consequently, a large fraction of polymer segments experience such transient interactions throughout the duration τ_R, and this induces a homogeneous slow down of dynamics on the time scale of τ_R. The effect is tantamount to an increase in the effective friction experienced by a chain. Higher particle concentrations lead to larger polymer-particle interfacial areas of interaction (assuming the particles do not aggregate appreciably) and enhance the effect on dynamics. The work of Pryamitsyn et al.[20] describes this type of behavior at low concentrations of a spherical filler in PNCs with weakly attractive polymer-particle interactions; such a mechanism is also commensurate with our experimental observations of τ_R as described below.

Evidence of the immobilization of polymer chain segments at the surface of the C_{60} particles can be discerned from incoherent elastic neutron scattering (IENS) measurements. Figure 4-9 reveals an increase of the elastic scattering intensity for the $\phi_{C_{60}}^{wt} = 0.01$ PNC relative to that of pure PMMA, indicating a decrease in atomic motions for the PNC relative to the homopolymer. Further, as will be described in detail in a future work, quasi-elastic neutron scattering measurements of the same systems, above T_g, reveal that the PNC exhibits a broader distribution of polymer relaxation times relative to the homopolymer. Hence the increased elastic intensity for the PNC melt is attributed to motional restriction of polymer segments at the polymer-particle interfaces on the nanosecond time scale of the INS measurements, while all other polymer segments
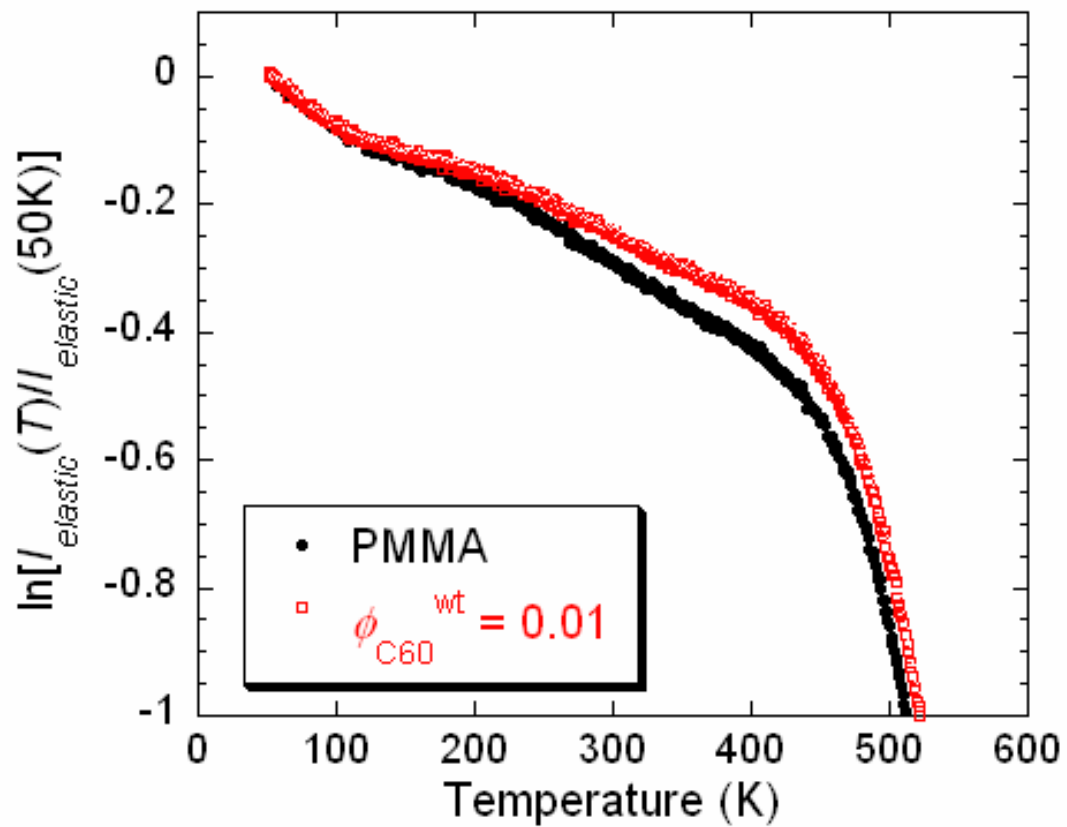
Figure 4-9: The decrease in the elastic scattering intensity, summed over all Q, as a function of temperature for PMMA and the ϕ_{C60}^{wt}=0.01 PNC.

retain homopolymer-like dynamics on this time scale. However, in contrast to this dynamic heterogeneity observed in the INS measurements, mechanical measurements suggest that the effect of C_{60} on polymer melt dynamics may be described in terms of a homogeneous increase in the local friction factor throughout the bulk of the material. Observations that support this latter suggestion include: the invariance of the shape of the PNC mechanical α-relaxation peak from that of pure PMMA (Figure 4-1a), the invariance of the temperature dependence of the PNC mechanical α-relaxation time from that of pure PMMA (Figure 4-1c), the invariance of the shape of the low frequency peak in the PNC melt loss modulus from that of pure PMMA (Figure 4-6), and the frequency shift in the rheological moduli over the entire frequency range of the measurements (Figure 4-3). The picture that emerges from these findings is that the heterogeneous PNC melt dynamics at the nanosecond time scale of the IENS measurements result in a homogeneous slowing of the bulk dynamics measured mechanically. The homogeneous effect on polymer dynamics on the time scale of τ_R can be attributed to the mechanism described above for the simulations. We also propose an alternative mechanism to describe the α-relaxation behavior as follows.

Motions associated with the mechanical α-relaxation peak are localized cooperative motions, and this begs the question as to how segments greater than 10 nanometers away from the particle surface would experience an equivalent reduction in dynamics as segments in direct contact with the surface. One way to interpret the shift in the α-relaxation dynamics of the PMMA-C_{60} PNCs may lie in the ideas presented by Long and Lequeux,[50] where a mechanism for the glass transition is proposed. In their work, Long and Lequeux regard system dynamics to be strongly heterogeneous, characterized by the presence of both slow domains and fast domains that result from thermally induced density fluctuations. They interpret the glass transition as a dynamical

effect that results from the percolation of slow domains throughout the system. In our case, the PMMA-C_{60} interactions enhance the fraction of slow domains in the PNC relative to the homopolymer. Consequently, the percolation of slow domains occurs at a higher temperature in the PNC than in the homopolymer, and hence the PNC T_g and associated α-relaxation motions are shifted to higher temperatures. Thus, in this framework, it is not necessary for the particles to influence all polymer segments uniformly to obtain a shift in the α-relaxation dynamics as found in the DMA measurements of the PMMA-C_{60} PNCs. Only a shift in the percolation temperature is necessary, and this can be accomplished via the polymer-particle interfacial interactions described heretofore.

4.5   CONCLUSIONS

We have shown how small concentrations of C_{60} in PMMA increase the melt shear moduli, the glass transition temperature and the longest relaxation time of the polymer. The increases in shear plateau modulus are associated with a so-called conventional "filler" effect; however the increases in T_g and τ_R are associated with a change in polymer matrix properties that reveals a breakdown of polymer "continuum solvent" behavior in the PNCs. Since the mechanical measurements resolve a uniform change in polymer dynamics with nanoparticle addition, it is tempting to attribute the decrease in dynamics to a decrease in free volume or an increase in polymer entanglement density associated tighter segmental packing due to the influence of the nanoparticles. However, no such structural changes are discerned; the increases in τ_R are shown to result from transient immobilization of polymer segments at the particle surface that lead to an increase in the effective friction experienced by the chains. An increase in the fraction of slowly relaxing polymer domains due to the PMMA-C_{60} interfacial

77

interactions is also proposed to account for the shift in T_g and the associated α-relaxation dynamics by increasing the temperature at which percolation of the slow domains occurs. The development of such dynamical heterogeneities upon the addition of nanoparticles is supported by simulations and by INS measurements that probe polymer segmental motions on a nanosecond time scale. Higher particle concentrations lead to more polymer-particle interfacial area and increase the magnitude of the observed effects. However, the growth of polymer-particle interfacial area is inhibited when increased particle concentration leads to the formation of larger particle agglomerates, and the magnitude of the effect on dynamics in this scenario is limited.

4.6 REFERENCES

[1]   W. B. Russel, D. A. Saville, and W. R. Schowalter, *Colliodal Dispersions* (Cambridge University Press, New York, 1989).

[2]   G. Tsagaropoulos, and A. Eisenburg, *Macromolecules* **28**, 396 (1995).

[3]   G. Tsagaropoulos, and A. Eisenberg, *Macromolecules* **28**, 6067 (1995).

[4]   C. Becker, H. Krug, and H. Schmidt, *Materials Research Society Symposium Proceedings* **435**, 237 (1996).

[5]   B. J. Ash, R. W. Siegel, and L. S. Schadler, *Journal of Polymer Science, Part B: Polymer Physics* **42**, 4371 (2004).

[6]   A. Bansal *et al.*, *Nat. Mater.* **4**, 693 (2005).

[7]   P. Rittigstein, and J. M. Torkelson, *Journal of Polymer Science, Part B: Polymer Physics* **44**, 2935 (2006).

[8]   R. Krishnamoorti, R. A. Vaia, and E. P. Giannelis, *Chemistry of Materials* **8**, 1728 (1996).

[9]   R. Krishnamoorti, and E. P. Giannelis, *Macromolecules* **30**, 4097 (1997).

[10]   K. Yurekli *et al.*, *Journal of Polymer Science, Part B: Polymer Physics* **39**, 256 (2000).

[11] Q. Zhang, and L. A. Archer, *Langmuir* **18**, 10435 (2002).

[12] M. E. Mackay *et al.*, *Nat. Mater.* **2**, 762 (2003).

[13] K. W. Putz *et al.*, *Journal of Polymer Science, Part B: Polymer Physics* **42**, 2286 (2004).

[14] F. Du *et al.*, *Macromolecules* **37**, 9048 (2004).

[15] A. Tuteja *et al.*, *Macromolecules* **38**, 8000 (2005).

[16] G. Galgali, C. Ramesh, and A. Lele, *Macromolecules* **34**, 852 (2001).

[17] M. J. Solomon *et al.*, *Macromolecules* **34**, 1864 (2001).

[18] P. Potschke, T. D. Fornes, and D. R. Paul, *Polymer* **43**, 3247 (2002).

[19] G. D. Smith *et al.*, *Journal of Chemical Physics* **117**, 9478 (2002).

[20] V. Pryamitsyn, and V. Ganesan, *Macromolecules* **39**, 844 (2006).

[21] R. Krishnamoorti, and K. Yurekli, *Current Opinion in Colloid & Interface Science* **6**, 464 (2001).

[22] T. Desai, P. Keblinski, and S. K. Kumar, *Journal of Chemical Physics* **122**, 134910/1 (2005).

[23] M. Vacatello, *Macromolecules* **34**, 1946 (2001).

[24] M. Vacatello, *Macromolecular Theory and Simulations* **11**, 757 (2002).

[25] F. W. Starr, T. B. Schroder, and S. C. Glotzer, *Physical Review E* **64**, 021802 (2001).

[26] F. W. Starr, T. B. Schroder, and S. C. Glotzer, *Macromolecules* **35**, 4481 (2002).

[27] D. Brown *et al.*, *Macromolecules* **36**, 1395 (2003).

[28] J. L. Keddie, R. A. L. Jones, and R. A. Cory, *Europhysics Letters* **27**, 59 (1994).

[29] J. H. van Zanten, W. E. Wallace, and W.-l. Wu, *Physical Review E: Statistical Physics, Plasmas, Fluids, and Related Interdisciplinary Topics* **53**, R2053 (1996).

[30] C. J. Ellison, and J. M. Torkelson, *Nat. Mater.* **2**, 695 (2003).

[31] J. Q. Pham, and P. F. Green, *Macromolecules* **36**, 1665 (2003).

[32]   C. L. Soles, J. F. Douglas, and W.-L. Wu, *Journal of Polymer Science, Part B: Polymer Physics* **42**, 3218 (2004).

[33]   B. M. Besancon, C. L. Soles, and P. F. Green, *Physical Review Letters* **97**, 057801 (2006).

[34]   A. Meyer *et al.*, *Review of Scientific Instruments* **74**, 2759 (2003).

[35]   S. Wu, *Journal of Polymer Science, Part B: Polymer Physics* **27**, 723 (1989).

[36]   P. Lomellini, and L. Lavagnini, *Rheologica Acta* **31**, 175 (1992).

[37]   K. Fuchs, C. Friedrich, and J. Weese, *Macromolecules* **29**, 5893 (1996).

[38]   M. Rubinstein, and R. H. Colby, *Polymer Physics* (Oxford University Press, New York, 2003).

[39]   J. D. Ferry, *Viscoelastic Properties of Polymers. 3rd Ed* (Wiley, New York, 1980).

[40]   M. E. Mackay *et al.*, *Science* **311**, 1740 (2006).

[41]   G. Chen, and G. Ma, *Applied Physics Letters* **72**, 3294 (1998).

[42]   E. T. Kopesky *et al.*, *Polymer* **46**, 4743 (2005).

[43]   E. Guth, *Journal of Applied Physics* **16**, 20 (1945).

[44]   H. M. Smallwood, *Journal of Applied Physics* **15**, 758 (1944).

[45]   J. L. Keddie, R. A. L. Jones, and R. A. Cory, *Faraday Discussions* **98**, 219 (1995).

[46]   J. A. Forrest *et al.*, *Physical Review Letters* **77**, 2002 (1996).

[47]   D. S. Fryer *et al.*, *Macromolecules* **34**, 5627 (2001).

[48]   C. J. Ellison *et al.*, *European Physical Journal E: Soft Matter* **8**, 155 (2002).

[49]   J. Berriot *et al.*, *Europhysics Letters* **64**, 50 (2003).

[50]   D. Long, and F. Lequeux, *European Physical Journal E: Soft Matter* **4**, 371 (2001).

Chapter 5: Local Polymer Dynamics in Polymer-C_{60} Mixtures[*]

The complexity of intermolecular interactions in polymer-nanoparticle systems leads to spatial variations in structure and dynamics at both the meso- and nano-scale. Much of this behavior is manifested in properties such as the glass transition and the viscosity. In the following, we will demonstrate that incoherent neutron scattering measurements of C_{60}-polymer mixtures reveal that local polymer chain backbone motions in the glassy state are suppressed relative to those of the pure polymer. Moreover, the scattering spectrum of the melt suggests that the influence of C_{60} on polymer dynamics is limited to the vicinity of the particles at nanosecond time scales. A model is presented to reconcile these observations with the bulk dynamical properties exhibited by the mixtures.

5.1 INTRODUCTION

Very small concentrations of nanoparticles, on the order of a percent, can significantly alter the phase behavior and the mechanical and electrical characteristics of polymeric materials. Insight into how nanoparticles influence the associated morphological structure[1-3] and system dynamics[4-6] of polymer-nanoparticle mixtures is only beginning to emerge, and the advancement of knowledge in these areas will be key to developing design rules to engineer materials with desired properties.

The complexity of interactions, polymer-particle, polymer-polymer and particle-particle, that determine the properties exhibited by polymer-based nanocomposites (PNCs) manifest a diverse range of effects on polymer dynamics. For example, dynamic

mechanical measurements show that PNCs containing silica particles exhibit two glass transition temperatures (T_gs).[7] Specifically, the particles are believed to induce two distinct regions of reduced polymer mobility near the particle surfaces: (1) chain segments tightly bound to the particle surfaces that do not relax over the experimental time scales and (2) loosely bound chains that give rise to an additional, higher, T_g when the particles are sufficiently close and the loosely bound chains around many particles overlap. Other investigations of PNCs reveal only a single T_g that is shifted due to the influence of nanoparticles.[5, 8-11] Particle-induced regions of altered polymer mobility are also suggested to underlie the T_g shifts in these materials. On the other hand, other PNC materials exhibit no change in the local dynamics associated with the T_g, while long-range motions of the chains are highly restricted.[12] Clearly, the effects of nanoparticles on polymer dynamics in each of these systems differ, and understanding the mechanism of influence is essential to discerning why this is the case.

Molecular dynamics (MD) simulations of PNCs reveal that changes in monomer packing near the polymer-particle interface lead to the formation of "shells" of perturbed polymer density around a nanoparticle which exhibit dynamics that differ from the neat polymer.[13, 14] These simulations further suggest that such dynamical heterogeneities can provide a rationale for the observed changes in T_g and viscosity in the PNCs.[13-15] The common conclusion that can be drawn from all the aforementioned experimental and simulated observations is that an understanding of the microscopic dynamics in PNCs is key to understanding material property enhancements (by "microscopic" here, we mean the length scale of a few bonds).

Neutron scattering measurements offer the unique possibility of analyzing the spatial dimensions of atomic processes in their development over time and provide an excellent means of evaluating the microscopic dynamics of interest in PNCs.[16, 17] In

82

this chapter, we use incoherent elastic neutron scattering (IENS) to examine three C_{60}-polymer PNCs: C_{60}-polystyrene (PS), C_{60}-poly(methyl methacrylate) (PMMA) and C_{60}-tetramethylbisphenol-A polycarbonate (TMPC). These materials exhibit an increase in their "bulk" T_g, as measured by differential scanning calorimetry and dynamic mechanical analysis and depicted in Figure 5-1. Here, we will demonstrate that insight into the mechanism by which C_{60} increases the T_g can be gained from IENS measurements of the materials in the glassy state. Further, mechanical measurements of these PNCs show no evidence of excess structural or dynamic heterogeneity relative to the neat polymer and suggest that the effect of the particles may be described in terms of an increased segmental friction coefficient for the polymer.[11] However, quasi-elastic neutron scattering (QENS) measurements reveal that the influence of C_{60} on polymer melt dynamics is limited to the vicinity of the particle surfaces at the nanosecond timescale. We use this finding to explain how the increases in the longest relaxation time of the polymer, τ_R, can be reconciled with a mechanism involving transient polymer segment-particle interactions.

5.2   EXPERIMENTAL DESCRIPTION

The C_{60}-polymer PNCs were made via a solution-dissolution/solvent-evaporation method. The C_{60} (Alpha Aesar[18], 99+ %) was added to organic solvents and sonicated (Sonicor, SC-40) for 15 minutes to disperse the fullerenes into solution. PMMA (Pressure Chemical; M_w = 254.7 kg/mol, M_w/M_n = 1.15), PS (Pressure Chemical; M_w = 152 kg/mol, M_w/M_n = 1.06), and TMPC (Bayer; M_w = 37.9 kg/mol, M_w/M_n = 2.75) were also dissolved in organic solvents, and the nanoparticle and polymer solutions were mixed in proportion to create the appropriate nanocomposite concentration. Toluene was
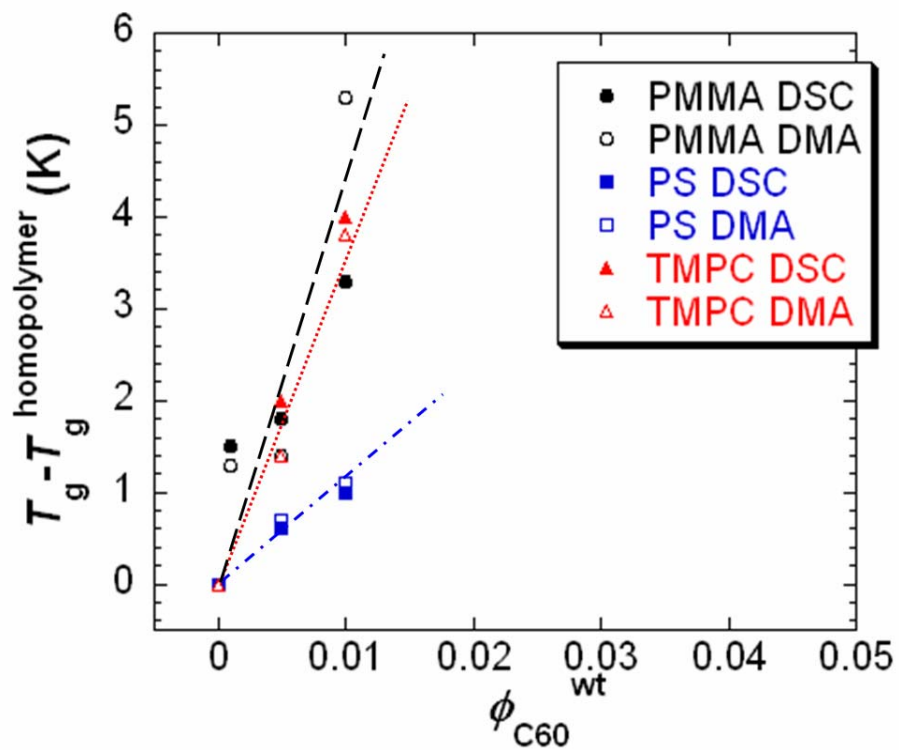
Figure 5-1: The change in glass transition temperature from that of the neat polymer as a function of C_{60} concentration. The dotted lines are a guide to the eye.

used to make the PMMA and PS samples, while 1,1,2,2-tetrachloroethane was used to make the TMPC samples. The solvent was evaporated from the mixtures at 348 K. Residual solvent was subsequently removed by drying the samples under high vacuum at 453 K for 15 h. The TMPC samples were further heated to 493 K for 30 min. We found that lower annealing temperatures were insufficient to completely remove residual solvent.

Aluminum boats containing the polymer samples were placed in an annular, thin-walled aluminum cell that was mounted on the High Flux Backscattering Spectrometer (HFBS)[19] on the NG2 beam line at the NIST Center for Neutron Research and cooled under vacuum. The spectrometer operated in two modes. The first was a fixed window mode (stationary Doppler drive), where the elastic intensity was recorded as the sample temperature, T, was increased from 50 K to 525 K at a rate of 1 K/min. The Doppler drive was also turned on to measure the QENS spectrum over a dynamic range of ± 11 μeV and over temperatures spanning 375 K to 525 K. This is a limited dynamic range, but the elastic scans, as will be seen in the following, suggest that faster processes, such as methyl rotations, are unaffected by C_{60}. Hence, measurements that resolve faster processes would not provide further information on the influence of C_{60} on polymer dynamics. Mechanical measurements that resolve the influence of C_{60} on slower processes have also been reported for one of the PNCs in a previous publication.[11] Raw data were normalized to monitor and to the intensity at the lowest measured temperature. Mean-square atomic displacements (MSD) and Fourier transforms of the QENS spectra were evaluated using software developed by NIST (Data Analysis and Visualization Environment).[20] For the evaluation of the QENS measurements, the resolution of the spectrometer was taken as the QENS spectrum of the sample at $T < 5$ K.

The incoherent scattering cross section of hydrogen is approximately 20 times greater than the total scattering cross section of C or O and approximately 40 times greater than its own coherent scattering cross section. Hence, in the C_{60}-polymer PNCs examined, the scattering is dominated by the incoherent scattering of the hydrogen atoms of the polymers and only the dynamics of the polymers is probed.

5.3   RESULTS AND DISCUSSION

We first discuss the polymer segmental dynamics, as determined from the incoherent elastic scattering intensity, $I_{el}(T)$. The focus of our attention will be on PNCs containing $\phi_{C60}{}^{wt}$ = 0.01; the most significant changes in T_g and τ_R occur at this concentration. C_{60} dispersion within each polymer host is qualitatively equivalent to that previously reported for PMMA;[11] micrographs which illustrate the C_{60} dispersion within the PS and TMPC hosts are included in Figure 5-2. Figure 5-3 shows I_{el}, summed over the momentum transfer range 0.25 Å^{-1} ≤ Q ≤ 1.75 Å^{-1}, plotted as a function of T for the neat polymers and the PNCs. In general, both Debye-Waller decay and anharmonic local segmental motions active in the time scale of the elastic window can contribute to the decrease in I_{el} with T for the polymers at $T < T_g$. In Figure 5-3a, ln[I_{el}] decreases linearly with T for PS, in a manner consistent with Debye-Waller predictions, up to the calorimetric T_g of the material. On the other hand, plots of ln[I_{el}] versus T show nonlinearities for both PMMA (Figure 5-3b) and TMPC (Figure 5-3c) for $T < T_g$. The nonlinearities can be attributed to methyl rotations ($T \approx$ 50 K to 100 K) and localized chain backbone motions[21] ($T \approx$ 200 K to 350 K) entering the elastic window of the spectrometer. All materials show a large drop in I_{el} near the calorimetric T_g.

I_{el} is increased for all PNCs relative to their homopolymer analogues, revealing a decrease in atomic motions of the polymer chain segments upon the addition of C_{60}. The
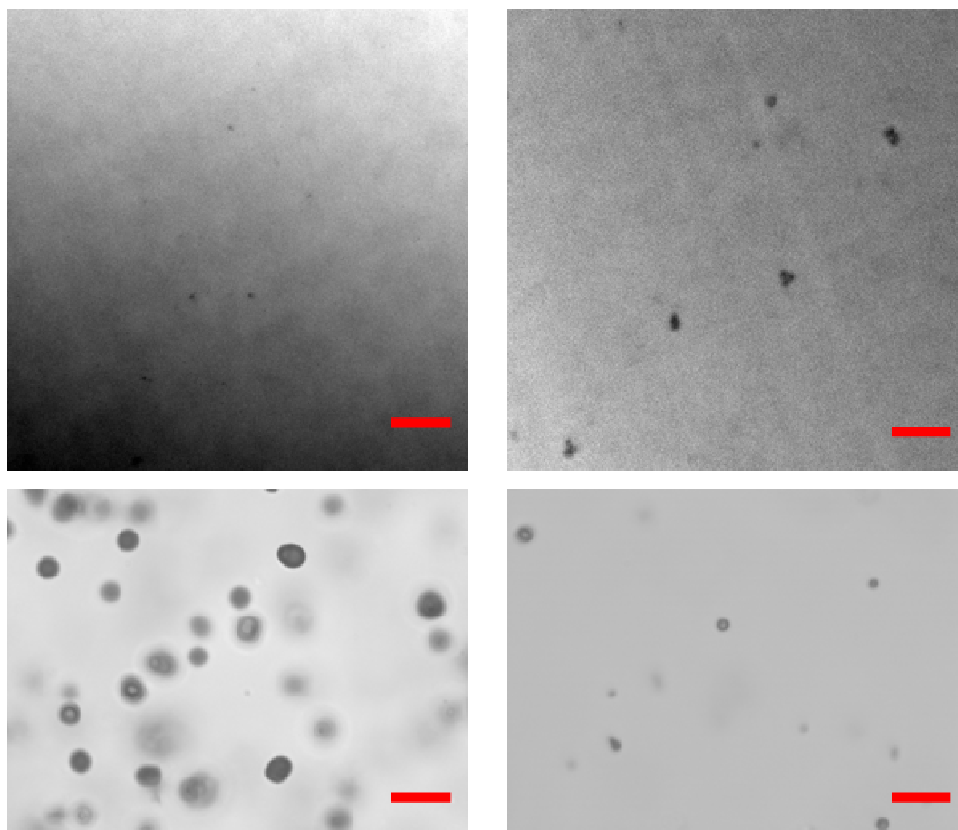
Figure 5-2: Micrographs depicting C_{60} dispersion within the PS and TMPC hosts at $\phi_{C60}{}^{wt} = 0.01$. Left column is PS, and right column is TMPC. Top row are TEM micrographs with 100 nm scale bars, and the bottom row are optical micrographs with 5 μm scale bars.
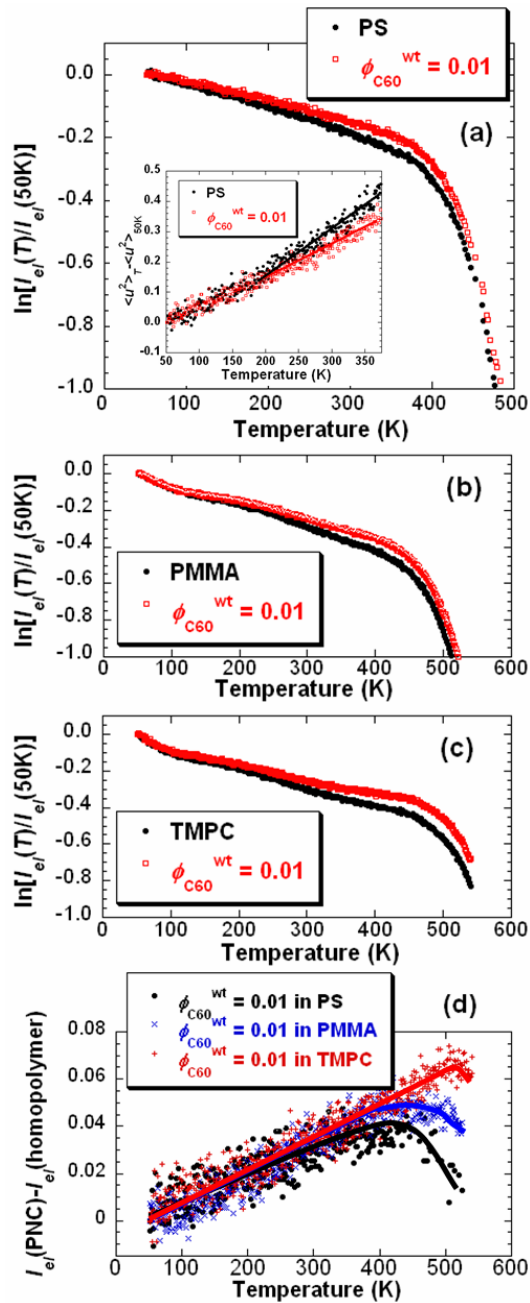
Figure 5-3: The decrease in the elastic scattering intensity as a function of temperature for (a) PS and $\phi_{C60}^{wt} = 0.01$ in PS, (b) PMMA and $\phi_{C60}^{wt} = 0.01$ in PMMA, and (c) TMPC and $\phi_{C60}^{wt} = 0.01$ in TMPC. The inset of (a) depicts the relationship between MSD and temperature described in the text. The difference between the elastic scattering intensity of the PNCs and neat polymers is given as a function of temperature in (d). The solid lines are a guide to the eye.

increase in I_{el} is observed over a very broad temperature range and cannot be explained solely by the increase in T_g for the composites; i.e., rescaling the x-axes in panels a-c in Figures 5-3 to $(T\text{-}T_g)/T_g$ will not result in a collapse of the PNC and neat polymer data. For PS, the decrease in the slope of $\ln[I_{el}]$ versus T, for $T < T_g$, upon C_{60} addition is indicative of a restriction of harmonic vibrations. For the PMMA and TMPC PNCs, the drop in I_{el} due to methyl rotations (at $T \approx 50$ K to 100 K) is unchanged from that of the neat polymers, indicating that the methyl rotations in the materials are unaffected by the C_{60} particles. At higher T, however, a suppression of the intensity drop associated with local backbone motions leads to an increase in I_{el} for the PMMA and TMPC PNCs relative to the neat polymers.

Figure 5-3d presents the difference between the elastic scattering intensities for the PNCs and the pure polymers, $[I_{el}(PNC) - I_{el}(homopolymer)]$, as a function of temperature. Interestingly, all the data superpose at low T and reach a peak that is positioned relative to the calorimetric T_g of the pure polymer. The superposition of the data indicates that the magnitude of the suppression of polymer dynamics in the glassy state, due to the C_{60} influence, is comparable for all systems. To further characterize the glassy behavior, we evaluate the MSD, $<u^2>$, of the materials using a linear fit of $\ln I_{el}$ vs. Q^2 in the Debye-Waller approximation,[16, 17]

$$\ln I_{el} \propto \left(-\frac{1}{3} Q^2 \langle u^2 \rangle \right). \tag{5-1}$$

The resulting MSD for PS and the PS-C_{60} PNC (evaluated for 0.38 Å^{-2} < Q^2 < 2.56 Å^{-2}) is plotted in the inset of Figure 5-3a. The behavior of the other polymer systems is similar, but methyl rotations that enter the time window of the spectrometer influence the relationship between $<u^2>$ and T, even at T as low as 50 K, and obscure the following analysis. Hence, we focus our attention on the PS materials.

89

We first note an observation that was not apparent from inspection of the I_{el} data; PS does not exhibit harmonic behavior above 200K. For $T < 200$ K, both PS and the PS-C_{60} PNC exhibit equivalent $<u^2>$; the linear dependence of $<u^2>$ on T enables a determination of the harmonic force constant of the materials, $\kappa \approx 3k_BT/<u^2>$, which is also equivalent for the pure polymer and composite. For $T > 200$ K, the PS $<u^2>$ exhibits a stronger dependence on T and exceeds that of the composite. Although the harmonic approximation is not strictly valid in this regime, the T dependence of $<u^2>$ for $200K < T < 350K$ can be well described by a linear fit for both the neat polymer and composite. The determination of a force constant within this temperature range, $\kappa^{200K-350K}$, provides a means to evaluate the restriction of the relaxation process associated with local polymer chain backbone motions due to the addition of C_{60}. This analysis yields an effective local "stiffness"[22] of the material and estimates an increase in $\kappa^{200K-350K}$ of 24% for the composite relative to the neat polymer.

The suppression of the local relaxation dynamics of the composite is consistent with an enhancement of cohesive interactions in the system, which may be the root of the increase in T_g for the PNCs; i.e., the system must acquire more thermal energy before polymer segments can overcome local energy barriers and thereby enable polymer center-of-mass motions. It has even been proposed that the local segmental relaxation processes restricted in the composite are associated with the short-time regime of the α-relaxation.[21] MD simulations of polymer melts by Smith et al.[23] have suggested that both increased polymer segment packing densities and the energy topography of a surface can lead to stronger caging of polymer segments near an attractive surface. Our results indicate that C_{60} induces similar effects in the glassy state of the polymers investigated, and that the effects can be discerned from the bulk IENS measurements.

Each curve in Figure 5-3d exhibits a maximum at $\approx$ 50 K above the neat polymer calorimetric T_g. The decrease of $[I_{el}(PNC) - I_{el}$ (homopolymer)$]$ for $T > T_g + 50$ K is consistent with the PNC melt density and relaxation dynamics homogenization toward that of the pure polymer with increasing temperature found in MD simulations.[13] It is noteworthy that the absence of a "kink" in the I_{el} versus T data for the PNCs at $T > T_g$ suggests that the decrease of $[I_{el}(PNC) - I_{el}$ (homopolymer)$]$ is not due to the sudden onset of diffusive motions associated with a fraction of polymers strongly influenced by the particle surfaces.[7] Rather, we suggest that a transient immobilization of polymer segments at the particle surfaces becomes less significant at higher T, as nearest neighbor distances increase and weaken the polymer-particle interactions relative to the thermal energy of the system.

To further explore this last suggestion, we consider the melt dynamics of the PNCs. The increased I_{el} for the PNCs in the melt ($T > T_g$) could be due to either of two effects: (1) a "permanent" adsorption of polymer segments to the particle surface that immobilizes the adsorbed atoms over long time scales, or (2) a transient immobilization of the polymer segments closest to the particle surface, which may slowly exchange locations with segments from neighboring chains. In the former, the dynamics of only a fraction of the polymer segments are affected by the particles, and the bulk of the polymer remains unaffected. This appears not to be the case in the C_{60} PNCs, as our measurements show an increase in the bulk T_g of the PNCs (Figure 5-1). Moreover, mechanical rheological measurements of the PMMA-C_{60} PNCs reveal an increase in the longest relaxation time that is not consistent with a permanent immobilization of only a fraction of polymer chains.[11] We argue that the latter description of a transient segmental immobilization is a more appropriate description of the behavior of the C_{60} PNCs.

91

Immobilization of polymer segments at the particle surface over nanosecond time scales is supported by the QENS data. To illustrate this, we evaluate the intermediate scattering function, $S(Q,t)$, for the PMMA samples at a melt temperature of 525 K in Figure 5-4. Figure 5-4 reveals an increase in $S(Q,t)$ for the PNC relative to the pure polymer over the entire resolvable time scale. In fact, the $S(Q,t)$ data of PMMA can be well fit to the $S(Q,t)$ data of PMMA-C_{60} by adding an elastic contribution according to the following relationship,

$$S(Q,t)_{PMMA-C_{60}} = \alpha + (1-\alpha)S(Q,t)_{PMMA} \qquad (5\text{-}2)$$

where $\alpha = 0.025$ represents the fraction of immobilized polymer chain segments. This relation holds over the entire Q range measured by the HFBS. Hence, we attribute the difference between the pure polymer and PNC $S(Q,t)$ to the immobilization of polymer segments at the polymer-particle interfaces over nanosecond time scales; all other polymer segments retain homopolymer-like dynamics. This finding is similar to observations in PDMS-silica mixtures.[24] The time scale associated with immobilization of the chain segments at the C_{60} surfaces, however, must be much less than the longest relaxation time of the polymer chains. In this case, the local influence of the particles can be felt by many polymer segments throughout the time scale of the longest relaxation. Consequently the increases in τ_R measured via rheology can be described by an increase in the local friction experienced by the chain.[11] We note that the relative dependence of α on T can be resolved from Figure 5-3d, as [I_{el}(PNC)-I_{el}(homopolymer)] is proportional to α.

Another way to interpret the increase in T_g for the C_{60} PNCs may be understood in terms of the dynamic percolation model of Long and Lequeux[25]. In this model the dynamics of a melt are characterized by the existence of "fast" and "slow" domains, associated with density fluctuations in the system. Percolation of the "slow" domains
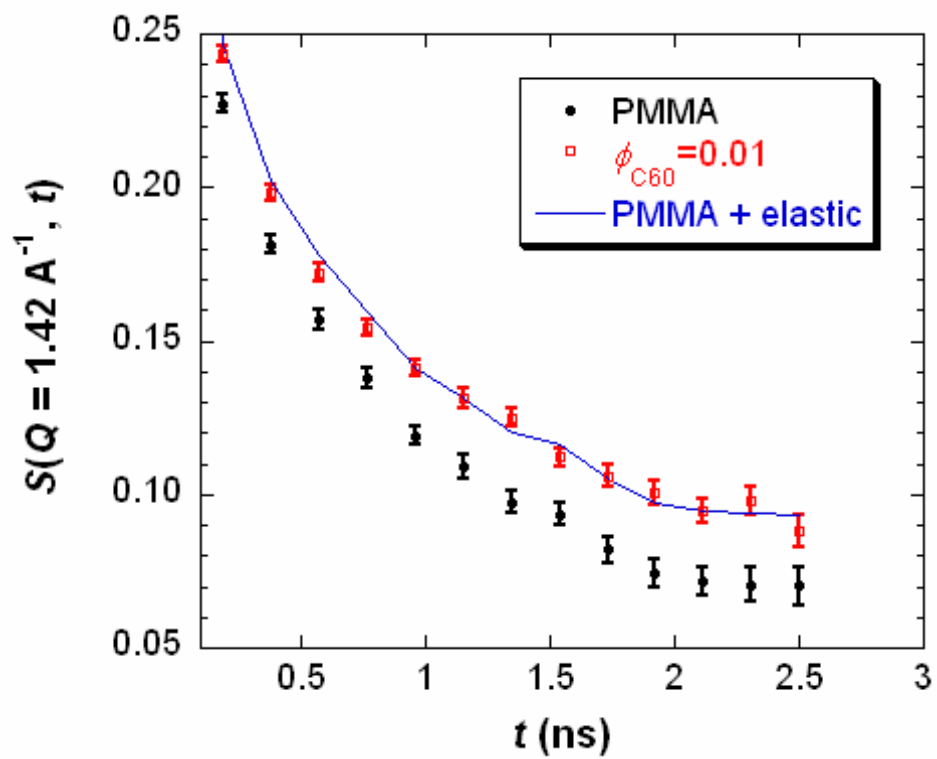
Figure 5-4: Intermediate scattering function for PMMA and the $\phi_{C60}{}^{wt} = 0.01$ in PMMA PNC at $Q = 1.42$ Å^{-1} and $T = 525$ K. The solid line represents the PMMA data corrected for an elastic contribution according to equation 2 with $\alpha = 0.025$.

occurs upon decreasing the temperature and is associated with the glass transition. The presence of immobilized polymer segments at the particle surfaces increases the fraction of "slow" domains in the PNC relative to the neat polymer; the enhancement in the fraction of slow domains in the PNC will induce their percolation at a higher temperature relative to the neat polymer and result in an increase in T_g for the PNC.

5.4   CONCLUSIONS

In summary, we have shown that the effect of adding C_{60} to three different polymer hosts, PS, PMMA, and TMPC, is to suppress the polymer segmental dynamics in all cases. Specifically, the local polymer chain backbone motions in the PNCs are suppressed relative to those of the neat polymer, which likely plays a role in the observed increases in T_g of the materials. In the melt, the dynamics of the polymer segments in the vicinity of the particle surfaces are suppressed relative to the neat polymer, and this effect results in an excess elastic fraction of polymer segments at the nanosecond time scale. The elastic fraction diminishes as the temperature is increased above $T_g + 50$ K. These results suggest that effects on polymer dynamics that are limited to the vicinity of particle surfaces at the nanosecond time scale can account for changes in bulk dynamics resolved with mechanical measurements.

5.5   REFERENCES

[1]   R. B. Thompson *et al.*, *Science* **292**, 2469 (2001).

[2]   M. E. Mackay *et al.*, *Science* **311**, 1740 (2006).

[3]   S. C. Warren, F. J. DiSalvo, and U. Wiesner, *Nat. Mater.* **6**, 156 (2007).

[4]   M. E. Mackay *et al.*, *Nat. Mater.* **2**, 762 (2003).

[5]   A. Bansal *et al.*, *Nat. Mater.* **4**, 693 (2005).

[6]   R. A. Narayanan *et al.*, *Physical Review Letters* **97**, 075505/1 (2006).

[7]   G. Tsagaropoulos, and A. Eisenburg, *Macromolecules* **28**, 396 (1995).

[8]   C. Becker, H. Krug, and H. Schmidt, *Materials Research Society Symposium Proceedings* **435**, 237 (1996).

[9]   B. J. Ash, R. W. Siegel, and L. S. Schadler, *Journal of Polymer Science, Part B: Polymer Physics* **42**, 4371 (2004).

[10]   P. Rittigstein, and J. M. Torkelson, *Journal of Polymer Science, Part B: Polymer Physics* **44**, 2935 (2006).

[11]   J. M. Kropka *et al.*, *Macromolecules* **40**, 5424 (2007).

[12]   F. Du *et al.*, *Macromolecules* **37**, 9048 (2004).

[13]   F. W. Starr, T. B. Schroder, and S. C. Glotzer, *Physical Review E* **64**, 021802 (2001).

[14]   G. D. Smith *et al.*, *Journal of Chemical Physics* **117**, 9478 (2002).

[15]   V. Pryamitsyn, and V. Ganesan, *Macromolecules* **39**, 844 (2006).

[16]   B. Frick, and D. Richter, *Science (Washington, D. C.)* **267**, 1939 (1995).

[17]   C. L. Soles *et al.*, *Physical Review Letters* **88**, 037401/1 (2002).

[18]   *The use of commercial products identified in this paper does not imply recommendation or endorsement by the National Institute of Standards and Technology, nor does it imply that the materials or equipment identified are necessarily the best available for the purpose.*

[19]   A. Meyer *et al.*, *Review of Scientific Instruments* **74**, 2759 (2003).

[20]   http://www.ncnr.nist.gov/dave.

[21]   J. Colmenero, and A. Arbe, *Physical Review B: Condensed Matter and Materials Physics* **57**, 13508 (1998).

[22]   R. A. Riggleman, J. F. Douglas, and J. J. de Pablo, *Journal of Chemical Physics* **126** (2007).

[23]   G. D. Smith, D. Bedrov, and O. Borodin, *Physical Review Letters* **90**, 226103/1 (2003).

[24]   V. Arrighi *et al.*, *Polymer* **39**, 6369 (1998).

[25]   D. Long, and F. Lequeux, *European Physical Journal E: Soft Matter* **4**, 371 (2001).

Chapter 6: Percolation Model to Describe the Glass Transition Temperature in Polymer Nanocomposites

6.1   INTRODUCTION

Despite decades of research on the subject, a detailed understanding of the glass transition remains elusive.   It is still controversial whether the phenomenon is a consequence of an underlying phase transition that is governed by thermodynamic variables such as specific volume and entropy,[1-4] or simply a dynamical phenomena that results in a freezing of motions due to relaxation times becoming large relative to observation times.[5-7]   Nonetheless, the topic still attracts a tremendous amount of interest, and a broad array of efforts are being actively pursued to try and answer many unresolved questions.[8-12]

One thing that has become clear in the past few years is that dynamics at or near the glass transition are spatially heterogeneous.[13-15] There is also a growing amount of evidence to support spatial correlations between such heterogeneities becoming long-ranged as the glass transition is approached.[3, 10, 16-18]   Using this idea, dynamic scaling laws have been derived for system relaxation times that are consistent with many experimental measurements.[18]   These findings support an interpretation of the glass transition based on the percolation of slow domains throughout the system, and within this framework, changes in the percolation threshold with the dimensionality of a system have even been shown to account for the thickness dependence of the glass transition temperature (T_g) in thin polymer films.[19, 20]

Inspired by these findings and the many analogies that have been drawn between polymer thin films and polymer-based nanocomposites (PNCs) in the literature,[21-23] we ask how these percolation ideas might apply to the T_g behavior of PNCs. A number

97

of experimental observations of PNC T_g have been consistent with a percolation interpretation,[24, 25] but to our knowledge no modeling work has been done to relate PNC T_g changes to percolation phenomena. Our primary interest was in determining whether a percolation model could be developed to emulate the T_g behavior of PNCs. For instance, could the model predict both increases and decreases in T_g with nanoparticle content, as is seen experimentally? Could the model also predict the experimentally observed particle size dependence of the T_g changes? Further, how could particle influence on the interfacial polymer behavior be accounted for? And lastly, would the results we get from such a model be strictly qualitative, or could quantitative information be extracted from it? We address these questions in the sections that follow.

6.2   THE MODEL

6.2.1   Percolation Theory

Percolation theory has been employed to model a wide variety of phenomena and continues to be of interest in a number of areas.[26, 27] Porous media problems have perhaps received the most attention; galactic star formation, the gelation of branched macromolecules, and the spread of epidemics in an ensemble of living things, to name a few, have all been associated with a percolation process as well. In fact, a number of types of percolation, site, bond, site-bond, correlated, directed bond, and more, have been employed to emulate specific processes of interest. Here, we develop a site percolation model to evaluate the behavior of PNC T_gs. As described in the introduction, one interpretation of the glass transition is based on the percolation of slow domains throughout the system. This interpretation is illustrated schematically in Figure 6-1 for the 2D case. Essentially, a material is viewed as being composed of both fast and slow
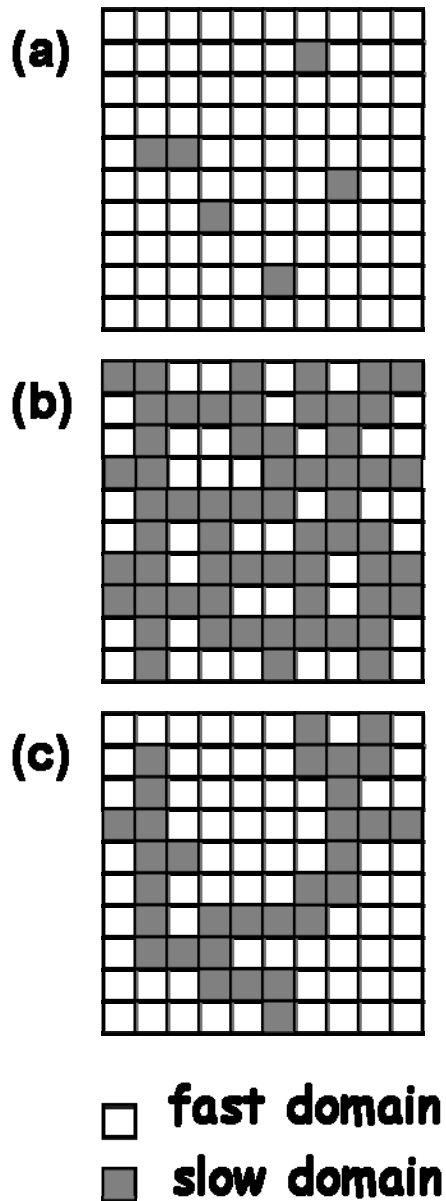
Figure 6-1: Schematic of the percolation interpretation of the glass transition temperature. The lattice represents a material broken down into individual dynamic domains that can be characterized as fast or slow. At high temperatures (a) the material is largely composed of fast domains, whereas at low temperatures (b) the material is largely composed of slow domains. The glass transition temperature is associated with the initial formation of a percolating cluster of slow domains (c).

domains. As the system is cooled from the melt state, a larger fraction of the domains become slow. The glass transition is associated with the temperature at which a percolating cluster of these slow domains, a series of nearest neighbor slow domains that spans to all outer interfaces of the system, fist appears and hence controls the bulk dynamics of the system. It is clear from experimental observations that nanoparticles can alter the T_g exhibited by polymers.[21, 22, 24, 25, 28, 29] It is tempting to attribute these effects to a change in the percolation behavior of slow domains in the system upon the addition of nanoparticles. Thus, a relevant question is how nanoparticles might affect the distribution, and eventual percolation, of slow domains in a PNC relative to the neat polymer. Our model will address this question by evaluating how lattice impurities affect the percolation threshold, p_c, of the system. There have been some recent efforts to study the effect of impurities on the percolation process.[30-32] These studies have focused on interpreting results in terms of the transfer of electronic excitation energy in porous matrices or the deposition of conducting particles onto contaminated surfaces and, in some cases, have dealt with cases specific to polyatomic species. This work not only extends these results to the T_g of PNCs, but also incorporates unique features to the model in order to account for specific aspects of PNCs observed experimentally.

To model PNCs, impurities are randomly placed on a periodic square lattice of linear size L, which contains $N = L \times L$ sites, subject to the constraint that impurities can not be nearest neighbors. The constraint against nearest neighbors allows us to unambiguously distinguish the effects of impurity size (nearest neighbor impurities would result in a larger effective impurity size and hence an impurity size dispersion for any given system). The lattice impurities represent the nanoparticles in the modeled PNC, and the remaining lattice sites represent polymer domains.

In the random site percolation problem, lattice sites are occupied (o) with probability p. The minimum occupation fraction that results in a cluster of occupied sites, i.e., slow domains in our context, that connects all external boundaries in an infinite lattice is denoted as the percolation threshold, p_c. Here, we establish that the sites labeled as impurities are not polymer and hence are not considered for occupation as in the random percolation problem. The impurity sites are treated strictly as either occupied or unoccupied sites in the percolation determination. As will be further illustrated in the results section, these two treatments realize unique physical situations observed experimentally: particles that are wet by the polymer and particles that are not wet by the polymer. In both treatments the particles can be viewed as dense slow domains, as would be expected for the addition of dense inorganic particles to a polymer host. The difference between the two cases is that when particles are wet by the polymer, two slow polymer domains can span across a particle. On the other hand, when particles are not wet by the polymer, a void remains between the polymer and particle and two slow polymer domains can not span across a particle. A schematic representation of these two cases is given in Figure 6-2.

To account for variations in the particle-polymer interaction strength, an additional modification to the lattice must be made. Thus, in some instances, we allow the lattice impurities, or nanoparticles, to have a "skin" of influence on the polymer sites. This interfacial region can be defined by two parameters: (1) the strength of the interaction, δ, which defines the occupation probability of the interfacial sites, $p' = p\pm\delta$; and (2) the number of neighboring lattice sights over which the interface exists. We note that the interfacial sites of different particles are allowed to overlap, but that all interfacial sites exhibit the same δ, i.e., the interfacial effects are not additive. We further note that the occupation probability used to determine p_c is the occupation probability of the bulk
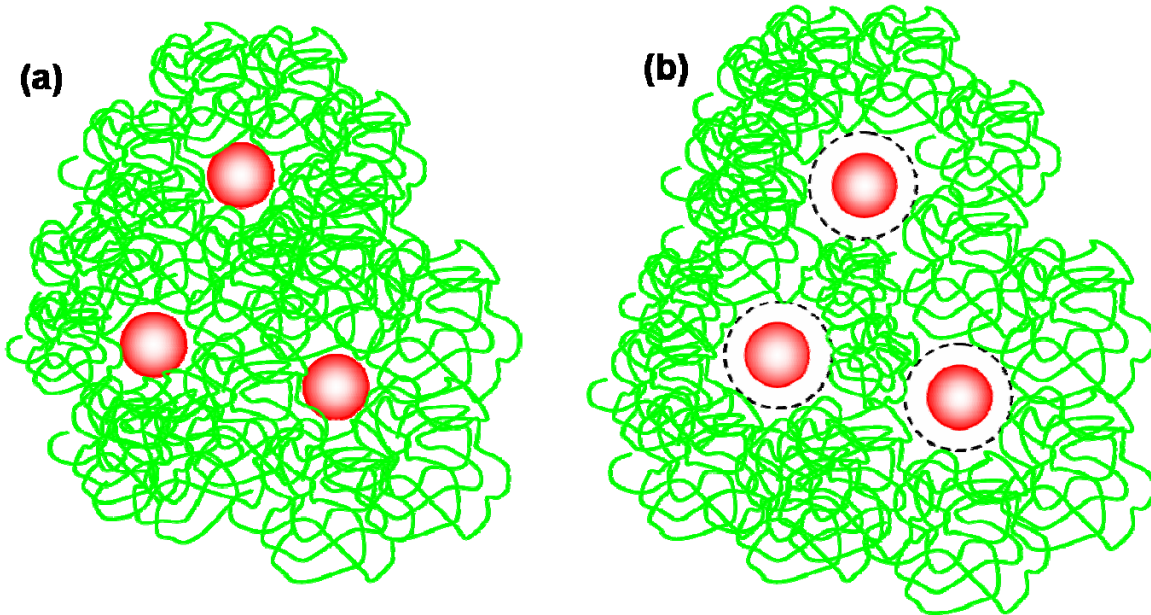
Figure 6-2: Schematic representation of PNCs when (a) particles are wet by the polymer
and (b) particles are not wet by the polymer. If two slow polymer domains
are adjacent to a particle in (a), a slow cluster will span the particle. In (b) a
void remains between the particle and polymer, and the particles are always
surrounded by a low density, fast region. Thus slow domains can not span
across a particle in this scenario.

polymer sites (not that of the total lattice), unless otherwise specified. This is an important distinction, because the addition of impurities to the lattice, with or without "skins", will alter the total lattice occupied fraction. However, our interest lies in how such impurities alter the percolation behavior at a given polymer occupation fraction, which, as will be described in further detail later, is representative of the system temperature.

In this work, impurity fractions, ϕ, up to 0.25 are evaluated for various impurity sizes and shapes and for $L = 32$, 64, 128, and 256. The percolation threshold of the system is evaluated according to the following steps: (1) a lattice configuration is generated and occupied according to the rules described above; (2) cluster analysis is performed using the Hoshen-Kopelman algorithm[33] to determine whether a percolating cluster of occupied domains exists; (3) this process is repeated a large number (≥ 500), n, of times to determine the number, m, of runs that generate a percolated cluster; (3) the probability of the system to percolate, $P(p) = m/n$, is determined and the procedure is repeated for all values of the system parameters of interest; (4) the common intersection point of $P(p)$ for all L, as depicted in Figure 6-3, of a given lattice configuration is taken as p_c. The algorithm was validated by evaluating the well known case of site percolation on a square lattice; the $P(p)$ curves obtained for all sizes of the square lattice intersect at an occupation probability $p_c^{2D} \approx 0.593$, in agreement with the result given by Stauffer.[27]

While many PNCs of interest are 3D, the systems evaluated here are 2D. Despite this discrepancy, we expect the 2D results will capture many of the qualitative aspects of the problem. A major advantage for the 2D systems is that they are very easily visualized and are less calculation intensive than for 3D. We can thus use the 2D results to gain insights into the important phenomena and focus the more calculation intensive 3D

103
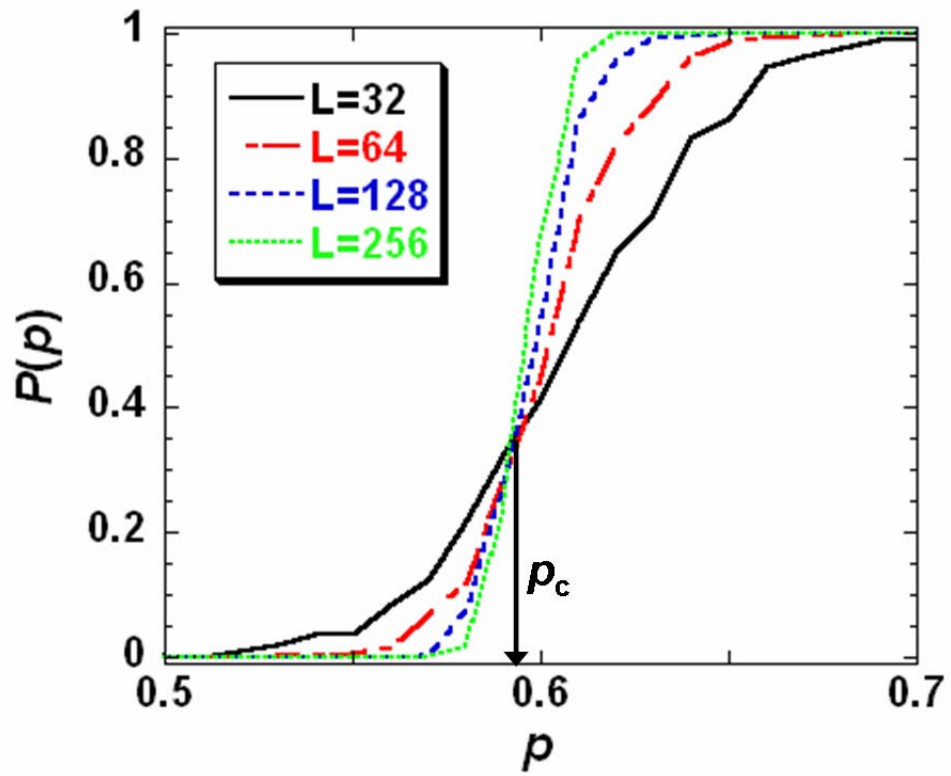
Figure 6-3: The probability of a pure lattice to percolate plotted against the occupation probability for a range of lattice sizes. The common intersection point of the curves for different lattice sizes represents the percolation threshold of the system.

efforts on these phenomena. The 3D systems are under study now, and the 2D and 3D results will be used as the extremes of a study to evaluate the behavior of the transition between the two dimensionalities in the frame work of thin film PNCs.

6.2.2   Connection Between p_c and T_g

Although there is evidence that points to the glass transition being associated with the percolation of domains of slow dynamics throughout the system,[10, 17, 34] the exact origin of the slow domains is still widely debated. Within the framework that the dynamic heterogeneities of the system stem from thermally induced density fluctuations, a relationship between the relative percolation thresholds of systems and their T_gs can be made.[19, 20] To facilitate the interpretation of our model results in terms of PNC T_g, we will use the relation derived by Long and Lequeux,[19] based on a Gaussian distribution of densities in the system, to convert changes in the system p_c to changes in T_g. An outline of the development of the relationship follows. We note, however, that the changes in p_c determined by the model predict a change in T_g *independent* of the underlying cause of the dynamic heterogeneities in the system.

It is first necessary to define a slow domain, for which a density ρ_c is designated above which a microscopic domain is in a very high viscosity state. In order to be in a viscous state, the domain must also contain a minimum number of monomers, N_c, such that the lifetime of the slow domain is sufficiently long. This defines the volume of a microscopic domain, v_o,

$$v_o \approx \frac{N_c}{\rho_{eq}}$$

(6-1)

where ρ_{eq} is the equilibrium bulk density.

The density fluctuations of the subunits of volume v_o are described to have Gaussian statistics according to the probability distribution,

$$P(T,\rho) \propto \exp\left(\frac{-(\rho-\rho_{eq})^2 K v_o}{2\rho_{eq}^2 T}\right)$$ (6-2)

where K is the bulk modulus and T is the temperature. As temperature is decreased from the melt state, the fraction of slow domains increases. At T_g domains of density larger than ρ_c percolate, hence

$$\int_{\rho_c}^{\infty} P(T_g,\rho)d\rho = p_c$$ (6-3)

This integral can be evaluated to give

$$\frac{\rho_c-\rho_g}{\sigma\rho_g} = F(p_c)$$ (6-4)

where $\sigma^2 = T/Kv_o$, ρ_g is the bulk density at T_g, and $F(x)$ is the reciprocal function of $Erf(x)$, which is defined by

$$Erf(x) = \frac{1}{(2\pi)^{1/2}} \int_x^{\infty} du \exp\left[\frac{-u^2}{2}\right]$$ (6-5)

For two systems of identical thermodynamic properties (bulk modulus, thermal expansion coefficient, and density) but varying percolation thresholds, the difference of the above equation for the two systems gives

$$\frac{\Delta T_g(n)}{T_g} = [F(p_c(n))-F(p_c)]\frac{1}{N_c^{1/2}}$$ (6-6)

where n represents the changing parameter of the systems. Long and Lequeux[19] used this relation to describe T_g changes in polymer thin films with film thickness. Here, we use it to describe T_g changes in systems with impurities, which we relate to PNCs. Our extension of the relation was motivated by the many parallels between polymer thin films and PNCs established in the literature[21-23] and the success of the Long and Lequeux method to describe T_g behavior in thin polymer films.[19]

106

We now further address a comment made previously about the relation between the occupation of polymer domains and the system temperature, and why the bulk polymer occupation fraction is used to determine p_c, rather than the total lattice occupation fraction. An occupied polymer domain represents a slow domain (versus a fast unoccupied domain). As the system temperature is decreased, the fraction of slow polymer domains in the system will increase. Hence, the polymer occupation fraction is inversely related to the temperature. Our interest is in how particles change the temperature at which slow domains percolate within in PNC. To compare the PNC and neat polymer in an equivalent manner, we must look at the occupation of the polymer only domains in the PNC.

6.3   RESULTS AND DISCUSSION

In the following analysis, we will focus on the critical percolation behavior of the system. In particular, the evolution of the percolation threshold, and hence glass transition temperature, with impurity concentration, impurity size, impurity shape, and impurity interfacial effects. The plots of $\Delta T_g/T_g$ that follow are all based on the relation in equation 6-5 above, with the only changing factor in the relation being the percolation threshold of the system. N_c is taken as $100^{2/3}$ for our calculations; this is the appropriate 2D conversion of the value that has been determined to give a good fit to experimental results in 3D systems.[19]

6.3.1   Impurity Treatment

Both increases and decreases in the T_g of polymers have been observed upon the addition of nanoparticles.[28, 29] Thus, a model to describe the effects of nanoparticles

on polymer T_g would need to be able to account for changes of T_g in either direction. As explained in the model description, the lattice impurities we employ are not occupied with probability, p, as in the random site percolation problem. Rather, the impurities are simply treated as either occupied or unoccupied during the percolation determination. The system $\Delta T_g/T_g$ predicted by our model for single site impurities of both treatments is depicted in Figure 6-4 as a function of ϕ. There are two main points we would like to draw from this data. The first is that the two impurity treatments change T_g in opposite directions, such as would be expected for the case of nanoparticles that are wet by the polymer $(+\Delta T_g)$ versus nanoparticles that are not wet by the polymer $(-\Delta T_g)$. In both treatments, the nanoparticles can be viewed as dense, slow domains, as would be the case for the addition of inorganic particles to a polymer host. However, if the polymer does not wet the particles, then slow polymer domains can not span a particle. In this case there is region of free volume surrounding the particle that prevents a percolating cluster from spanning through its vicinity. On the other hand, slow polymer domains can span particles that are wet by the polymer. The second point is that the two impurity treatments give qualitatively similar results on opposite sides of the $\Delta T_g = 0$ axis. Thus, it is only necessary to evaluate one of these impurity treatments to understand the physical predictions of the model (this holds for different impurity sizes and impurity interfacial effects as well). For this reason, the remaining portions of this manuscript will consider only unoccupied treatment of impurities.

Physically, the decrease in T_g that results from unoccupied site impurities can be explained in terms of an increase in the number of sites required to connect any two points in the system. The impurities introduce obstacles to the formation of clusters in the system, requiring a large cluster to form many paths that travel around these obstacles in order to percolate the system.
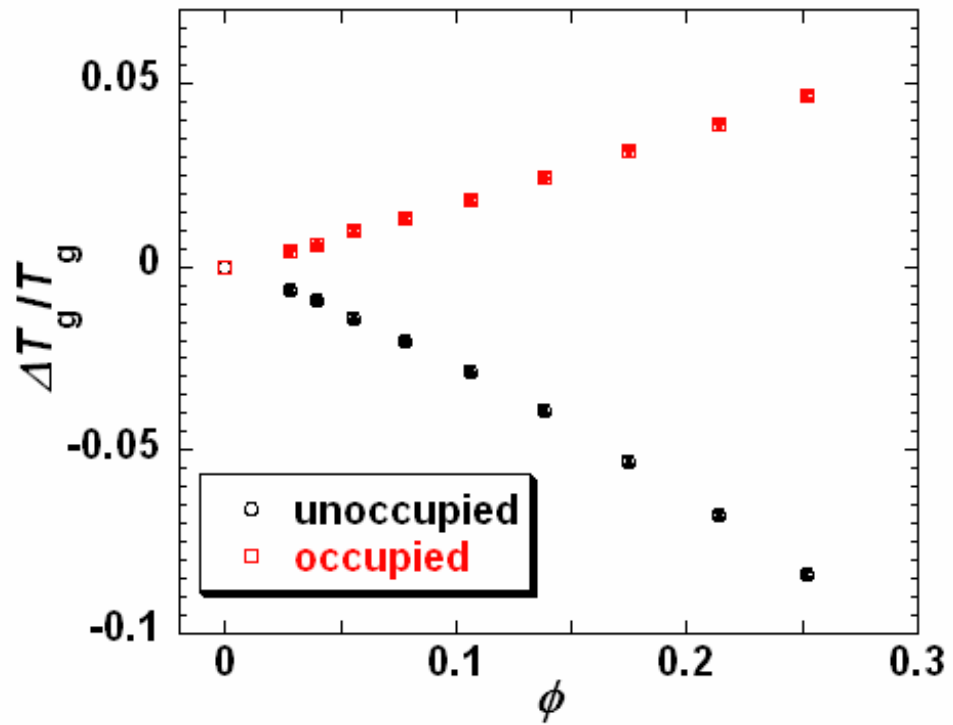
Figure 6-4: The change in the glass transition temperature as a function of single site impurity concentration for occupied and unoccupied impurity treatment.

6.3.2 Impurity Size

Our interest in the effect of impurity size on ΔT_gs predicted by our model stems from experimental observations that particles with dimensions of the order of tens of nanometers or less can influence the T_g of polymers, while larger particles of the same chemical make-up have no resolvable influence on the T_g of the same polymer.[35] The ability of nanometer dimensioned particles to affect the bulk T_g of PNCs is attributed to the large surface-to-volume ratio of the nanoparticles and the influence they exhibit on polymer segments that neighbor the particle surface[24, 25] and/or the small interparticle distances within which the polymer chains are confined.[21, 22] Figure 6-5b shows the change in T_g determined from our percolation model for a range of square impurity sizes as a function of impurity concentration. A clear decrease in the magnitude of $\Delta T_g/T_g$, for a given ϕ, with impurity size is observable. The very small changes in T_g for the largest impurities are consistent with an inability to experimentally resolve changes in T_g for micron-sized particles. We can understand the impurity size dependence of the T_g changes in terms of the correlated location of impure sites for the case of the larger impurities. Relative to the single site impurities, larger impurities leave larger regions of the lattice pure, with the impure sites all bound together. This leads to a less effective obstacle to cluster growth and percolation.

The monotonic dependence of the magnitude of $\Delta T_g/T_g$ on impurity size is also consistent with speculation based on experimental observations that the effect of nanoparticles on T_g scales with the polymer-particle interfacial interaction area or the nearest neighbor interparticle distance. To evaluate the correspondence of these experimental observations to our model results, we calculated the concentration of impurity perimeter sites (based on the number of nearest neighbors to lattice impurities) and nearest neighbor interparticle distances (calculated based on a circular impurity of
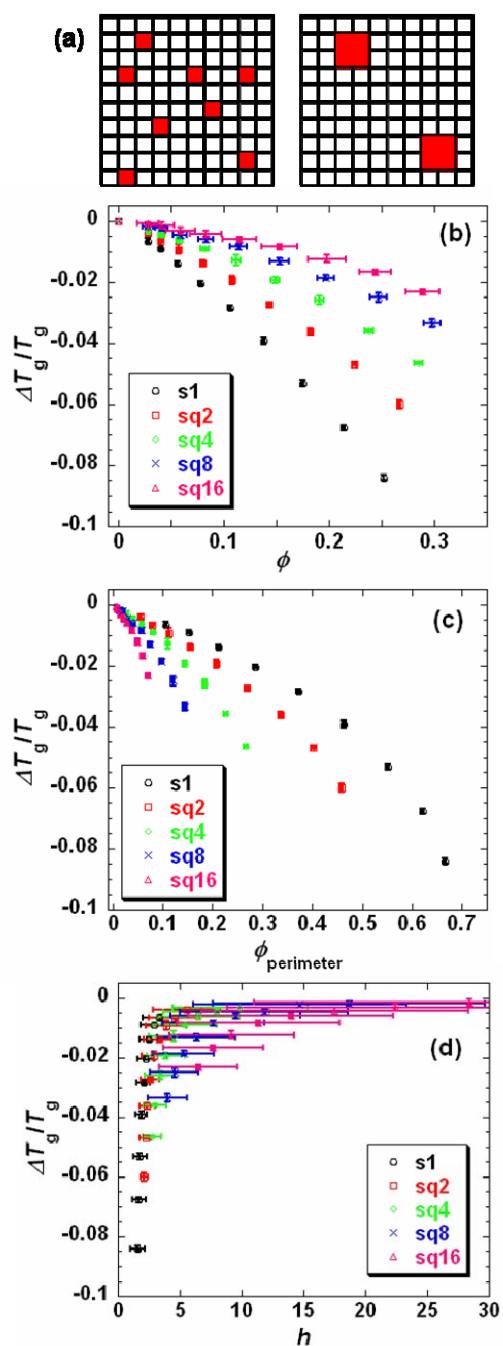
Figure 6-5: (a) Schematic of impurity placement in lattice. A red site represents an impurity and a clear site represents polymer. The left lattice is the case of single site (s1) impurities and the right lattice is the case of 2x2 (sq2) impurities. The change in the glass transition temperature for a range of square impurity sizes as a function of (b) impurity concentration, (c) interfacial site concentration, and (d) interparticle distance.

111

radius half the impurity linear dimension). Figure 6-5 (panels c and d) shows $\Delta T_g/T_g$ plotted against these parameters. We observe that there is not an exact collapse of the data for different particle sizes in either case, although the interparticle distance plot comes closer to giving a particle size independent description of the T_g changes. The inability to completely describe PNC T_g changes in terms of a single parameter suggests that there may be a complex interplay between effects. Percolation of slow domains throughout the system is inherently a multi-body effect. Thus, the fact that particle surface perimeters, which only accounts the for role of individual particles, or interparticle particle distances, which only accounts for the role of particle pairs, do not completely capture the changes in the percolation behavior is not too surprising.

6.3.3   Interfacial Effects

Experimental measurements on PNCs often suggest that the polymer properties at the polymer-particle interface are altered from those exhibited by the neat polymer.[22, 24, 25]   Our percolation model takes this into account by altering the occupation probability of sites neighboring the impurity site to $p' = p \pm \delta$. This interfacial region around the impurity is defined by both a strength, δ, and a length scale, the number of lattice neighbors over which the interface exists. The role that these factors play in the T_g changes can be systematically evaluated with the framework of our percolation model. Nearest neighbor interfacial regions for both a range of impurity sizes at a given δ and for a single site impurity over a range of δ are depicted in Figure 6-6. For a given δ, both the magnitude of the ΔT_g for a given impurity size and the magnitude of the size dependence of ΔT_g increase relative to $\delta = 0$. The latter is due to the fact that as impurity size decreases, the ratio of nearest neighbor sites to impurity sites increases. For the single site impurity, an increase in δ leads to a larger change in T_g, especially at high ϕ. The

Figure 6-6: The change in the glass transition temperature as a function of impurity concentration for (a) a range on square impurity sizes with a nearest neighbor interfacial layer of δ=0.4 and (b) single site impurities with a nearest neighbor interfacial layer over a range of δ.

qualitative behaviors of the T_g changes are the same in all cases.

When the interfacial region is allowed to extend beyond nearest neighbors to next nearest neighbors, we see a plateau in the ϕ dependence of $\Delta T_g/T_g$ for low δ at $\phi < 0.25$, as depicted in Figure 6-7. At high δ, percolation is completely prevented in the system before the plateau can occur. In this analysis, skin layers are allowed to overlap each other but not overlap impurities. This leads to the lattice organization depicted in the inset of Figure 6-7 when the maximum impurity loading in the lattice is reached. The plateau in the T_g behavior is thus related to approaching the maximum impurity occupation fraction under the given interfacial condition. Figure 6-7 demonstrates that the plateau occurs at even lower concentrations when the skin extends to even more remote neighbors; again, the plateau is associated with approaching the maximum impurity occupation fraction at the given interfacial conditions. We do note that experimental measurements by Ash et al.[24] have shown that the T_g of polymers can display large changes upon the addition of small concentrations of nanoparticles and then plateau with further increases in nanoparticle concentration. Exactly how this may be related to our model results is still unclear; especially in the case of the repulsive particle-polymer interactions in the materials of Ash et al.,[24] where particles would be expected to agglomerate before reaching the maximum occupation fraction described by the model. On the other hand, simulations have shown that when particle-polymer interactions are attractive, discrete bound layers of polymer can form at the particle surface and prevent the particles from agglomerating.[36] Hence, a limit to the effectiveness of particles to change the T_g of these systems may be reached when the average interparticle distance reaches twice the thickness of the bound layer.
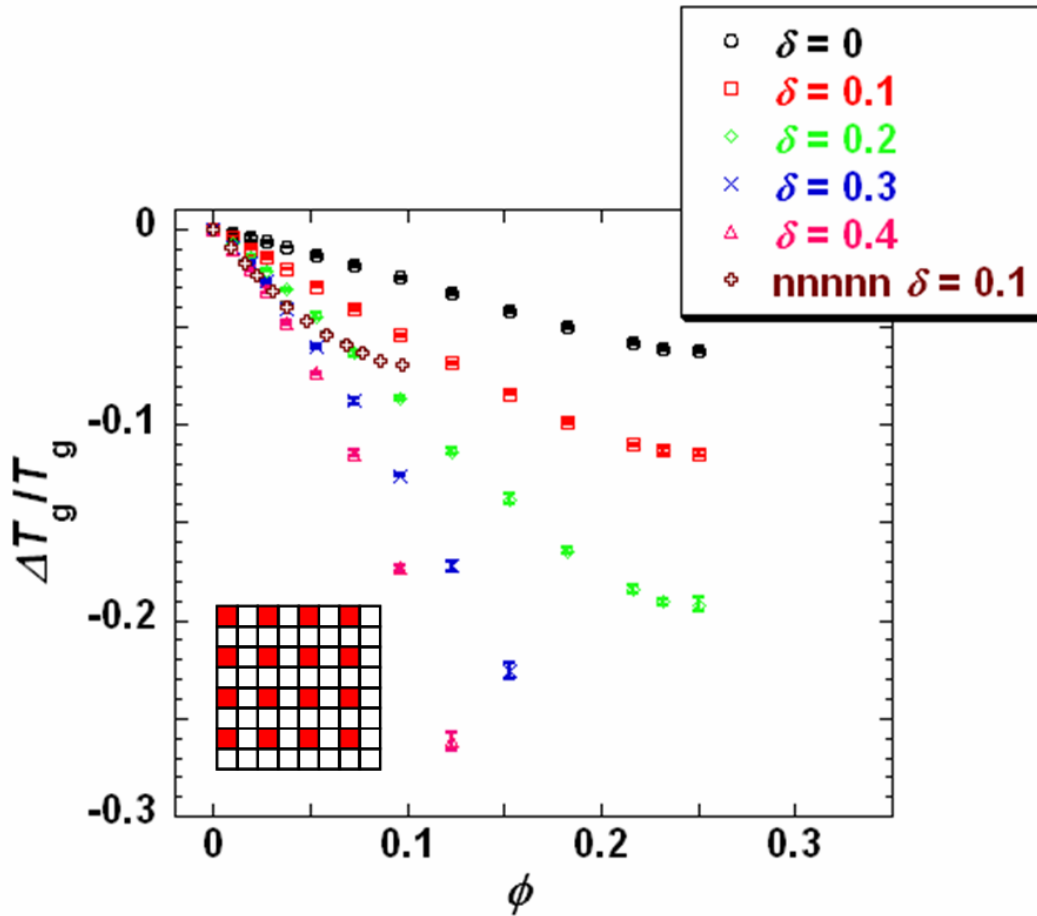
Figure 6-7: The change in the glass transition temperature as a function of impurity concentration for single site impurities with nearest and next-nearest neighbor interfacial layers over a range of δ. The case of nnnnn and $\delta = 0.1$ gives an example of what occurs when the impurity skin is extended to even more remote neighbors. The inset schematic depicts particle (red site) organization within the lattice at the maximum particle loading fraction for single site particles with nearest and next nearest neighbor interfacial layers.

6.3.4   Impurity Shape

Nanoparticle shape may also play a role in the effect on polymer T_g. Throughout this paper, we have been discussing the T_g of a system based on the percolation of slow domains. Often times, it is the percolation of the filler material itself that is of interest, as in the formation of an electrically conductive network of particles in the material. In this case, anisotropic particles exhibit a lower particle percolation threshold than the isotropic case.[37]   Thus, we would expect particle anisotropy to play a role in shaping the percolation of slow domains in our systems as well.

We can use our percolation model to evaluate such questions by varying the shape of the impurities and measuring the effect on $\Delta T_g/T_g$. A single site impurity can be extended in one dimension to transition from a square to a rod-like particle. The resulting change in T_g for these systems is given in Figure 6-8a. Interestingly, $\Delta T_g/T_g$ is found not to exhibit a monotonic dependence on the impurity line length. For small increases in the impurity line length, the magnitude of ΔT_g decreases relative to the single site impurities, similar to the behavior when increasing the size of square impurities. However, when line length is greater than eight sites, T_g changes increase relative to the single site impurity. The non-monotonic behavior is likely the result of two competing effects on ΔT_g with increasing impurity line length: impurity site correlations and impurity anisotropy.

In light of our analysis of the square impurities, we realize that impurity site correlations reduce T_g changes relative to random placement of individual impurity sites. Site correlations increase with increasing impurity line length. Hence, the effect of site correlations would act to decrease the magnitude of ΔT_g with increasing impurity line length.   As impurity line length is increased, the impurity shape also becomes increasingly anisotropic. The unoccupied anisotropic impurities are more effective at
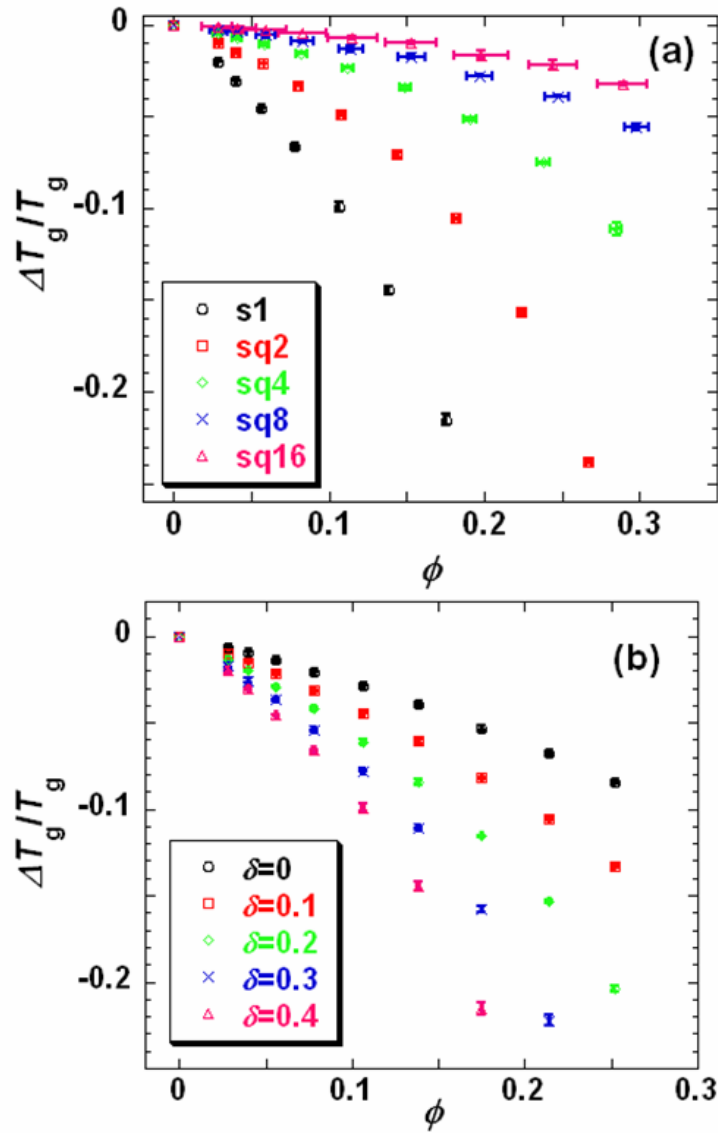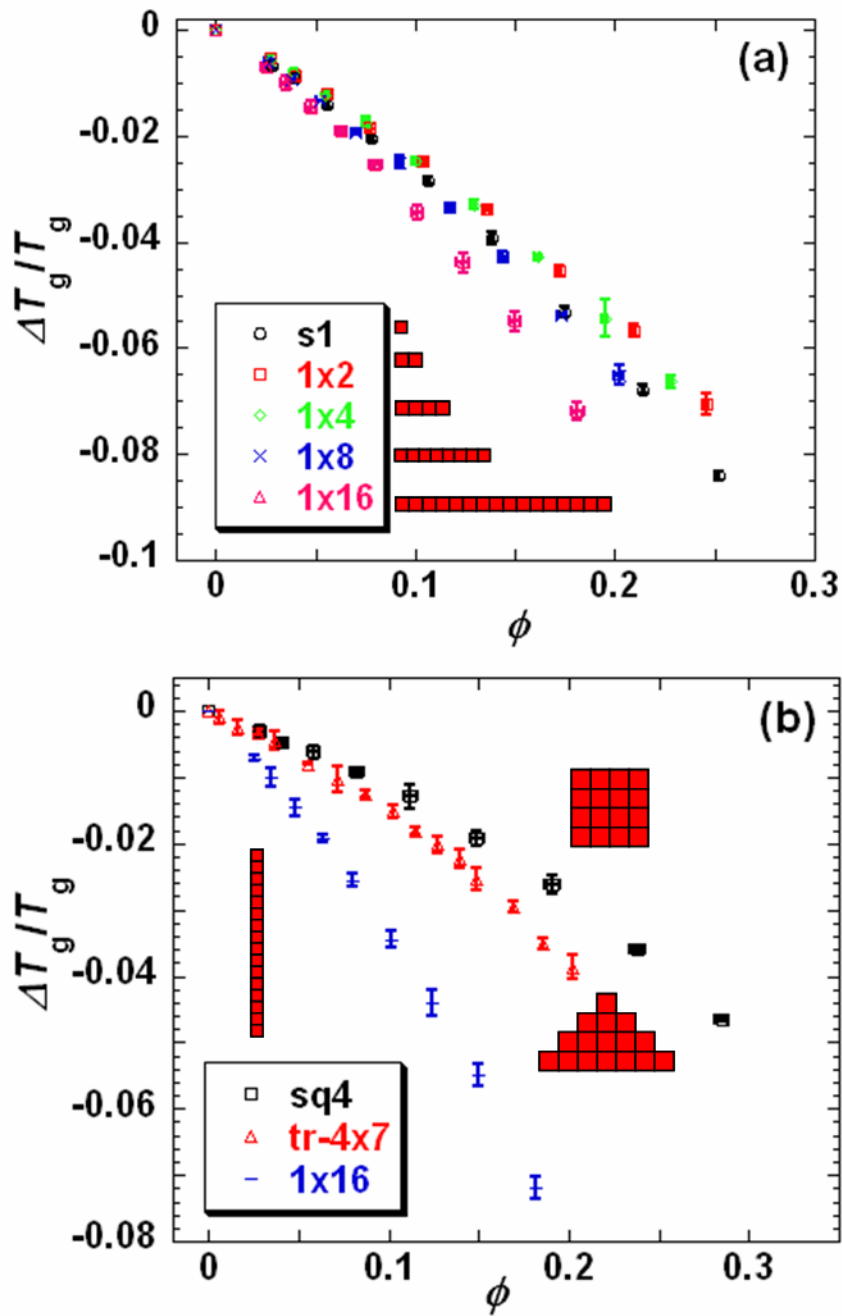
Figure 6-8: The change in the glass transition temperature as a function of impurity concentration for (a) a range of linear impurity sizes and (b) a range of impurity shapes, square, triangle, and line, composed of an equal number sites.

forming clusters that isolate polymer domains within the cluster than their isotropic counterparts, and this isolation renders the polymer domains unable to contribute to a percolated polymer network throughout the system. This effect will increase the magnitude of ΔT_g with increasing impurity line length. Thus, with increasing line length impurity site correlations act to decrease the magnitude of ΔT_g and increasing particle anisotropy acts to increase the magnitude of ΔT_g. The observed behavior indicates which effect is dominant. The effect of impurity anisotropy is further demonstrated in Figure 6-8b. Here, a comparison of impurities of different shapes, all composed of an equal number of sites, is given. As the shape transitions from sphere-like to line-like, the magnitude of ΔT_g increases.

6.3.5 PNC versus Thin Film

Of interest in this section is the correspondence of behaviors in PNCs and thin polymer films. The properties in both of these systems are strongly influenced by the presence of polymer-surface interactions: in thin polymer films, polymer segments interact with the external interfaces that confine the film geometry, while in PNCs the particle-polymer surface interactions are within the bulk of the material. The manner in which these surface interactions affect the T_g of the materials has been of particular interest over the last decade.[19, 21, 22, 25, 28, 29, 38-50] Recent experimental investigations have even suggested that polystyrene (PS)-silica PNC T_gs at a given interparticle distance, h_p, are equivalent to that of free standing PS thin films with thickness $h_f = h_p$.[21] However, similar experiments exploring the relations between real PNCs and model PNCs, films bound by two surfaces of the same chemical make-up as the nanoparticles, have suggested that the quantitative equivalence between PNCs and

118

thin polymer films found for the PS-silica systems may not be universal for all materials.[22]

The percolation model developed here provides a means to address some important questions that must be answered to determine whether there is an intrinsic relation between PNC and thin polymer film T_gs. To this end, we compare the 2D PNC ΔT_g results to the crossover between 2D and 1D percolation, i.e., the change in T_g that results from reducing the size of one side of the 2D lattice, approaching the 1D case. Figure 6-9b presents the comparison between the $\Delta T_g/T_g$ values determined for PNCs and thin films, with h representing the average nearest neighbor interparticle distance and height of the 2D lattice for the PNC and thin film, respectively. Both the PNC and thin film exhibit the same qualitative behavior for $\Delta T_g/T_g$ vs. h, but a clear quantitative difference is observed; the quantitative differences are evident despite the dispersion of PNC $\Delta T_g/T_g$ at a given h for the range of particle sizes.

To further characterize the differences between the PNC and equivalent thin film ΔT_g, we asses the h dependence of the T_g changes. Earlier work has shown that the thickness dependence of polymer film T_g can be characterized by a power law behavior, $\Delta T_g/T_g = -(\alpha/h_f)^x$;[19, 44, 45] where α is a proportionality constant. Log-log plots of the change in T_g from the percolation model versus h for both the PNCs and thin films (Figure 6-9c) can be well described by a linear fit; this indicates that the ΔT_g resolved from our percolation model can also be described by a power law relation in terms of h. The fitting parameters, α and x, attained from the best fit of the power law relation to the data are given in Table 6-1. The fits resolve an increase in the power law exponent x, from 1.48 for sq16 particles to 1.94 for the s1 particles, with decreasing particle size. The power law exponent for the film, x = 0.71, is considerably smaller than that found for the PNCs; the smaller exponent for the film results in the film exhibiting a broader T_g
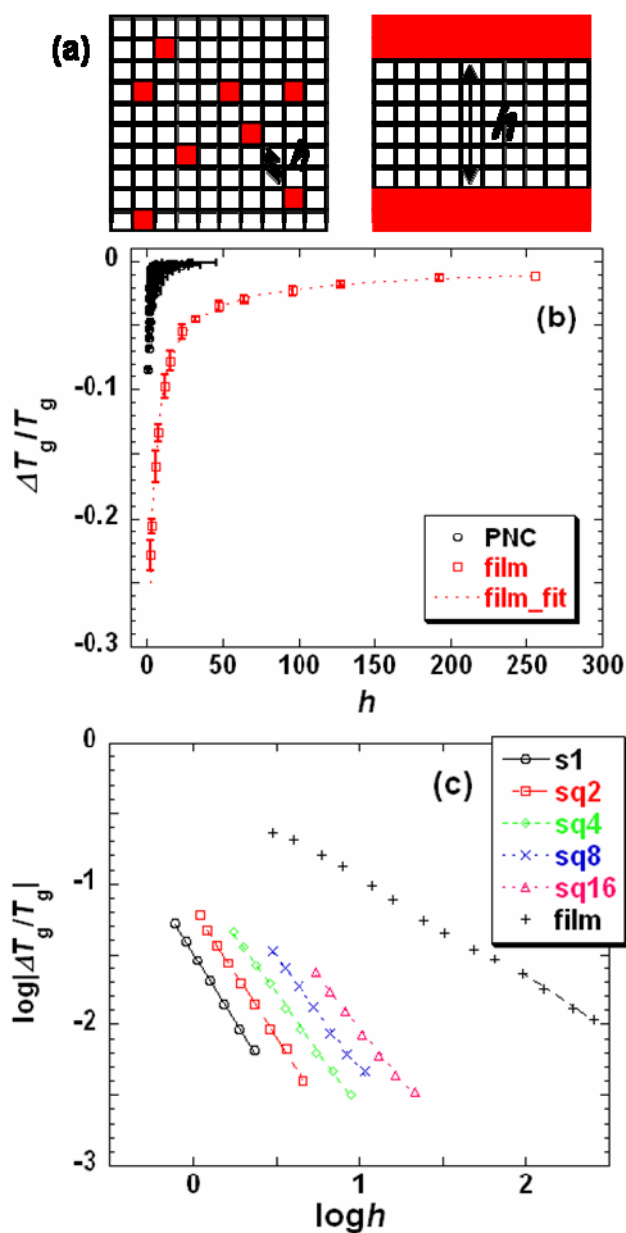
Figure 6-9: (a) Schematic showing the relation between the interparticle distances in PNCs (left) and the film thickness in polymer thin films (right). (b) The change in the glass transition temperature determined from the percolation model for all PNCs and the equivalent thin film plotted against the interparticle distance and film thickness for the PNCs and films, respectively. (c) log-log plot of the change in the glass transition temperature versus interparticle distance and film thickness for the PNCs and films, respectively. The lines connecting the points represent the best linear fit to the data.

	Interfacial Layer Thickness (lattice spacing)	δ	α	x
s1	1	0	0.17	1.94
sq2	1	0	0.23	1.85
sq4	1	0	0.26	1.65
sq8	1	0	0.34	1.57
sq16	1	0	0.49	1.48
film	1	0	0.42	0.71
s1	3	0.4	1.59	5.22
sq2	3	0.4	1.53	3.13
sq4	3	0.4	1.51	2.73
sq8	3	0.4	1.36	2.35
sq16	3	0.4	1.11	1.87
film	3	0.4	2.13	1.07

Table 6-1:   The fitting parameters resolved for the best fit of the T_g data from the percolation model to the power law expression described in the text.

transition regime than the equivalent PNCs. A narrower T_g transition regime for the real PNCs relative to the model PNC films could explain the relation between the T_gs of the materials in Torkelson's experimental measurements,[22] where the films exhibited larger T_g changes than the real PNCs at film thicknesses comparable to the "theoretical" interparticle spacing; particularly since the experimental data is taken at the onset of deviations from bulk, neat polymer behavior.

We now address whether the relationship between PNC and thin film T_g just described is universal for all systems, or whether the relation depends on the specific polymer-surface interactions in the system. Figure 6-10b depicts $\Delta T_g/T_g$ vs. h for both PNCs and films when interfacial interactions extend ~3 lattice spacings and decrease the occupation probability of the sites, $p' = p - \delta$, with $\delta = 0.4$. The extended influence on polymer dynamics leads to a sharper T_g transition regime for both the film and PNCs relative to the cases without influence on the neighboring polymer domains. This is characterized by increases in the exponent of power law fits to the h dependence of T_g; x = 1.07 for the film and increases from 1.87 to 5.22 with decreasing particle size in the PNCs, as resolved from linear fits to the log-log plots in Figure 6-10c and shown in Table 6-1. The difference between the PNC and thin film T_g, $[T_g^{PNC} - T_g^{film}]/ T_g^{pure, bulk}$, with and without effects on neighboring polymer dynamics is shown in Figure 6-10d as a function of h. In Figure 6-10d we focus on the region $3 < h < 100$; this is likely the most relevant region of the plot to compare to experimental observations. We note a couple of observations from Figure 6-10d. The first is that in all systems the films show larger decreases in T_g from the bulk than the PNCs (this does not always hold in the extreme case of $h < 3$, however). This results from the broader T_g transition regime for the films relative to the PNCs as described above. The second observation is that the stronger the surface influence on the polymer, the larger the difference between PNC and thin film
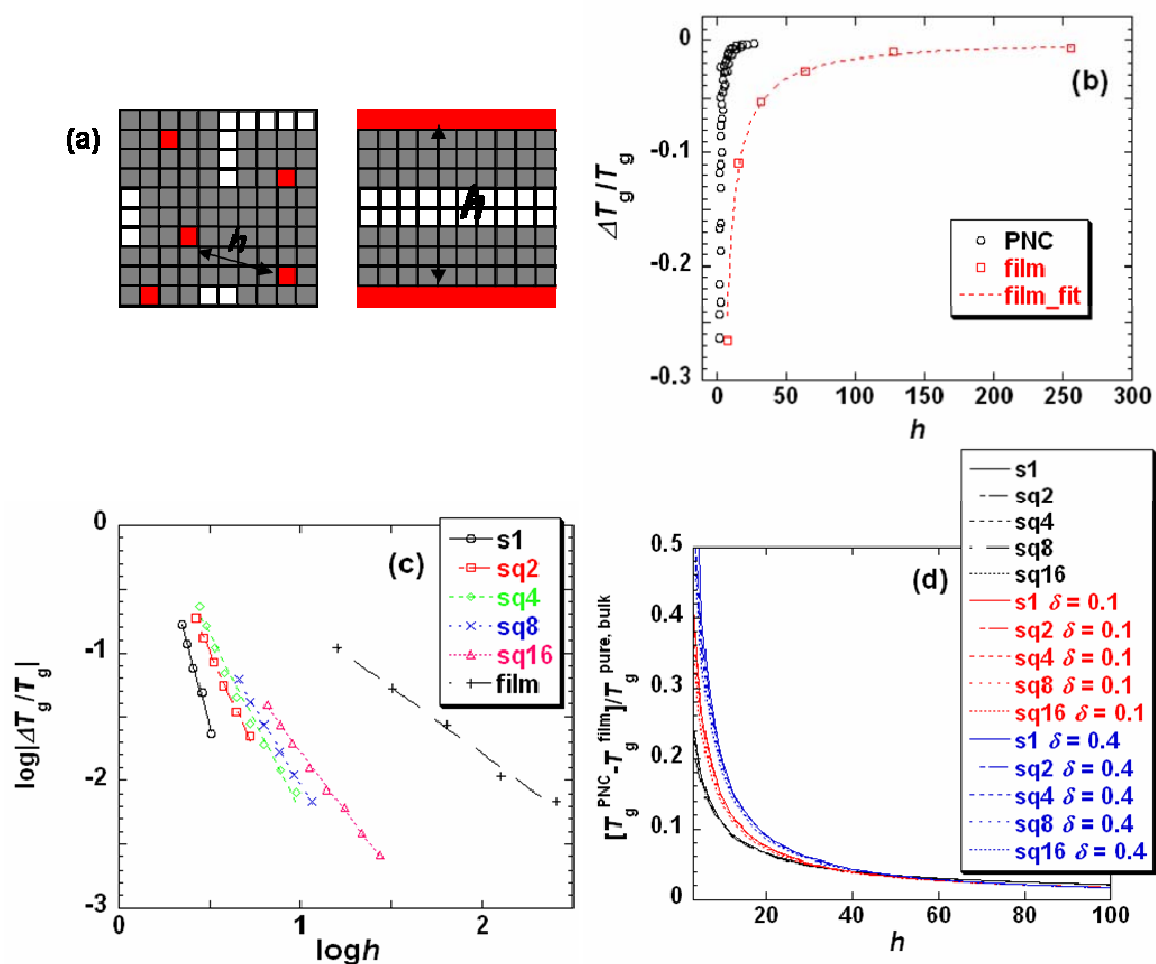
Figure 6-10: (a) Schematic showing the PNC (left) and film (right) when interfacial interactions extend three lattice spacings (dark squares). (b) The change in the glass transition temperature determined from the percolation model for all PNCs and the equivalent thin films plotted against the interparticle distance and film thickness for the PNCs and films, respectively. In this case, the surfaces are allowed to influence polymer domains up to three lattice spacings from the surface, altering the occupation probability of the interfacial domains by $p'=p-\delta$ with $\delta=0.4$. (c) log-log plot of the change in T_g versus h, interparticle distance or film thickness, for the systems with an interfacial zone. The lines connecting the points represent the best linear fit to the data. (d) Plot of the difference in T_g between the PNCs and equivalent films as a function of film thickness, or interparticle distance, for the systems with and without a region on influence on polymer dynamics extending from the interfaces.

123

T_gs. This clear dependence of the relation between PNC and thin film T_g on the extent of interfacial interactions in the system may explain why some experimentalists find a quantitative equivalence in T_gs of films and PNCs[21] while others do not.[22]

6.4   CONCLUSIONS

We have shown that many of the behaviors of PNC T_g can be explained in the context of a percolation model. The placement of impurities on a lattice changes the percolation threshold of the system and this can be related to a change in T_g. Specific treatments of the impurities result in either increases or decreases in T_g relative to the pure system, and the magnitude of the changes in T_g are related to the size of the lattice impurities. The magnitude of the changes in T_g can be enhanced relative to the impurity effect alone by allowing the impurities to influence the occupation probability of neighboring sites, essentially accounting for variations in polymer-particle interaction strengths. The model further suggests that nanoparticle shape can play a significant role in the magnitude of T_g changes. In particular, largely anisotropic impurities can enhance the magnitude of T_g changes relative to their isotropic analogues. The chemical similarity of materials like C_{60}, carbon nanotubes and graphene sheets may provide an opportunity to evaluate the effect of particle anisotropy on PNC T_g if the particles can be ideally dispersed in a polymeric medium.

The development of the percolation model for PNCs also enabled a comparison of PNC T_g changes to those of thin polymer films. The same qualitative behavior was found for both PNCs and thin films, but a clear quantitative difference was discerned. A relation was developed for the differences and shown not to be universal, i.e., when the particles, or surfaces, were allowed to influence the neighboring polymer domains a new relation between PNC and thin film T_g was required. The lack of universality suggests

that although thin films may be a good tool to examine qualitative behaviors in real PNCs, quantitative relations between the two systems may have to be determined for each system individually.

The attractiveness of the percolation model stems from its ability to predict changes in bulk T_g behavior based solely on local changes in system dynamics by determining the manner in which dynamic heterogeneities in the system interact to cease bulk flow of the material. The ability of local changes in polymer dynamics, induced by interfacial interactions with nanoparticles, to affect the bulk T_g in PNCs has been suggested by both experiments and simulations.[23-25, 51, 52] However, a complete understanding of how the increased dynamic heterogeneity of these systems leads to changes in T_g is not fully understood. This computational percolation model provides additional insight into the problem. The simplicity of the percolation model presented suggests that it is likely only a tool to evaluate qualitative trends in T_g behavior; particularly since the computations are completed in 2D, whereas real systems are 3D.

6.5 REFERENCES

[1]   J. H. Gibbs, and E. A. DiMarzio, *Journal of Chemical Physics* **28**, 373 (1958).

[2]   E. A. DiMarzio, and J. H. Gibbs, *Journal of Chemical Physics* **28**, 807 (1958).

[3]   G. Adam, and J. H. Gibbs, *Journal of Chemical Physics* **43**, 139 (1965).

[4]   G. S. Grest, and M. H. Cohen, *Advances in Chemical Physics* **48**, 455 (1981).

[5]   J. Jackle, *Rep. Prog. Phys.* **49**, 171 (1986).

[6]   R. Zallen, *The Physics of Amorphous Solids* 1983).

[7]   G. H. Fredrickson, *Annual Review of Physical Chemistry* **39**, 149 (1988).

[8]   P. A. O'Connell, and G. B. McKenna, *Science* **307**, 1760 (2005).

[9]   L. Berthier *et al.*, *Science* **310**, 1797 (2005).

[10]   J. C. Conrad *et al.*, *Physical Review Letters* **97**, 265701 (2006).

[11]   X. H. Lu *et al.*, *Physical Review Letters* **1**, 045701 (2008).

[12]   R. D. Priestley *et al.*, *Science* **309**, 456 (2005).

[13]   M. D. Ediger, *Annual Review of Physical Chemistry* **51**, 99 (2000).

[14]   H. Sillescu, *Journal of Non-Crystalline Solids* **243**, 81 (1999).

[15]   R. Richert, *J. Phys.-Condes. Matter* **14**, R703 (2002).

[16]   P. H. Poole, C. Donati, and S. C. Glotzer, *Physica A* **261**, 51 (1998).

[17]   C. Bennemann *et al.*, *Nature* **399**, 246 (1999).

[18]   R. H. Colby, *Physical Review E* **61**, 1783 (2000).

[19]   D. Long, and F. Lequeux, *European Physical Journal E: Soft Matter* **4**, 371 (2001).

[20]   P. Sotta, and D. Long, *Eur. Phys. J. E* **11**, 375 (2003).

[21]   A. Bansal *et al.*, *Nat. Mater.* **4**, 693 (2005).

[22]   P. Rittigstein *et al.*, *Nat. Mater.* **6**, 278 (2007).

[23]   F. W. Starr, T. B. Schroder, and S. C. Glotzer, *Physical Review E* **64**, 021802 (2001).

[24]   B. J. Ash, R. W. Siegel, and L. S. Schadler, *Journal of Polymer Science, Part B: Polymer Physics* **42**, 4371 (2004).

[25]   J. M. Kropka *et al.*, *Macromolecules* **40**, 5424 (2007).

[26]   M. Sahimi, *Applications of percolation theory* (Taylor & Francis, Bristol, PA 1993).

[27]   D. Stauffer, *Introduction to percolation theory* (Taylor & Francis, London 1992).

[28]   A. Bansal *et al.*, *Journal of Polymer Science Part B-Polymer Physics* **44**, 2944 (2006).

[29]   P. Rittigstein, and J. M. Torkelson, *Journal of Polymer Science, Part B: Polymer Physics* **44**, 2935 (2006).

[30]   S. A. Bagnich, and A. V. Konash, *J. Phys. A-Math. Gen.* **36**, 1 (2003).

[31]   V. Cornette, A. J. Ramirez-Pastor, and F. Nieto, *Journal of Chemical Physics* **125** (2006).

[32]   G. Kondrat, *Journal of Chemical Physics* **122** (2005).

[33]   J. Hoshen, and R. Kopelman, *Physical Review B* **14**, 3438 (1976).

[34]   A. R. C. Baljon, J. Billen, and R. Khare, *Physical Review Letters* **93** (2004).

[35]   C. Becker, H. Krug, and H. Schmidt, *Materials Research Society Symposium Proceedings* **435**, 237 (1996).

[36]   J. B. Hooper, and K. S. Schweizer, *Macromolecules* **38**, 8858 (2005).

[37]   E. M. Sevick, P. A. Monson, and J. M. Ottino, *Phys. Rev. A* **38**, 5376 (1988).

[38]   D. S. Fryer, P. F. Nealey, and J. J. De Pablo, *Macromolecules* **33**, 6439 (2000).

[39]   D. S. Fryer *et al.*, *Macromolecules* **34**, 5627 (2001).

[40]   J. Q. Pham, and P. F. Green, *Journal of Chemical Physics* **116**, 5801 (2002).

[41]   J. Q. Pham, and P. F. Green, *Macromolecules* **36**, 1665 (2003).

[42]   C. J. Ellison *et al.*, *European Physical Journal E: Soft Matter* **8**, 155 (2002).

[43]   C. J. Ellison, and J. M. Torkelson, *Nat. Mater.* **2**, 695 (2003).

[44]   J. L. Keddie, R. A. L. Jones, and R. A. Cory, *Europhysics Letters* **27**, 59 (1994).

[45]   J. L. Keddie, R. A. L. Jones, and R. A. Cory, *Faraday Discussions*, 219 (1994).

[46]   J. A. Forrest *et al.*, *Physical Review Letters* **77**, 2002 (1996).

[47]   J. A. Forrest, and K. Dalnoki-Veress, *Advances in Colloid and Interface Science* **94**, 167 (2001).

[48]   J. H. van Zanten, W. E. Wallace, and W.-l. Wu, *Physical Review E: Statistical Physics, Plasmas, Fluids, and Related Interdisciplinary Topics* **53**, R2053 (1996).

[49]   J. A. Torres, P. F. Nealey, and J. J. de Pablo, *Physical Review Letters* **85**, 3221 (2000).

[50]   P. G. de Gennes, *European Physical Journal E: Soft Matter* **2**, 201 (2000).

[51]   F. W. Starr, T. B. Schroder, and S. C. Glotzer, *Macromolecules* **35**, 4481 (2002).

[52]   G. D. Smith *et al.*, *Journal of Chemical Physics* **117**, 9478 (2002).

Chapter 7: Summary and Outlook

This work has contributed to the development of an understanding of the factors that control both (1) interfacial instabilities associated with dewetting in thin polymer films and (2) the dynamical properties exhibited by polymer-based nanocomposites (PNCs). In this closing chapter, a summary of the research detailed within this dissertation is presented, followed by proposed recommendations for future work.

7.1   SUMMARY OF RESEARCH

The investigations of the morphological structure of thin film mixtures of polystyrene (PS) and tetramethyl bisphenol-A polycarbonate (TMPC) highlighted the ability to stabilize the characteristically unstable PS thin films, supported on oxidized silicon substrates, with the addition of as little as a few weight percent TMPC. The nature of the stabilization was evaluated in terms of the compositional dependence of both the macroscopic wetting parameters and the effective interface potential. We showed that while films can be stabilized over long periods of time, which exceed the decrease in film dynamics anticipated from the addition of TMPC, the long-range forces in the system actually become more destabilizing with TMPC addition. This finding led us to propose that the development of surface heterogeneities at the substrate interface may play a role in stabilizing the thin polymer films; particularly, that a more dense covering of TMPC on the substrate could lead to an increased resistance to dewetting. However, the exact underlying forces that resist the destabilizing van der Waals interactions in these systems remain elusive.

While investigating the morphological stability of the PS-TMPC thin films, we found that the secondary nanoscopic dewetting structures[1, 2] change with both film

composition and initial film thickness. Changes in the system thermodynamic parameters, the film surface tension, Hamaker constant, and wetting layer thickness, were shown unlikely to be the origin of changes in nanodroplet structure. Mechanisms for changes in film composition and dynamics local to the supporting substrate were proposed that could explain the changes in structure observed.

In addition to the structural stability of thin films, we were also interested in the role that particle-polymer interfacial interactions play in shaping the properties exhibited by PNCs. Studies on the thermal and rheological properties of PMMA-C_{60} PNCs resulted in the detection of increases in the glass transition temperature (T_g) and melt relaxation times with C_{60} addition, without any resolution of increased dynamic heterogeneity of the mixtures relative to the neat polymer. The compositional dependence of the dynamics could be accounted for by the changes in T_g, and an analysis of the dispersion of C_{60} within the polymer allowed for the determination that particle-polymer interfacial interactions alone, not polymer confinement between particles or polymer bridging of particles, were responsible for the changes in properties observed in the mixtures. A mechanism involving transient interactions between the particles and polymer segments was described to account for the changes in the longest relaxation time of the system. The homogenization of the particle effects throughout the system that can occur on the timescale of the longest relaxation time of the polymer, however, is not possible in the case of the localized cooperative motions associated with the mechanical α-relaxation peak. To account for the changes in α-relaxation dynamics, ideas relating the glass transition to a percolation process were invoked.[3-8] These ideas allow for changes in local dynamics in the system, associated with the addition of nanoparticles, to account for a shift the in the bulk T_g and associated α-relaxation dynamics.

Similar effects of C_{60} on the dynamics associated with T_g occurred in other amorphous polymers, PS and TMPC, providing some generality to the observations. Incoherent neutron scattering measurements of these materials in the melt state also provided evidence of immobilization of polymer chain segments at the surface of the C_{60} particles over nanosecond time scales. This observation provided support for the proposal that the nanoparticles increase the fraction of slow polymer domains in the material relative to the neat polymer. Under these conditions, percolation of slow domains would occur at a higher temperature in the PNCs than in the neat polymer, and this could explain the increases in T_g observed for the PNCs.

Finally, the effects of nanoparticles on the percolation of slow domains in a system, and hence the observed T_g, was characterized computationally. A very simple model was shown to be able to account for many experimental observations of PNC T_g, including: (1) increases[9-12] or decreases[12-14] in T_g with particle loading, (2) particle size effects on the magnitude of T_g changes,[13-15] and (3) variations in the magnitude of T_g changes with particle-polymer interaction strength. These consistencies with experimental observations provided some confidence that even such a simple model may be able to give some insight into the physical behaviors of PNC T_gs. The percolation model also provided a means to test other experimental observations, such as the equivalence of PNC T_gs at a given particle-polymer interfacial interaction area[13] or a given interparticle distance in the system.[14] We further showed that, within the percolation model, the relationship between PNC and thin film T_g is dependent upon the polymer-surface interactions in the system. This may explain the apparent contradictions in experimental observations for different polymer-surface combinations.[10, 14]

7.2   RECOMMENDATIONS FOR FUTURE WORK

The work completed in this dissertation presents new insights into the behaviors of both polymer thin film wetting properties and the dynamical properties of polymer nanocomposites, but it also introduces new questions that remain to be answered. In the following, possible directions for future research that will help to better understand the physics in these situations are proposed.

7.2.1   Role of Surface Roughness on the Morphological Stabilization of Thin Polymer Films

In Chapter 2, a combination of (1) strong specific interactions between TMPC and the oxidized silicon substrate and (2) surface roughening of the substrate due to TMPC coverage were proposed to account for the stabilization of PS thin films, supported on oxidized silicon substrates, by the addition of TMPC. The exact role that surface roughening may play, however, could not be discerned from the experiments. A study to systematically resolve the influence of surface roughness on the stability of thin polymer films may help to resolve the stabilization mechanism in the PS-TMPC thin film mixtures as well as answer questions about how nanoparticles[16, 17] and dendrimers[18] stabilize thin polymer films by segregating to the substrate interface.

Such a study will require both the creation and characterization of rough substrates composed of a material from which films are known to dewet from the smooth surface. Methods to fabricate rough oxidized silicon surfaces are available,[19, 20] and the detailed structure of these substrate surfaces can be characterized using x-ray reflectivity and atomic force microscopy. These substrates would provide a means to test the ability of surface roughness to stabilize PS films on oxidized silicon substrates,

132

particularly if substrate surface patterns could be fabricated with a range of roughness characteristics. If rough substrates could be fabricated out of a range of different materials, one could also evaluate whether the ability of substrate roughness to stabilize a polymer film depends on the specific polymer-substrate interactions in the system.

7.2.2   Uniqueness Versus Universality in PNC Dynamical Behavior

As has been discussed in earlier chapters of this dissertation, the addition of nanoparticles to a polymer host can have a range of effects on the α-relaxation dynamics of the system. Differential scanning calorimetry can resolve the following types of results: (a) the elimination of a fraction of segments from participating in the glass transition,[21] (b) a broadening of the temperature range over which the glass transition occurs along with a shift in the midpoint of the transition,[14] or (c) a mere shift in the transition temperature.[11] Similarly, the α-relaxation of PNCs measured by dynamic mechanical analysis can exhibit the following behaviors: (a) two separate peaks,[22] (b) a broadening of the neat polymer peak along with a change in the peak temperature,[14] or (c) just a shift in the neat polymer peak temperature without any broadening of the peak.[11, 13] In both types of measurements, (a) is generally associated with strong specific particle-polymer interactions in the system that slow the dynamics of a fraction of the polymer segments considerably from the neat polymer state. On the other hand, (b) and (c) are generally attributed to weakly attractive or repulsive interactions between the particle and polymer. A question that remains is whether these systems are truly unique from one another or whether they can all be fit into the same universality class, where the differences described above are merely artifacts of the analysis technique and associated with the time scale of the measurement relative to the strength of the particle-polymer interactions.

Nanoparticles grafted with polymer chains of the same chemistry as the polymer host in which they are embedded may provide an ideal PNC system by which to make measurements to answer this question. These systems have been shown to exhibit increases, decreases, or no changes in the T_g of the system, depending on the relative molecular weights of the grafted and matrix chains.[12] If this behavior could be exploited in such a way as to generate PNCs that exhibit two separate α-relaxation peaks, peak broadening, and peak shift by changing only the molecular weight of the polymer chains, it may provide direct evidence for a single universality class for PNC dynamical behaviors.

7.2.3 Cluster Structure Details, 3D Effects, and Thin Film PNC T_g

The focus of the work on the 2D percolation model for PNC T_g described in Chapter 6 was the critical percolation threshold. A number of other parameters in the problem might be of interest as well. For instance cluster size distributions might provide more information about the role nanoparticles play in the dynamic heterogeneity exhibited by PNCs.[23] Evaluation of the relationship between cluster mass (the number of sites in a cluster) and cluster size (radius of gyration of the cluster) as a function of nanoparticle concentration might also provide insights into the manner in which these composite materials approach their glass transition relative to the neat polymer.

The computations we have performed can also be extended to 3D, where they can be compared to experimental measurements on a more quantitative basis. The relevance of more elaborate features to the model, such as specific decay functions for polymer-particle interfacial interactions or additive effects of overlapping interfacial layers, could also be evaluated.

Maybe the most exciting extension of this work would be an evaluation of the role of nanoparticles on the T_g behavior of thin polymer films. Thin film PNCs hold potential for novel technological applications such as optoelectronics, and a better understanding of the physical properties they exhibit may help in designing stable, operational devices. The percolation model should be able to answers questions like whether the effects of confinement and nanoparticles are additive in these systems, whether one effect dominates the other, or whether a more complicated relationship exists. It will also be interesting to see if there are specific regimes where each of these conditions prevails.

7.3 REFERENCES

[1]   P. Muller-Buschbaum *et al.*, *Europhysics Letters* **40**, 655 (1997).

[2]   M. Muller *et al.*, *Journal of Chemical Physics* **115**, 9960 (2001).

[3]   G. Adam, and J. H. Gibbs, *Journal of Chemical Physics* **43**, 139 (1965).

[4]   P. H. Poole, C. Donati, and S. C. Glotzer, *Physica A* **261**, 51 (1998).

[5]   C. Bennemann *et al.*, *Nature* **399**, 246 (1999).

[6]   D. Long, and F. Lequeux, *European Physical Journal E: Soft Matter* **4**, 371 (2001).

[7]   A. R. C. Baljon, J. Billen, and R. Khare, *Physical Review Letters* **93** (2004).

[8]   J. C. Conrad *et al.*, *Physical Review Letters* **97** (2006).

[9]   P. Rittigstein, and J. M. Torkelson, *Journal of Polymer Science, Part B: Polymer Physics* **44**, 2935 (2006).

[10]   P. Rittigstein *et al.*, *Nat. Mater.* **6**, 278 (2007).

[11]   J. M. Kropka *et al.*, *Macromolecules* **40**, 5424 (2007).

[12]   A. Bansal *et al.*, *Journal of Polymer Science Part B-Polymer Physics* **44**, 2944 (2006).

[13] B. J. Ash, R. W. Siegel, and L. S. Schadler, *Journal of Polymer Science, Part B: Polymer Physics* **42**, 4371 (2004).

[14] A. Bansal *et al.*, *Nat. Mater.* **4**, 693 (2005).

[15] C. Becker, H. Krug, and H. Schmidt, *Materials Research Society Symposium Proceedings* **435**, 237 (1996).

[16] K. A. Barnes *et al.*, *Macromolecules* **33**, 4177 (2000).

[17] R. S. Krishnan *et al.*, *Langmuir* **21**, 5770 (2005).

[18] M. E. Mackay *et al.*, *Langmuir* **18**, 1877 (2002).

[19] I. Karapanagiotis, D. F. Evans, and W. W. Gerberich, *Colloid Surf. A-Physicochem. Eng. Asp.* **207**, 59 (2002).

[20] F. J. Zhang *et al.*, *Langmuir* **21**, 7427 (2005).

[21] D. Fragiadakis, and P. Pissis, *Journal of Non-Crystalline Solids* **353**, 4344 (2007).

[22] G. Tsagaropoulos, and A. Eisenberg, *Macromolecules* **28**, 6067 (1995).

[23] R. H. Colby, *Physical Review E* **61**, 1783 (2000).

Bibliography

Adam, G. and J. H. Gibbs, *Journal of Chemical Physics* **43**, 139 (1965).

Arceo, A. and P. F. Green, *Journal of Physical Chemistry B* **109**, 6958 (2005).

Arrighi, V., J. S. Higgins, et al., *Polymer* **39**, 6369 (1998).

Ash, B. J., R. W. Siegel, et al., *Journal of Polymer Science, Part B: Polymer Physics* **42**, 4371 (2004).

Ashley, K. M., D. Raghavan, et al., *Langmuir* **21**, 9518 (2005).

Bagnich, S. A. and A. V. Konash, *J. Phys. A-Math. Gen.* **36**, 1 (2003).

Baljon, A. R. C., J. Billen, et al., *Physical Review Letters* **93** (2004).

Bansal, A., H. Yang, et al., *Nat. Mater.* **4**, 693 (2005).

Bansal, A., H. C. Yang, et al., *Journal of Polymer Science Part B-Polymer Physics* **44**, 2944 (2006).

Barnes, K. A., A. Karim, et al., *Macromolecules* **33**, 4177 (2000).

Becker, C., H. Krug, et al., *Materials Research Society Symposium Proceedings* **435**, 237 (1996).

Bennemann, C., C. Donati, et al., *Nature* **399**, 246 (1999).

Berriot, J., H. Montes, et al., *Europhysics Letters* **64**, 50 (2003).

Besancon, B. M. and P. F. Green, *Physical Review E: Statistical, Nonlinear, and Soft Matter Physics* **70**, 051808/1 (2004).

Besancon, B. M. and P. F. Green, *Macromolecules* **38**, 110 (2005).

Besancon, B. M., C. L. Soles, et al., *Physical Review Letters* **97** (2006).

Binder, K., *Advances in Polymer Science* **138**, 1 (1999).

Bonderer, L. J., A. R. Studart, et al., *Science* **319**, 1069 (2008).

Brown, D., P. Mele, et al., *Macromolecules* **36**, 1395 (2003).

Chen, G. and G. Ma, *Applied Physics Letters* **72**, 3294 (1998).

Colby, R. H., *Physical Review E* **61**, 1783 (2000).

Cole, D. H., K. R. Shull, et al., *Macromolecules* **32**, 771 (1999).

Colmenero, J. and A. Arbe, *Physical Review B: Condensed Matter and Materials Physics* **57**, 13508 (1998).

Conrad, J. C., P. P. Dhillon, et al., *Physical Review Letters* **97**, 265701 (2006).

Cornette, V., A. J. Ramirez-Pastor, et al., *Journal of Chemical Physics* **125** (2006).

Costa, A. C., R. J. Composto, et al., *Macromolecules* **36**, 3254 (2003).

Dalnoki-Veress, K., B. G. Nickel, et al., *Physical Review E* **59**, 2153 (1999).

De Gennes, P. G., *Reviews of Modern Physics* **57**, 827 (1985).

de Gennes, P. G., *Eur. Phys. J. E* **2**, 201 (2000).

Desai, T., P. Keblinski, et al., *Journal of Chemical Physics* **122**, 134910/1 (2005).

DiMarzio, E. A. and J. H. Gibbs, *Journal of Chemical Physics* **28**, 807 (1958).

Dimitrakopoulos, C. D. and D. J. Mascaro, *IBM J. Res. Dev.* **45**, 11 (2001).

Du, F., R. C. Scogna, et al., *Macromolecules* **37**, 9048 (2004).

Ducker, W. A., T. J. Senden, et al., *Nature (London, United Kingdom)* **353**, 239 (1991).

Ediger, M. D., *Annual Review of Physical Chemistry* **51**, 99 (2000).

Ellison, C. J., S. D. Kim, et al., *European Physical Journal E: Soft Matter* **8**, 155 (2002).

Ellison, C. J. and J. M. Torkelson, *Nat. Mater.* **2**, 695 (2003).

Feng, Y., A. Karim, et al., *Macromolecules* **31**, 484 (1998).

Ferry, J. D., *Viscoelastic Properties of Polymers. 3rd Ed* (Wiley, New York, 1980).

Forrest, J. A. and K. Dalnoki-Veress, *Advances in Colloid and Interface Science* **94**, 167 (2001).

Forrest, J. A., K. Dalnoki-Veress, et al., *Physical Review Letters* **77**, 2002 (1996).

Frank, B., A. P. Gast, et al., *Macromolecules* **29**, 6531 (1996).

Frank, C. W., V. Rao, et al., *Science* **273**, 912 (1996).

Fredrickson, G. H., *Annual Review of Physical Chemistry* **39**, 149 (1988).

Frick, B. and D. Richter, *Science (Washington, D. C.)* **267**, 1939 (1995).

Fryer, D. S., P. F. Nealey, et al., *Macromolecules* **33**, 6439 (2000).

Fryer, D. S., R. D. Peters, et al., *Macromolecules* **34**, 5627 (2001).

Fuchs, K., C. Friedrich, et al., *Macromolecules* **29**, 5893 (1996).

Galgali, G., C. Ramesh, et al., *Macromolecules* **34**, 852 (2001).

Gibbs, J. H. and E. A. DiMarzio, *Journal of Chemical Physics* **28**, 373 (1958).

Grest, G. S. and M. H. Cohen, *Advances in Chemical Physics* **48**, 455 (1981).

Guth, E., *Journal of Applied Physics* **16**, 20 (1945).

Henn, G., D. G. Bucknall, et al., *Macromolecules* **29**, 4305 (1996).

Hooper, J. B. and K. S. Schweizer, *Macromolecules* **38**, 8858 (2005).

Hoshen, J. and R. Kopelman, *Physical Review B* **14**, 3438 (1976).

Huang, Y. and D. R. Paul, *Polymer* **45**, 8377 (2004).

Israelachvili, J. N., *Intermolecular and Surface Forces* (Academic Press, London, 1991).

Jackle, J., *Rep. Prog. Phys.* **49**, 171 (1986).

Jacobs, K., S. Herminghaus, et al., *Langmuir* **14**, 965 (1998).

Karim, A., T. M. Slawecki, et al., *Macromolecules* **31**, 857 (1998).

Keddie, J. L., R. A. L. Jones, et al., *Faraday Discussions*, 219 (1994).

Keddie, J. L., R. A. L. Jones, et al., *Europhysics Letters* **27**, 59 (1994).

Kerle, T., R. Yerushalmi-Rozen, et al., *Europhysics Letters* **38**, 207 (1997).

Kim, E., E. J. Kramer, et al., *Journal of Polymer Science, Part B: Polymer Physics* **33**, 467 (1995).

Kim, E., G. Krausch, et al., *Macromolecules* **27**, 5927 (1994).

Kondrat, G., *Journal of Chemical Physics* **122** (2005).

Kopesky, E. T., T. S. Haddad, et al., *Polymer* **46**, 4743 (2005).

Krishnamoorti, R. and E. P. Giannelis, *Macromolecules* **30**, 4097 (1997).

Krishnamoorti, R., R. A. Vaia, et al., *Chemistry of Materials* **8**, 1728 (1996).

Krishnamoorti, R. and K. Yurekli, *Current Opinion in Colloid & Interface Science* **6**, 464 (2001).

Krishnan, R. S., M. E. Mackay, et al., *Langmuir* **21**, 5770 (2005).

Kropka, J. M. and P. F. Green, *Macromolecules* **39**, 8758 (2006).

Kropka, J. M., K. W. Putz, et al., *Macromolecules* **40**, 5424 (2007).

Limary, R., P. F. Green, et al., *European Physical Journal E: Soft Matter* **8**, 103 (2002).

Lin, E. K., R. Kolb, et al., *Macromolecules* **32**, 3753 (1999).

Lin, E. K., C. L. Soles, et al., *Science* **297**, 372 (2002).

Lin, H. Q., E. Van Wagner, et al., *Science* **311**, 639 (2006).

Liu, Y., M. H. Rafailovich, et al., *Physical Review Letters* **73**, 440 (1994).

Lomellini, P. and L. Lavagnini, *Rheologica Acta* **31**, 175 (1992).

Long, D. and F. Lequeux, *European Physical Journal E: Soft Matter* **4**, 371 (2001).

Mackay, M. E., T. T. Dao, et al., *Nat. Mater.* **2**, 762 (2003).

Mackay, M. E., A. Tuteja, et al., *Science* **311**, 1740 (2006).

Masson, J.-L. and P. F. Green, *Physical Review Letters* **88**, 205504/1 (2002).

Masson, J.-L. and P. F. Green, *Physical Review E: Statistical, Nonlinear, and Soft Matter Physics* **65**, 031806/1 (2002).

McCoy, J. D. and J. G. Curro, *Journal of Chemical Physics* **116**, 9154 (2002).

Merkel, T. C., B. D. Freeman, et al., *Science* **296**, 519 (2002).

Meyer, A., R. M. Dimeo, et al., *Review of Scientific Instruments* **74**, 2759 (2003).

Mueller-Buschbaum, P., E. Bauer, et al., *Journal of Physics: Condensed Matter* **17**, S363 (2005).

Muller-Buschbaum, P., J. S. Gutmann, et al., *Journal of Macromolecular Science, Physics* **B38**, 577 (1999).

Muller-Buschbaum, P., P. Vanhoorne, et al., *Europhysics Letters* **40**, 655 (1997).

Muller, M., L. G. MacDowell, et al., *Journal of Chemical Physics* **115**, 9960 (2001).

Narayanan, R. A., P. Thiyagarajan, et al., *Physical Review Letters* **97**, 075505/1 (2006).

Oslanec, R., A. C. Costa, et al., *Macromolecules* **33**, 5505 (2000).

Pashley, R. M., *Journal of Colloid and Interface Science* **83**, 531 (1981).

Pham, J. Q. and P. F. Green, *Journal of Chemical Physics* **116**, 5801 (2002).

Pham, J. Q. and P. F. Green, *Macromolecules* **36**, 1665 (2003).

Pham, J. Q., C. A. Mitchell, et al., *Journal of Polymer Science, Part B: Polymer Physics* **41**, 3339 (2003).

Podsiadlo, P., A. K. Kaushik, et al., *Science* **318**, 80 (2007).

Poole, P. H., C. Donati, et al., *Physica A* **261**, 51 (1998).

Potschke, P., T. D. Fornes, et al., *Polymer* **43**, 3247 (2002).

Pryamitsyn, V. and V. Ganesan, *Macromolecules* **39**, 844 (2006).

Pu, Y., M. H. Rafailovich, et al., *Physical Review Letters* **87**, 206101/1 (2001).

Putz, K. W., C. A. Mitchell, et al., *Journal of Polymer Science, Part B: Polymer Physics* **42**, 2286 (2004).

Reiter, G., *Physical Review Letters* **68**, 75 (1992).

Reiter, G., *Europhysics Letters* **23**, 579 (1993).

Reiter, G., *Langmuir* **9**, 1344 (1993).

Reiter, G., *Macromolecules* **27**, 3046 (1994).

Reiter, G., P. Auroy, et al., *Macromolecules* **29**, 2150 (1996).

Reiter, G., J. Schultz, et al., *Europhysics Letters* **33**, 29 (1996).

Reiter, G., A. Sharma, et al., *Langmuir* **15**, 2551 (1999).

Richert, R., *J. Phys.-Condes. Matter* **14**, R703 (2002).

Riggleman, R. A., J. F. Douglas, et al., *Journal of Chemical Physics* **126** (2007).

Rittigstein, P., R. D. Priestley, et al., *Nat. Mater.* **6**, 278 (2007).

Rittigstein, P. and J. M. Torkelson, *Journal of Polymer Science, Part B: Polymer Physics* **44**, 2935 (2006).

Rubinstein, M. and R. H. Colby, *Polymer Physics* (Oxford University Press, New York, 2003).

Russel, W. B., D. A. Saville, et al., *Colliodal Dispersions* (Cambridge University Press, New York, 1989).

Russell, T. P., *Current Opinion in Colloid & Interface Science* **1**, 107 (1996).

Sahimi, M., *Applications of percolation theory* (Taylor & Francis, Bristol, PA 1993).

Seemann, R., S. Herminghaus, et al., *Physical Review Letters* **86**, 5534 (2001).

Seferis, J. C. and R. J. Samuels, *Polymer Engineering and Science* **19**, 975 (1979).

Semenov, A. N., *Physical Review Letters* **80**, 1908 (1998).

Sharma, A., *Langmuir* **9**, 861 (1993).

Sharma, A. and A. T. Jameel, *Journal of Colloid and Interface Science* **161**, 190 (1993).

Sharma, A. and R. Khanna, *Physical Review Letters* **81**, 3463 (1998).

Sillescu, H., *Journal of Non-Crystalline Solids* **243**, 81 (1999).

Smallwood, H. M., *Journal of Applied Physics* **15**, 758 (1944).

Smith, G. D., D. Bedrov, et al., *Physical Review Letters* **90**, 226103/1 (2003).

Smith, G. D., D. Bedrov, et al., *Journal of Chemical Physics* **117**, 9478 (2002).

Soles, C. L., J. F. Douglas, et al., *Journal of Polymer Science, Part B: Polymer Physics* **42**, 3218 (2004).

Soles, C. L., J. F. Douglas, et al., *Physical Review Letters* **88**, 037401/1 (2002).

Solomon, M. J., A. S. Almusallam, et al., *Macromolecules* **34**, 1864 (2001).

Sotta, P. and D. Long, *Eur. Phys. J. E* **11**, 375 (2003).

Stange, T. G., D. F. Evans, et al., *Langmuir* **13**, 4459 (1997).

Starr, F. W., T. B. Schroder, et al., *Physical Review E* **64**, 021802 (2001).

Starr, F. W., T. B. Schroder, et al., *Macromolecules* **35**, 4481 (2002).

Stauffer, D., *Introduction to percolation theory* (Taylor & Francis, London 1992).

Thompson, R. B., V. V. Ginzburg, et al., *Science* **292**, 2469 (2001).

Torres, J. A., P. F. Nealey, et al., *Physical Review Letters* **85**, 3221 (2000).

Tsagaropoulos, G. and A. Eisenberg, *Macromolecules* **28**, 6067 (1995).

Tsagaropoulos, G. and A. Eisenburg, *Macromolecules* **28**, 396 (1995).

Tuteja, A., M. E. Mackay, et al., *Macromolecules* **38**, 8000 (2005).

Vacatello, M., *Macromolecules* **34**, 1946 (2001).

Vacatello, M., *Macromolecular Theory and Simulations* **11**, 757 (2002).

Van Oss, C. J., *Journal of Dispersion Science and Technology* **12**, 201 (1991).

Van Oss, C. J., M. K. Chaudhury, et al., *Advances in Colloid and Interface Science* **28**, 35 (1987).

Van Oss, C. J., M. K. Chaudhury, et al., *Chemical Reviews (Washington, DC, United States)* **88**, 927 (1988).

van Zanten, J. H., W. E. Wallace, et al., *Physical Review E: Statistical Physics, Plasmas, Fluids, and Related Interdisciplinary Topics* **53**, R2053 (1996).

Vitt, E. and K. R. Shull, *Macromolecules* **28**, 6349 (1995).

Voronov, A. and O. Shafranska, *Langmuir* **18**, 4471 (2002).

Vrij, A., *Discussions of the Faraday Society* **No. 42**, 23 (1966).

Wang, H. and R. J. Composto, *Journal of Chemical Physics* **113**, 10386 (2000).

Wang, H. and R. J. Composto, *Europhysics Letters* **50**, 622 (2000).

Warren, S. C., F. J. DiSalvo, et al., *Nat. Mater.* **6**, 156 (2007).

Wisniewsky, C., G. Marin, et al., *European Polymer Journal* **20**, 691 (1984).

Wu, S., *Polymer interface and adhesion* (M. Dekker, New York, 1982).

Wu, S., *Journal of Polymer Science, Part B: Polymer Physics* **27**, 723 (1989).

Yerushalmi-Rozen, R. and J. Klein, *Journal of Physics: Condensed Matter* **9**, 7753 (1997).

Yerushalmi-Rozen, R., J. Klein, et al., *Science* **263**, 793 (1994).

Yurekli, K., R. Krishnamoorti, et al., *Journal of Polymer Science, Part B: Polymer Physics* **39**, 256 (2000).

Zallen, R., *The Physics of Amorphous Solids* 1983).

Zhang, Q. and L. A. Archer, *Langmuir* **18**, 10435 (2002).

Zheng, X., M. H. Rafailovich, et al., *Physical Review Letters* **79**, 241 (1997).

Zheng, X., B. B. Sauer, et al., *Physical Review Letters* **74**, 407 (1995).

Ziemelis, K., *Nature* **393**, 619 (1998).

Vita

Jamie Michael Kropka was born in Clear Lake, Texas on May 6th, 1976, the son of Marilyn Kay (Nettles) and John Michael Kropka. After graduating from Azle High School, Azle, Texas in May 1994, he entered The University of Texas at Austin. In the summer of 1996, he began a co-op with Hoechst Celanese Corporation and spent two semesters at the corporate research facility in Charlotte, NC. He continued his co-op assignment with Dow Chemical Company and spent a semester each in contract manufacturing services in Midland, MI and in Epoxy I/HAA in Freeport, TX. He graduated with High Honors in May 1999 with a Bachelor of Science in Chemical Engineering. In June of 1999, he joined Applied Science Fiction, Inc. in Austin, Texas where he worked to develop unique digital imaging technologies. In June of 2003, he enrolled in the Chemical Engineering graduate program at The University of Texas at Austin where he has conducted research in polymer physics with Peter F. Green and Venkat Ganesan.

Permanent address: 206 Pecan Drive, Fort Worth, TX 76114

This dissertation was typed by the author.